A

Distributions of Tunnel Splittings in Quantum Tunneling of Magnetization in the Single Molecule Magnet, Mn12-acetate

by

Kevin Mathias Mertes

A dissertation submitted to the Graduate Faculty in Physics in partial fulfillment of the requirements for the degree of Doctor of Philosophy, The City University of New York.

2002

UMI Number: 3063862

ProQuest Information and Learning Company
300 North Zeeb Road
P.O. Box 1346
Ann Arbor, MI 48106-1346

This manuscript has been read and accepted for the Graduate Faculty in Physics in satisfaction of the dissertation requirement for the degree of Doctor of Philosophy.

09/18/02 Myriam P. Sarachik

Date Chair of Examining Committee

09/18/02 Sultan Catto

Date Executive Officer

J. Birman

E. Chudnovsky

H. Cummins

S. Vitkalov

Supervisory Committee

THE CITY UNIVERSITY OF NEW YORK

Acknowledgments

There are many people I would like to thank, for so many people have influenced my life in such a positive way to bring me to this point. First and foremost. I would like to thank my advisor. Myriam Sarachik. I can't imagine having had a better advisor. Her insight and kindness have been an inspiration. Her ability to focus my mind when I was lost in confusion by asking probing questions and recalling crucial information proved invaluable. I am very grateful for the freedom she has given me while conducting research. I've learned a great deal from her not only in matters scientific. but also personal.

I would also like to thank Eugene Chudnovsky. who has been essentially a second advisor. My first two years of research were supported by a grant he received from the United States Air Force of Scientific Research. Without him most of the interpretations of my data would not have been possible. He has provided many enlightening and interesting conversations that made this thesis possible.

I am also indebted to Dimitri Garanin. His attentive nature and kind sole are a blessing. Without his discussions about the implications of distributions much of the analysis made in this thesis would not have been possible.

I am also grateful to Dave Hendrickson and George Christou for many informative discussions on the chemistry of single molecule magnets. Of course. my research would have been impossible without their efforts. for they provided the samples I studied. I would also like to thank Evan Rumberger. a graduate student of Dave Hendrickson. who actually grew the samples for us. He also provided some important information on the chemistry of Mn_{12}-acetate.

All the measurements were made with Hall bars that were provided by Eli Zeldov and Hadas Shtrikman of the Weizmann Institute of Science. Their efforts enabled me to obtain clean accurate data which has in turn improved our understanding of the underlying physics of Mn_{12}-acetate. The Hall bars were manufactured by Yossi Paltiel. a graduate student in their group. I would like to thank him for quickly providing new detectors after each time I broke one.

Working within our group is Sergey Vitkalov. I would like to thank him for the numerous conversations about quantum mechanics. I would also like to thank him

for his help when trouble shooting problems in the lab. He saved many hours of head scratching.

Linden Langhorne and Russel of the Machine Shop helped me build the detector assembly unit. The precise craftsmanship contributed to directly to the quality of the data.

When I first begin working with Myriam, Dimitri Simonian and Sergey Kravchenko were members of her group. Both Dima and Sergey taught me how to run the He^3 system. I am grateful for their tutelage. YiCheng Zhong also helped get started with my studies in Mn_{12}-acetate. I would like to thank all three of them for their help.

Mark Jackson of Oxford Research Instruments helped me keep the He^3 system going. He provided many helpful tips to keep the system running smoothly.

I must also thank Jonathan Friedman, for he is the one who introduced me to Myriam. He also helped me through many conversations about Mn_{12}-acetate.

I would also like to thank Yoko Suzuki. She has provided many useful conversations.

George Collison, my high school physics teacher is an important person in my life. He set me out on this long journey when he showed me the wonder and beauty of the laws of physics. Samual Holland, one of my undergraduate professors also had a hand in my career when he encouraged me to continue with my education in physics.

The Seeley family provide many years of support. They are all wonderful people.

I would also like to thank the members of my thesis committee, Joe Birman, Eugene Chudnovsky, Herman Cummins, Myriam Sarachik and Sergey Vitkalov for taking the time to read my thesis. I would like to thank Herman for reminding me to stay on top of all subject matters in solid state physics and to thank Joe Birman for his wonderful lectures in group theory.

None of the research would have been possible without funding. I would like to thank the United States Air Force's Office of Scientific Research as well as the National Science Foundation.

Thank you all.

Table of Contents

List of Tables

List of Figures

List of Equations

1 Introduction

1.1 Single Molecule Magnets

Single molecule magnets are an interesting form of magnetic material. At low temperatures macroscopic samples of these materials exhibit dramatic quantum mechanical phenomena such as tunneling of magnetization[1, 2, 3] and Berry phase oscillations[4, 5]. This stems from the fact that single molecule magnets provide an ensemble of nominally identical molecules with negligible inter-molecular[6, 7, 8, 9] and sufficiently small environmental interactions[10, 11, 12, 13, 14, 15, 16, 17, 18, 19, 20, 21, 22]. The behavior can be measured easily because the large number of molecules in a macroscopic crystal will amplify the tiny signals of a single molecule. Moreover, measuring an ensemble of identical molecules simultaneously yields information that is very similar to measuring an individual molecule many times. Thus, single molecule magnets have the interesting property of exhibiting the laws of quantum mechanics which describe the behavior at molecular, atomic and sub-atomic scales on a macroscopic scale.

Another interesting feature of some single molecule magnets is that the total spin of each molecule lies in the middle ground between classical and quantum physics[11, 13, 20]. In addition, they may have practical uses such as memory storage devices or quantum computers[23, 24, 25].

Molecular magnets have attracted a great deal of attention from chemists and experimental and theoretical physicists and have been extensively studied over the past decade. Much of the basic physics and chemistry of these materials is now understood[26, 18, 27, 28]. However, there are still several important questions left open. The main purpose of this research is to try to answer some of these open questions. In order to effectively convey the main ideas behind this research, I will first review what is known about single molecule magnets and what is still not understood before delving into the details.

1.1.1 Basic Characteristics

Single molecule magnets are organic materials which contain a large (Avogadro's) number of identical magnetic molecules. Single molecule magnets contain magnetic clusters composed of several or many magnetic atoms coupled together at low temperatures to form a cluster of moderate to large total spin. The net spin of each molecule is determined by the exchange interaction between the magnetic moments of the atoms in the molecule. At sufficiently low temperatures, the individual magnetic moments couple together to form a composite spin particle or "single molecule magnet".

The magnetic properties can be understood by examination of the Hamiltonian. In the first approximation, the spin Hamiltonian of a uniaxial single molecule magnet with anisotropy can be modeled by:

$$\hat{\mathcal{H}} = -D\hat{S}_z^2 - g_z\mu_B H_z\hat{S}_z + \hat{V}_T, \tag{1}$$

where $D\hat{S}_z^2$ represents the anisotropy (taken to be along the z-axis) in the molecule, $g_z\mu_B H_z\hat{S}_z$ represents the effective Zeeman interaction the molecule experiences when placed in an external magnetic field, H_z, applied along the anisotropy axis of the molecule and $\hat{V}_T$ represents terms that do not commute with $\hat{S}_z$ and thus break the symmetry in the Hamiltonian. The magnetic anisotropy is an inherent property of the molecule itself[29, 30, 6, 31, 32].

For small $\hat{V}_T$, the energy eigenvalue for this Hamiltonian are given by:

$$E_m = -Dm^2 - g_z\mu_B H_z m, \tag{2}$$

where m is the energy eigenvalue of the $\hat{S}_z$ spin operator. The zero field energy eigenvalues are plotted in part (a) of Fig. 1 for an $S = 10$ single molecule magnet. The vertical axis denotes the energy of the eigenvalues and the horizontal axis denotes the angle the spin operator makes when projected along the z-axis: $\cos(\theta) = m/\sqrt{S(S+1)}$.

The continuous smooth curve results from allowing θ to vary smoothly and forms a double well structure. The energy barrier is due to the anisotropy. For an $S = 10$ spin system, m is an integer that increments equally from -10 to $+10$ and there are $2S + 1 = 21$ eigenvalues. These values are shown by the green dots in Fig. 1. The horizontal green lines connect two equivalent angles and serve as a reminder that the spin is precessing about the z-axis. Part (b) of Fig. 1. shows the double well structure when the molecule is placed in an external magnetic field. Clearly, the effect of the external magnetic field is to "unbalance" the wells producing a stable well and a metastable well.

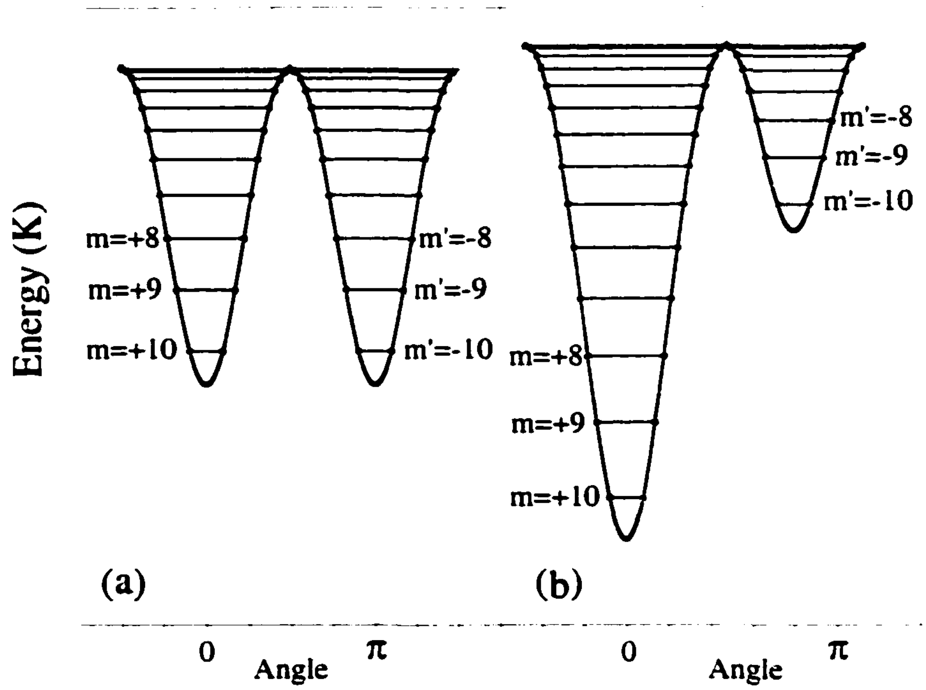

Figure 1: Double Well Potential for $\hat{\mathcal{H}} = -D\hat{S}_z^2 - g_z\mu_B H_z\hat{S}_z + \hat{V}_T$, with $S = 10$. Parts (a) and (b) depict the double well potential for $H_z = 0$ and $H_z \neq 0$, respectively.

For the Hamiltonian of Eq. 1 at zero magnetic field, all the energy levels are pairwise degenerate as can been seen in part (a) of Fig. 1. As the magnetic field increases, the potential wells will unbalance. Eventually, at a particular applied magnetic field, all the energy levels in the metastable well will once again become degenerate with energy levels in the stable well. For the simple Hamiltonian of Eq. 1, the fields at which eigenvalues in the stable well, E_m, equal the eigenvalues in the metastable well, $E_{m'}$, are given by:

$$H_z = \frac{D}{g_z \mu_B} N, \tag{3}$$

where $N = -(m + m')$ is called the step number. For the Hamiltonian listed in Eq. 1. each N corresponds to a family of energy "crossings" that occur at exactly the same magnetic field. The $N = 5$ family is shown in part (b) of Fig. 1.

1.1.2 Population of Energy Levels

These double well potential diagrams provide a convenient means of understanding the basic physical processes occurring in single molecule magnets. For temperatures below a certain value, T_G, the vast majority of the molecules will occupy the bottom (ground state) of one of the potential wells. This is because the population of the levels obey Boltzmann statistics. If most of the molecules in a sample are in the bottom of the same well, then the magnetization is said to be saturated. When the sample is heated above a certain temperature, then there is sufficient energy for each molecule to thermally activate to the top of the barrier and drop down the other side. Thus, heating a sample above this "blocking temperature", T_B, will cause the magnetization to reach equilibrium. For temperatures between T_G and T_B, molecules will thermally activate to the excited states. For even higher temperatures, each molecule will hop back and forth between the potential wells.

1.2 Mn_{12}-acetate

A quintessential example of a single molecule magnet is Mn_{12}-acetate (the other is Fe_8). Its chemical formula is given by: $[Mn_{12}O_{12}(CH_3COO)_{16}(H_2O)_4]\cdot 2CH_3COOH\cdot 4H_2O$. This complicated molecule was first synthesized by Lis in 1980.[33] The magnetic properties come from twelve Mn ions that are located near the center of the molecule. As shown in Fig. 2 the magnetic core consists of eight Mn^{3+} ($S = 2$) ions situated on an outer noncoplanar ring that surrounds four inner Mn^{4+} ($S = 3/2$) ions symmetrically arranged on the corners of a cubane. The four inner Mn ions couple anti-ferromagnetically via superexchange through oxygen bridges to the eight outer Mn ions. As determined by ac-susceptibility measurements[6, 30, 34] and EPR measurements[6, 30, 35], the molecule has an $S = (8 \times 2) - (4 \times 3/2) = 10$ ground state. Large anisotropy originates from the single-ion anisotropy of the Mn^{3+} ions[6]. The net result is that the single molecule magnet, Mn_{12}-acetate, acts like a giant $S = 10$ spin particle with large uniaxial anisotropy.

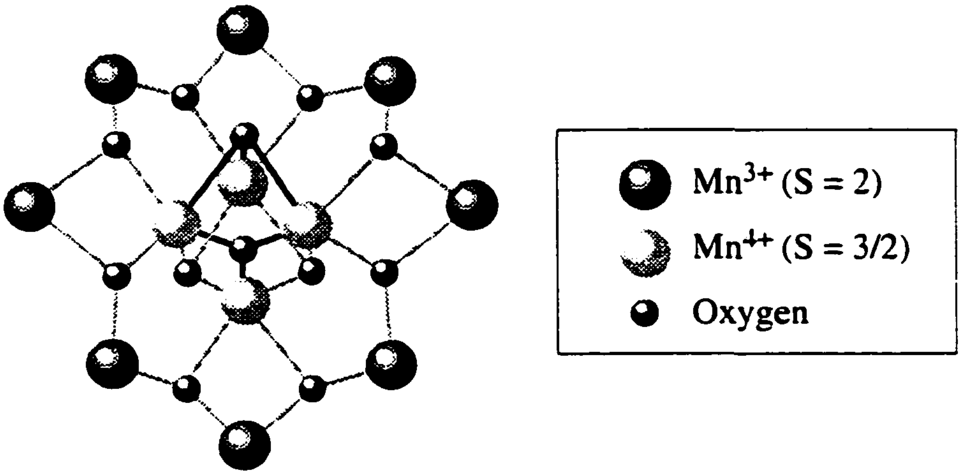

Figure 2: The magnetic core of the $S = 10$ single molecule magnet Mn_{12}-acetate. The four inner Mn ions couple anti-ferromagnetically via superexchange through oxygen bridges to the eight outer Mn ions.

The crystalline form of Mn_{12}-acetate has a tetragonal body centered lattice with lattice spacings of $a = b = 17.3\,\text{Å}$ and $c = 12.1\,\text{Å}$[33]. Since the inter-molecule distance is so large for the crystalline form of Mn_{12}-acetate, the exchange interaction is negligible[8, 9] and the dipole field due to a neighboring molecule is rather small ($\approx 0.01\,\mathrm{T} - 0.05\,\mathrm{T}$)[7, 9, 8]. This means that each molecule acts nearly independently and the entire crystal can be considered an ensemble of weakly interacting, nearly identical $S = 10$ spin particles. X-ray diffraction measurements have determined that Mn_{12}-acetate belongs to the $\mathrm{I}\bar{4}(S_4)$ space group[33].

Neutron scattering experiments[36, 37, 38] as well EPR measurements[39, 40] have determined Mn_{12}-acetate is modeled by the effective spin-Hamiltonian:

$$\hat{\mathcal{H}} = -D\hat{S}_z^2 - A\hat{S}_z^4 - g_z\mu_B H_z\hat{S}_z + \hat{V}_T, \tag{4}$$

where $D = 0.5477\,\mathrm{K}$ is the second order anisotropy constant, $A = 1.173 \times 10^{-3}\,\mathrm{K}$ is the fourth order anisotropy constant and $g_z \approx 1.94$ is the g-factor. The last term, $\hat{V}_T$, is the symmetry breaking term. $\hat{V}_T$ may include terms such as transverse field, $g_x\mu_B H_x$, fourth order transverse anisotropy, $C(\hat{S}_+^4 + \hat{S}_-^4)$, or other terms. Second order transverse anisotropy, $E(\hat{S}_x^2 - \hat{S}_y^2)$ is forbidden by the tetragonal symmetry for *perfect* Mn_{12}-acetate crystals. The nature of the symmetry breaking term, $\hat{V}_T$, is unknown and is the main subject of this research.

For small $\hat{V}_T$, the energy eigenvalues are given to good approximation by:

$$E_m = -Dm^2 - Am^4 - g_z\mu_B H_z m. \tag{5}$$

The fields at which the energy level resonances occur are given by:

$$H_z = N\frac{D}{g_z\mu_B}\left[1 + \frac{A}{D}\left(m^2 + m'^2\right)\right]. \tag{6}$$

where $N = -(m + m')$ is the step number defined earlier. Inclusion of the second order longitudinal anisotropy, $A\hat{S}_z^4$, has the effect of shifting the energy levels so that the energy eigenvalues no longer come into resonance simultaneously. Rather, each step N now represents a family of energy resonances that occur at slightly different magnetic fields. We will see later that the second order longitudinal anisotropy has important consequences for the temperature dependence measurements.

1.3 Tunnel Splittings

The eigenvalues can be calculated numerically by diagonalizing the Hamiltonian. For example, consider the following Hamiltonian,

$$\hat{\mathcal{H}} = -D\hat{S}_z^2 - A\hat{S}_z^4 - g\mu_B H_z\hat{S}_z + g_x\mu_B H_x\hat{S}_x, \tag{7}$$

where $\hat{V}_T = g_x \mu_B H_x \hat{S}_x$ is the symmetry breaking term with $H_x = 0.03T$ and $g_x = g_z$. H_x could arise from an externally applied field or from an internal dipole field. Fig. 3 shows the numerically determined eigenvalues of Eq. 7 as a function of field, from $H_z = 0$ to $H_z = 5.5\,\mathrm{T}$. Without the symmetry breaking term, the eigenvalues would cross at the fields given by Eq. 6 with energies given by Eq. 7 for each resonance.

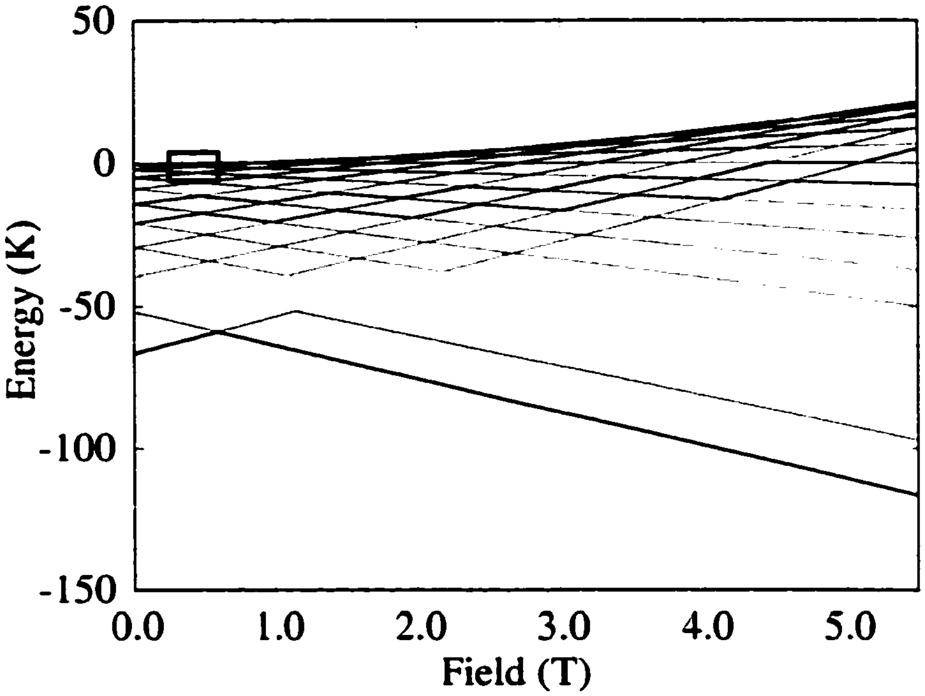

Figure 3: Energy eigenvalues for Eq. 7 (which includes the presence of the symmetry breaking term, $g_x \mu_B H_x \hat{S}_x$) determined by numerically diagonalizing the Hamiltonian. Because of the presence of the symmetry-breaking term, the eigenvalues do not cross. A close-up view of one of the crossings appearing in the rectangle is shown in Fig. 4.

However with the symmetry breaking term, we realize from quantum mechanics that the eigenvalues do not actually cross. They form "anti-crossings". This behavior can be understood by examining the Hamiltonian in Eq. 7 in terms of the eigenstates of $\hat{S}_z$. These eigenstates are also the eigenstates of the "unperturbed" Hamiltonian of Eq. 7 (i.e. without the symmetry-breaking term, $g_x \mu_B H_x \hat{S}_x$). For fields that do not place the system near a resonance, the eigenstates of the full Hamiltonian in Eq. 7 are accurately given by the eigenstates of the unperturbed Hamiltonian (i.e.

m is a "good" quantum number). However, for fields that place the system close to a resonance, substantial mixing occurs between the two states that are near the resonance. For fields that place the system just beyond the resonance, m is again a good quantum number and the eigenstates of the full Hamiltonian are accurately approximated by the eigenstates of the unperturbed Hamiltonian.

As the field is swept, the eigenstates "exchange character" after passing through the resonance. For example, consider the $E_{m'=-2} = E_{m=+1}$ energy resonance which is one of the resonances located in the black rectangle in Fig. 3. For fields below the resonance, the lower curve in Fig. 4 corresponds to the eigenstate, $|-2\rangle$ and the upper curve corresponds to the eigenstate, $|+1\rangle$. However, above the resonance, the lower curve corresponds to the eigenstate, $|+1\rangle$ and the upper curve corresponds to $|-2\rangle$. In other words, the eigenstates have exchanged character.

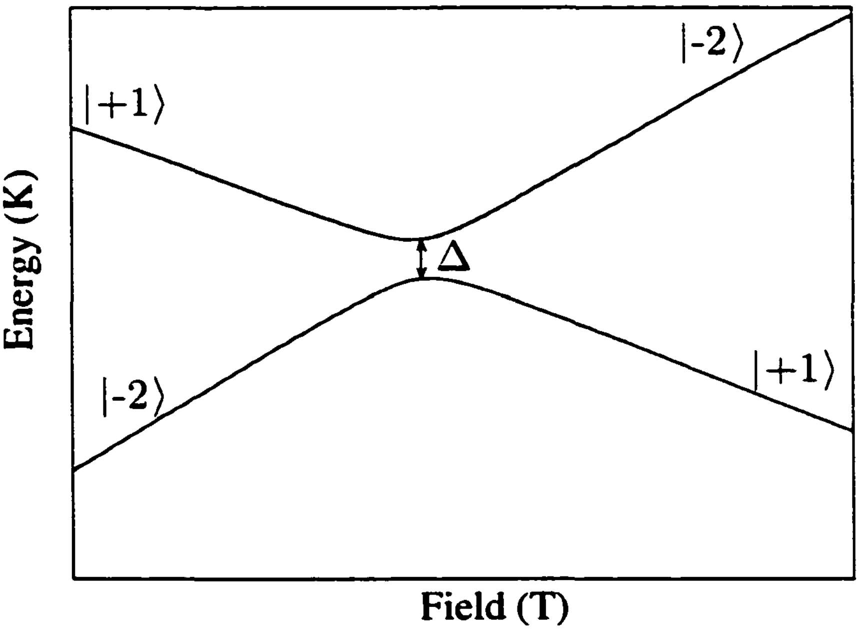

Figure 4: Energy eigenvalues near the energy resonance, $E_{m'=-2} = E_{m=+1}$ for the Hamiltonian shown in Eq. 7 which includes the presence of the symmetry breaking term. $g_x \mu_B H_x \hat{S}_x$. The eigenvectors exchange characters at the anti-crossing. The size of the gap is called the tunnel splitting and can be calculated through high order degenerate perturbation theory.

The minimum gap formed between the eigenvalues near a transition is called the tunnel splitting. Garanin showed that the tunnel splitting can be calculated through high order degenerate perturbation theory[41]. If the perturbing term, $\hat{V}_T$, is small then the fields and energies at which the anti-crossing occur are given to good approximation by Eq. 6 and Eq. 5 respectively. Also, from Ref. [41] it is clear that the tunnel splitting increases as one proceeds up the ladder to levels higher in the potential wells.

1.4 Tunneling of Magnetization

The above discussion describes what happens to the eigenvectors of the system as a function of field. For a swept field, the wavefunction obeys the Schrödinger Equation with a time-dependent Hamiltonian. In this case, there is a probability for a molecule originally in the metastable well to tunnel to the stable well due to the presence of the symmetry breaking terms, $\hat{V}_T$, in the Hamiltonian. For a swept field, time-dependent perturbation theory can be applied in two extreme cases: the adiabatic approximation and the sudden approximation[42]. In both cases, the eigenvectors, ψ_i, of the system to depend explicitly on time. However, the wavefunction, Ψ, behaves differently in these two cases.

For the case of a sudden perturbation, the eigenvectors change instantaneously. In this case, the wavefunction cannot adjust itself in a timely fashion and should be reexpressed as a linear combination of the new eigenstates. However, as was described earlier, the eigenstates exchange character as the system is swept through the resonance. In particular, if the system was originally in the $|-2\rangle$ just before the $m' = -2$, $m = +1$ energy resonance state as shown in Fig. 4, then it will still be in that state after the energy resonance. This means the molecule remains in the metastable well and there is no tunneling

On the other hand in the adiabatic limit, the eigenvectors change so slowly with time that the wavefunction "keeps up" with the eigenvectors. If Ψ was originally in an eigenstate, then it will adjust itself to remain in the time-evolving eigenstate. Again considering the same $E_{m'=-2} = E_{m=+1}$ energy resonance shown in Fig. 4, if the wavefunction was originally in the $|-2\rangle$ eigenstate, then it will evolve into the $|+1\rangle$ state as the system passes through the resonance. In other words, the spin tunnels from the metastable well to the stable well.

The Landau-Zener-Stueckelberg solution describes the middle ground between these two extremes. It is the exact solution to the Schrödinger equation for a two-level system with diagonal terms that change linearly with time and off-diagonal symmetry-breaking terms that are constant. The Landau-Zener-Stueckelberg formula[43, 44, 45] is the asymptotic solution for the probability of a two state system to tunnel as the magnetic field brings the energy eigenvalues in and out of resonance. It is given by:

$$P_{LZS} = 1 - \exp(-\pi\Delta^2/v\hbar). \tag{8}$$

where Δ is the tunnel splitting and v is the energy sweep rate. Δ is the size of the gap formed by the anti-crossing (see Fig. 4). v is the rate at which the energy levels approach each other (in the absence of any symmetry breaking terms) and is proportional to the magnetic field sweep rate, dH_z/dt. From Eq. 8, it is clear that the *slower* the field is swept, the *greater* the probability of tunneling to occur. Also, the probability of tunneling *increases* with *increasing* tunnel splitting.

1.5 Environmental Effects

The above analysis only considered the ideal case of an ensemble of identical molecules without any interaction with the environment. It leaves out nuclear spin coupling, spin-phonon coupling as well as dipolar and exchange coupling with neighboring molecules. This is not an unreasonable approach since these interactions are sufficiently small and the solution to the complete Schrodinger equation is (with present day mathematics) hopelessly complex due to the very large dimensionality of the

Hilbert space. For the "limited" case of spin-spin coupling of the electrons of the Mn ions, the dimension of the Hilbert space is $(2(3/2+1))^4 \times (2(2+1))^8 = 10^8$.

The model also assumes that the molecules are strictly identical. In real crystals of Mn_{12}-acetate there are imperfections. Imperfections can occur at the molecular level by isomeric molecules or from missing or misplaced atoms. Imperfections may also occur at the crystal level due to chemical impurities and dislocations. All of these effects may have measurable consequences.

1.6 Temperature Effects

Even though temperature is not formally included in the analysis, the double well potential diagram can be used to understand what will happen at different temperatures. This leads to the classification of three magnetic relaxation processes. Consider the case of a sample placed in an external field with some of the molecules in the metastable well. As stated earlier, when the sample is heated above the blocking temperature, T_B, then there is sufficient energy for the molecules to thermally activate to the top of the barrier and drop down the other side. This is called over the barrier hopping. This process is shown by the curved solid arrow in Fig. 5. If the sample is at a lower temperature then most of the molecules cannot reach the top of the barrier. However, if the molecules are excited to a state within the metastable well that is degenerate with another state in the stable well, then molecules can escape from the metastable well by tunneling from the excited state. This is called thermally assisted tunneling and is depicted by the two dashed arrows in Fig. 5. Finally, if the temperature is sufficiently low, then the molecules spend most of the time in the lowest lying level in the metastable well. If this state is degenerate with another state of the stable well then the molecules can tunnel. This is termed ground state tunneling and is depicted by a single dotted arrow in Fig. 5. The three magnetic relaxation processes just described can also occur for an out-of-equilibrium sample in zero magnetic field. Paulsen and Novak were the first to suggest the possibility of experimentally determining the presence of thermally assisted tunneling[46, 7, 47] in Mn_{12}-acetate.

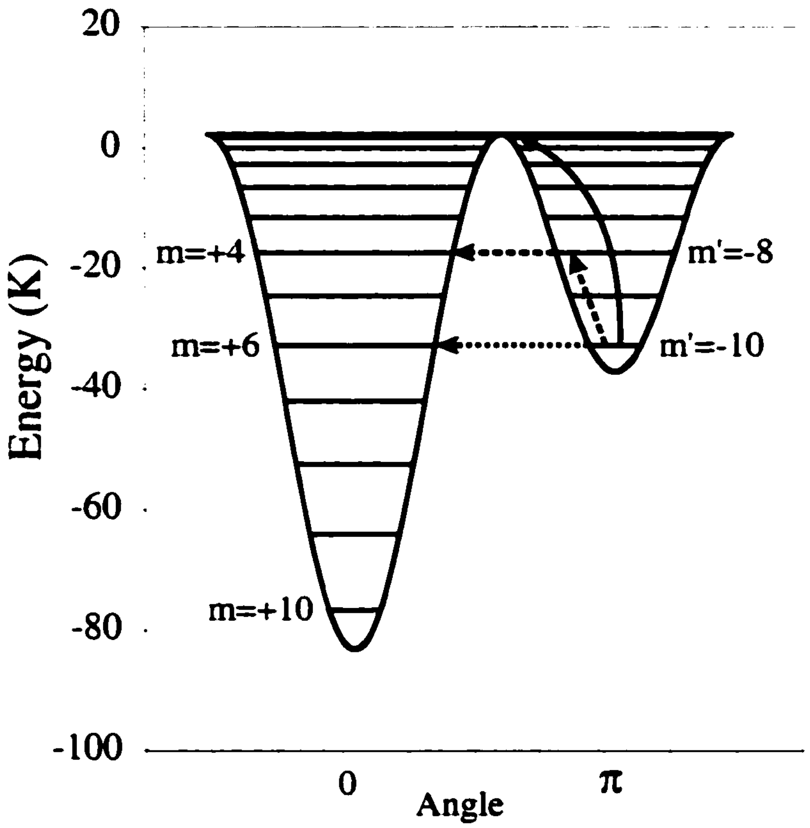

Figure 5: Double well potential illustrating the different classifications of tunneling processes. Ground state tunneling is depicted by the single dotted horizontal arrow. Thermally assisted tunneling is depicted by the two dashed arrows. Over the barrier hopping is depicted by the long solid curved arrow.

1.7 Incoherent Quantum Tunneling

Many attempts have been made to generalize the Landau-Zener-Stueckelberg solution to include environmental factors. Garanin and Chudnovsky solved the time dependent density matrix equation[18] for the case of a large spin coupled to a thermal bath. Interestingly, the probability of tunneling for this incoherent system turns out be of exactly the same form as the coherent system, but with an additional factor of 2. Miyashita, who first applied the Landau-Zener-Stueckelberg formula to the case of spin tunneling[48], working with Nishino *et al.* , added stochastic noise to the Schrodinger equation and solved the system numerically[49]. They also found that the probability of tunneling obeys the Landau-Zener formula. However, there is a noise dependent correction to the tunnel splitting. Leuenberger and Loss have also generalized the problem to include thermal relaxation by solving the master equation[50] for the system. They found that the probability has the same form as P_{LZS}, but with an additional factor of 2. The fact that all these calculations have reproduced very similar formulae, suggests that the form of the equation is correct. However, inclusion of environmental decohering effects requires replacement of the coherently determined tunnel splitting with an effective tunnel splitting. All calculations later in this thesis will use the incoherent formula of Eq. 9.

$$P_{inc} = 1 - \exp(-\pi\Delta^2/2v\hbar), \tag{9}$$

where P_{inc} is the probability of tunneling for an incoherent system.

1.8 Motivation

The aim of this research was two-fold: 1) to study the nature of the crossover from thermally assisted to ground state tunneling as the temperature is reduced, and 2) to identify and investigate the symmetry-breaking term that drives the tunneling.

The next section will describe in detail the experimental techniques employed during the research. Section 3 will describe three experiments. The first was designed to investigate the crossover from thermally assisted to ground state tunneling. The second will identify and investigate the dominant symmetry-breaking that drives the tunneling process. The third experiment is aimed at obtaining additional evidence of the finding of the second experiment, namely that the tunneling in Mn_{12}-acetate is due to locally varying transverse anisotropy which gives rise to a distribution of tunnel splittings.

2 Experimental Techniques

Before describing the experimental results and their interpretations, I will present a detailed account of the techniques used to measure the magnetization of the samples. In addition, I will describe how the samples were handled and produced.

2.1 Sample Preparation and Mounting

Samples of Mn_{12}-acetate were grown by Evan Rumberger, a student of David Hendrickson of the Department of Chemistry and Biochemistry at the University of California at San Diego in collaboration with George Christou at the University of Florida at Gainesville. The samples were grown in solution using the techniques specified inRef. [33]. To prevent degradation, the samples were stored in a commercial refrigerator at −20 C except for the brief times during which crystals were selected for experiments.

Figure 6: A typical Mn_{12}-acetate crystal mounted on a Hall sensor. In the left image, the camera was focused on the Mn_{12}-acetate crystal. In the right image, the camera was focused on the surface of the Hall sensor. The oval shape surrounding the sample in the right image is the eicosen wax used to hold the sample on the Hall sensor.

Selection of a particular crystal was made by examining several hundred crystals under a microscope and selecting individual crystals that had parallel surfaces (without bumps or extraneous growths), sharp edges and well defined corners. Since the crystals are rather fragile special techniques were developed to handle them. A small quantity of Dow Corning® high vacuum grease was applied to the end of a fine wooden fiber. Gently placing the greased wooden fiber in contact with the crystal sample was sufficient to pick up the sample. The sample was pried off the greased wooden fiber with the use of a second ungreased wooden fiber.

To hold the sample on the detector, a small quantity of eicosen wax which is solid at room temperature was placed on top of the sample. The eicosen was heated by an incandescent lightbulb. Heat was applied for approximately 2 minutes until the wax began to melt. The wax surrounds the sample and holds it in place. From trial and error it was found that the lamp could be placed no closer than 5 cm for at most 30 minutes before damage to the sample occurred. Significantly less heat was applied to the samples studied here. The magnetic signal from both the eicosen and vacuum grease were determined to be negligibly small.

2.2 Hall Sensor

The magnetization of the Mn_{12}-acetate crystals were measured using an array of microscopic Hall sensors[51, 52, 53] that were provided by Yossi Paltiel, a student of Eli Zeldov working with Hadas Shtrikman at The Weizmann Institute of Science. The active layer in these sensors is a 2DEG formed at the interface of GaAs/AlGaAs heterostructures. The sensors are defined photolithographically, as shown in Fig. 7. The size of each sensor is $10 \times 10\ \mu m^2$. The current is driven through all the sensors and the corresponding Hall voltage of each sensor is directly proportional to the perpendicular component of the local magnetic field within the active area of the sensor. Since the 2DEG resides only about 1000 Å below the surface, this technique allows a very sensitive mapping of the local magnetic field across the sample.

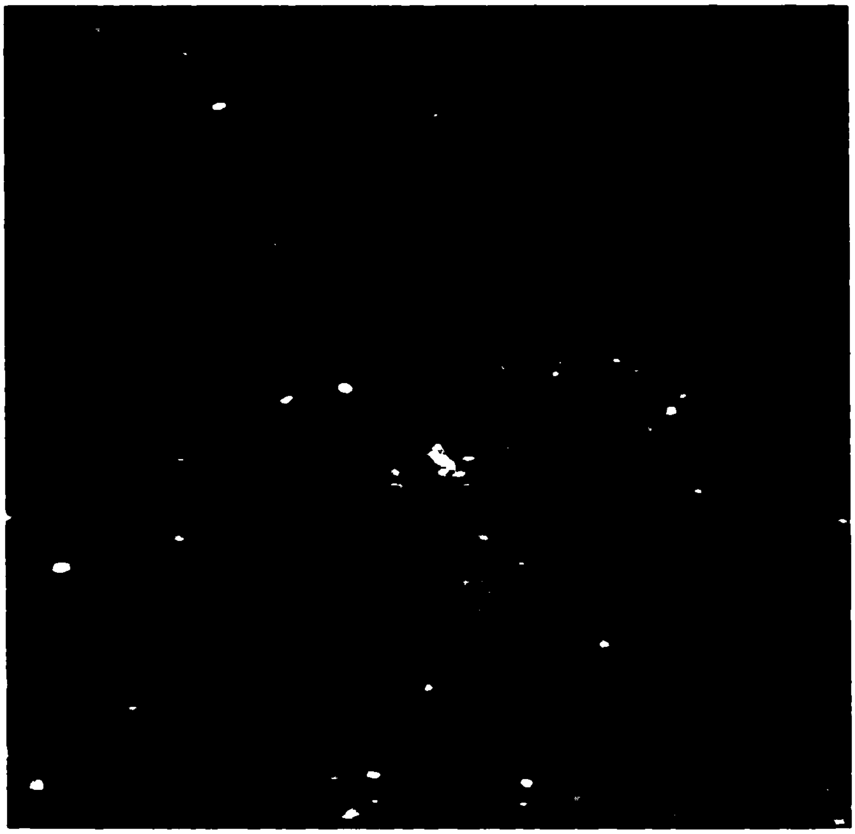

Figure 7: An image of the Hall sensor array used to measure magnetic induction. There are 11 $10 \times 10\ \mu m^2$ sensors arranged in an array.

2.3 Electronics

The electronic circuit used to measure the Hall voltage is particularly simple. The basic idea is to apply a current through the source and drain of the Hall sensor and then measure the Hall voltage. The measured Hall voltage will be proportional to the perpendicular component of the magnetic field passing through the Hall sensor area. There are many possible ways to implement such a circuit. The circuit used for the experiments studied in this thesis is shown in Fig. 8. The excitation voltage from a Stanford Research Systems model SR-850 Lock-In amplifier was converted into a current by placing two resistors in series with the Hall sensor as shown in Fig. 8. The frequency of the ac excitation voltage from the SR-850 was set to 17 Hz. The Hall voltage was measured by the SR-850 with a time constant of 300 ms. To compensate for the small changes in current due to the changes in the impedance of the Hall sensor, R_{SD}, a Princeton Applied Research®model PAR™-116 Lock-In amplifier was used to measure the current directly. This was accomplished by measuring the voltage drop across a 1 kΩ resistor. It was not possible to measure the voltage drop across the 1 MΩ resistor because the input impedance of the PAR-116 is only 10 MΩ. The 1 MΩ resistor sets the current to approximately 1 μA. In summary:

$$\begin{aligned} I_{SD} &= V_{PAR}/R_2 \\ R_{Hall} &= V_{Hall}/I_{SD}, \end{aligned} \tag{10}$$

where V_{PAR} is voltage drop across R_2, I_{SD} is the current passing through both resistors and through the Hall sensor, V_{Hall} is the voltage measured across one Hall contact, and R_{Hall} is the measured Hall resistance. R_{Hall} is proportional to the perpendicular component of the local magnetic field.

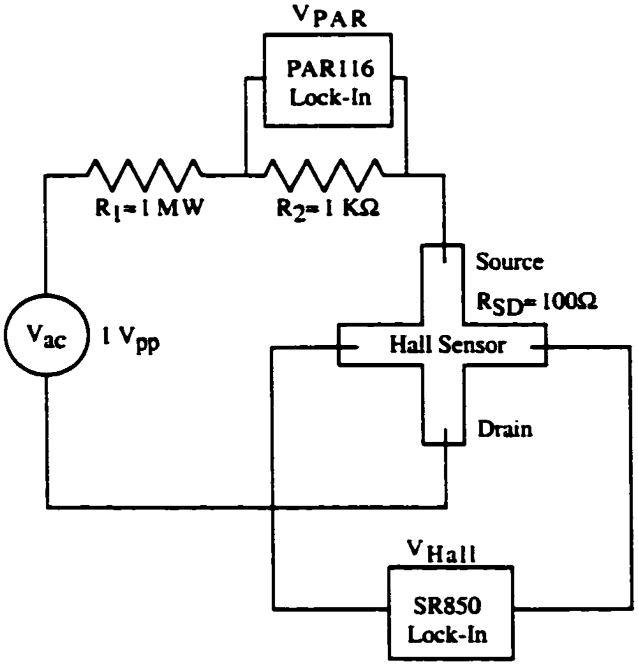

Figure 8: Schematic diagram of measuring apparatus. An ac voltage source is applied across two resistors in series with the Hall sensor. Typical resistances of the Hall sensor for temperatures around 2 K is about 100 Ω. For clarity only one of the eleven Hall sensors is shown. The PAR-116 Lock-In amplifier is used to measure the current through the Hall sensor. The SR-850 Lock-In amplifier measures the Hall voltage.

2.4 Data Acquisition Software

The data acquisition software was written in G using National Instruments' LabVIEW software package. Because of the graphical nature of the programming language, it is not practical to list the the source code here. Instead the pseudo-code that models the main algorithm is listed below.

```
Begin {
      Initialize Variables
      Initialize Instruments
      Create Data File
      Write Column Headers
      Start Ramping the Field
      While Still Running and $He^4$ level high enough {
            Read Clock
            Trigger Instruments
            Read PAR
            Read SR850
            Read Temperature
            Read Magnetic Field
            Read $He^4$ Level
            Compute $R_{Hall}$
            Write Data to File
            Update Display
      }
      Reset Instruments
}
```

All instruments were accessed through the GPIB interface. And a group trigger event was sent to all the instruments simultaneously. This requests that all the instruments make a measurement at the same time. This is important because in some measurements the field was swept rapidly.

2.5 Oxford He^3 Heliox System

An Oxford Research Instruments He^3 cryostat was used to bring the sample and detector down to milliKelvin temperatures. Mounted within the liquid He^4 is a 12 T superconducting solenoid manufactured by Cryogenic Consultants Limited. A stainless steel He^3 insert is mounted within the bore of the superconducting solenoid. A rotatable probe containing a Ruthenium Oxide thermometer and the homemade detector assembly unit are inserted within the He^3 insert. Unfortunately, the rotator does not provide smooth action nor does it provide reliable angular increments. Nevertheless, it can rotate the sample so that the detector's surface is parallel to the field. For temperatures below 1.9 K, the sample is immersed in liquid He^3.

An important aspect of the research presented here is good temperature control in a high magnetic field. Some of the experiments presented later depend sensitively on temperature. Unfortunately, most thermometers have a magnetic field dependent response. A simple way to determine how large an effect the field has on the sample thermometer is to cool the system down to base temperature. The system will stay at base temperature for several hours before the temperature starts to slowly creep up. Since the temperature is known to be constant at base temperature, the field dependence of the thermometer can be determined. The field response of the sample thermometer is shown in Fig. 9.

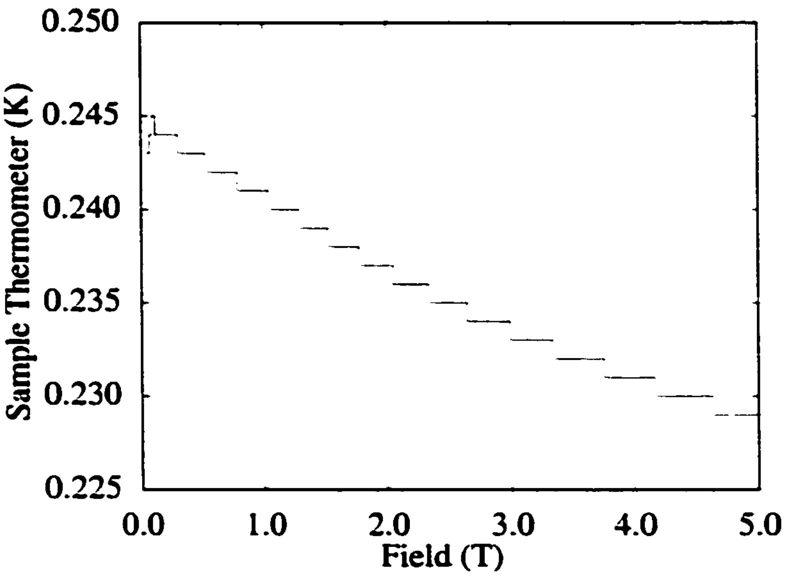

Figure 9: Response of the sample thermometer to a magnetic field. Since the system is at base temperature, the response of the thermometer should be independent of magnetic field. The temperature read from the thermometer decreases as field increases.

As can be clearly seen from Fig. 9, the temperature read from the thermometer decreases as field increases. This has serious consequences if one attempts to control the temperature of the system during a field swept measurement using this thermometer. As the field increases, the temperature read from the thermometer decreases. Consequently, the temperature monitoring system will add more heat to compensate for the perceived decrease in temperature. As a result, the temperature control system will actually steadily increase the temperature of the system.

Evidence of this is clearly seen by examining the response of the system as the field is swept up to 5 T. The upper curve in part (a) of Fig. 10 shows that the measured temperature of the sample thermometer is fairly constant. However, the upper curve in part (b) shows that the amount of heat added by the temperature monitoring system steadily increases with increasing field. The net result is that the temperature of the sample is not held truly constant during a swept field measurement.

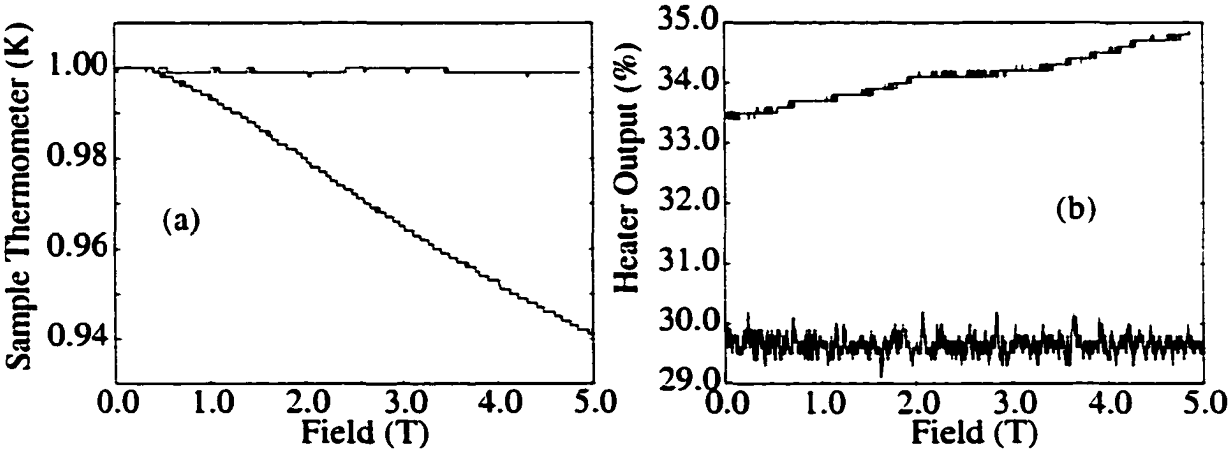

Figure 10: Response of the sample thermometer to a magnetic field while the system is held. Since the system is at base temperature, the response of the thermometer should be independent of magnetic field. The temperature read from the thermometer decreases as field increases.

To resolve this issue a different temperature control system was implemented instead of the manufacturer's recommended method of temperature control. Fortunately, there is a second thermometer in the system far from the center of the solenoid.

This thermometer is not affected by the magnetic field since it is outside the solenoid. Using this thermometer for the feedback loop in the temperature control system means that additional heat will not be added to the system as the field is swept. The lower curves in Fig. 10 are the responses using the new method of temperature control. The lower curve in part (a) of Fig. 10 shows that the measured temperature decreases as it should since the magnetic field increases. The lower curve in part (b) shows that the heater output fluctuates around a constant value, so no additional heat is added to the system. We can safely conclude that the actual temperature of the system does not change since the amount of heat added is constant.

As an additional check of the new method of temperature control, the field was swept slowly up to high field and then swept quickly back to zero. The temperature of the sample thermometer had the same value before sweeping the field as it did after sweeping up and back down. This indicates that the new temperature control method is not hysteretic and provides good temperature control in a magnetic field.

2.6 Hall Sensor Response Curves

The linearity of the detector can be checked by measuring the response of the detector at various angles as show in part (a) of Fig. 11. The detector was first aligned by eye to a parallel position and the rotator "zeroed" to this position. The rotator was then moved counter-clockwise past the 3° mark and then clockwise to the 3° mark to take up any backlash. The response of the detector was measured for 3°, 2°, 1°, 0° and −1° as shown in Fig. 11. The angle was adjusted until the detector had a flat response. This is indicated by thick black curve labeled "True 0".

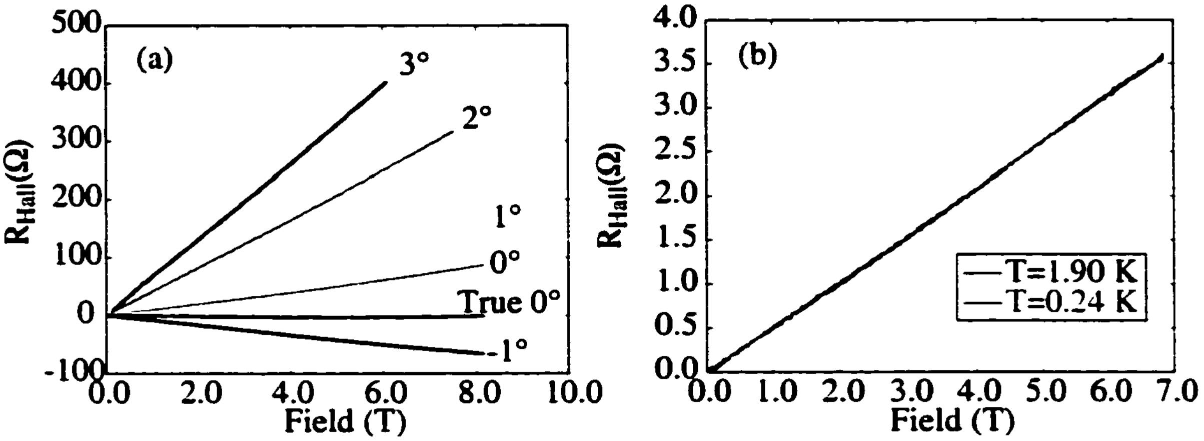

Figure 11: Hall sensor response curves for various small angles are shown in part (a). Part (b) shows the response at 0.24 K and 1.90 K. The response is linear and independent of temperature.

An important fact that can be determined from part (a) of Fig. 11 is that the detector has a linear response to an applied field. It should also be noted that these curves simulate what happens when a sample is mounted on the detector. When the detector (without a sample) is rotated to a small angle. θ. relative to the direction of the field. it will experience a small magnetic field perpendicular to the surface. $B_\perp = Bsin(\theta)$. In addition, the detector will also experience a strong field parallel to the surface. $B_\parallel = Bcos(\theta)$. This is similar to the situation when the sample is mounted on the detector and the detector is mounted parallel to the field. In this case, $B_\perp$ will be due primarily to the magnetization of the sample. $B_\parallel$ will be due primarily to the applied magnetic field. How the magnetization is measured is discussed in more detail below.

Since the sample will be measured at various temperatures it is important to verify that the Hall sensor is temperature independent. Part (b) of Fig. 11 shows the response of the detector to the field when orientated at a small angle relative to the magnetic field at two different temperatures, 0.24 K and 1.90 K. There is no discernible difference between the response curves of the Hall sensor. These temperatures represent the two extremes at which the Mn_{12}-acetate samples were measured. Thus, the detector has a linear response over the entire range of temperatures considered.

2.7 Magnetization Measurements

To measure the magnetization of the sample, the sample is mounted with the easy c-axis of the crystal aligned parallel to the surface of the detector and the applied magnetic field, as shown schematically in Fig. 12. As the sample becomes magnetized, the field lines of the sample penetrate the active area of the Hall sensor. If the Hall sensor is mounted exactly parallel, there will be no signal from the external field. Any signal will then be entirely due to the sample. However, there is always some misalignment. With a misaligned detector, the measured response will contain a linear component in addition to the response from the sample. This linear component can be easily subtracted off from the data as will be shown presently.

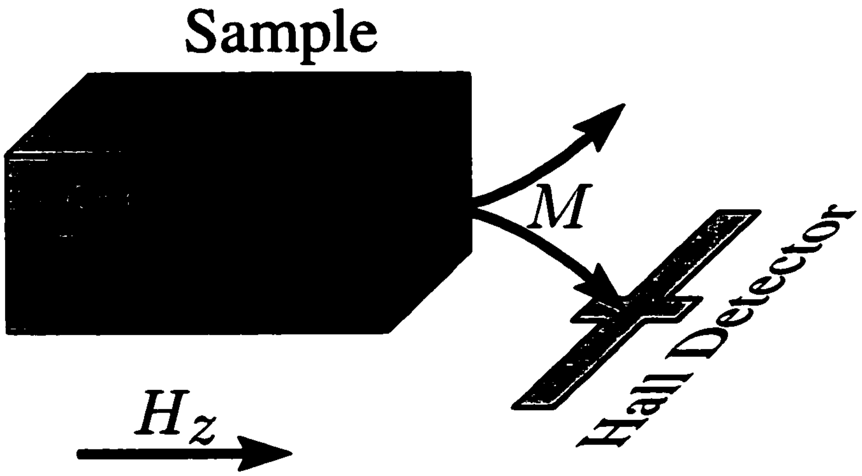

Figure 12: The experimental setup used to measure the magnetization of the sample. The easy c-axis of sample was aligned along the direction of the external field. The Hall detector's surface was perpendicular to the applied field.

The raw data for a zero field cooled magnetization measurement is shown in Fig. 13. In this measurement, it is clear that there is a large misalignment of the Hall detector. When the Hall detector is misaligned, in addition to the magnetic field generated from the sample penetrating the 2DEG of the Hall sensor, the magnetic field of the solenoid itself penetrates the Hall sensor. Since the Hall sensor is a linear device, the Hall resistance is proportional to the sum of the flux lines from the applied field and the flux lines from the sample. If the Hall detector is at angle θ relative to the applied field, then $R_{Hall} = \alpha(\mu_0 H \sin(\theta) + M)$, where α is the sensitivity of the Hall sensor and $\mu_0 H$ is the applied external magnetic field and M represents the perpendicular field produced by the sample at the detector.

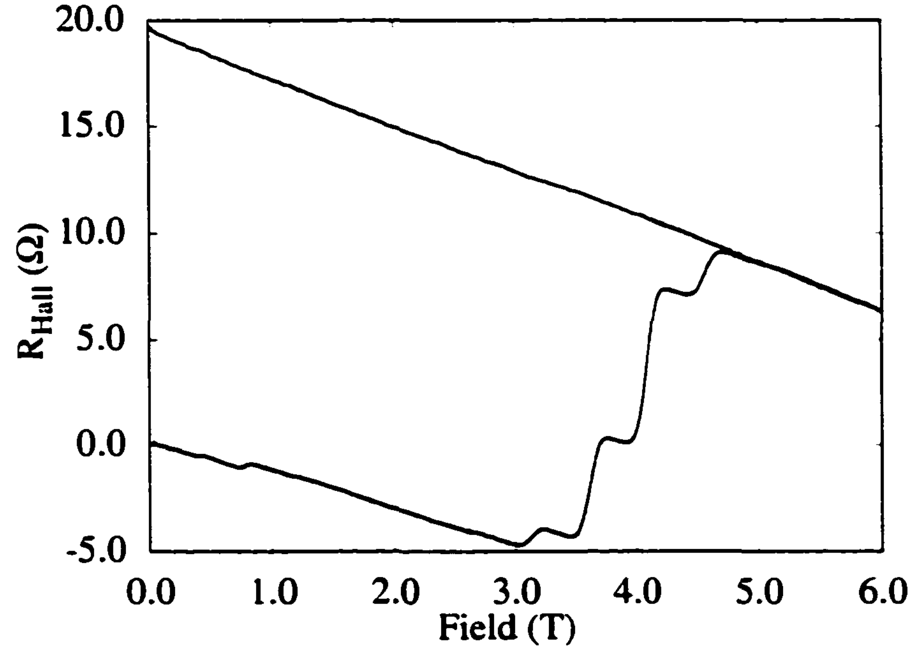

Figure 13: The measured Hall resistance, $R_{Hall} = V_{Hall}/I_{SD}$ for a measurement that has the Hall detector poorly aligned with the magnetic field. The sample was cooled in zero magnetic field, so the initial Hall resistance was near zero. At approximately 6 T the sample is fully magnetized and the field was swept back toward zero. Slope of R_{Hall} while the field is swept back toward zero determines the misalignment of the Hall detector.

Once the magnetization of the sample reaches saturation, M_{sat}, the magnetization no longer changes and any changes in R_{Hall} must come from the applied external field, $\mu_0 H$. Thus removal of the applied external field from R_{Hall} is easily accomplished by examining the R_{Hall} after the sample has reached saturation and the field is swept back toward zero. This part of R_{Hall} is a straight line with slope $\alpha \sin(\theta)$ and intercept αM_{sat}. The slope is used to remove the linear component of the external applied field by subtracting from each measured value of R_{Hall} the amount $\alpha\sin(\theta)\mu_0 H$, so that $\alpha M = R_{Hall} - \alpha\sin(\theta)\mu_0 H$. The results of this procedure are shown in Fig. 14.

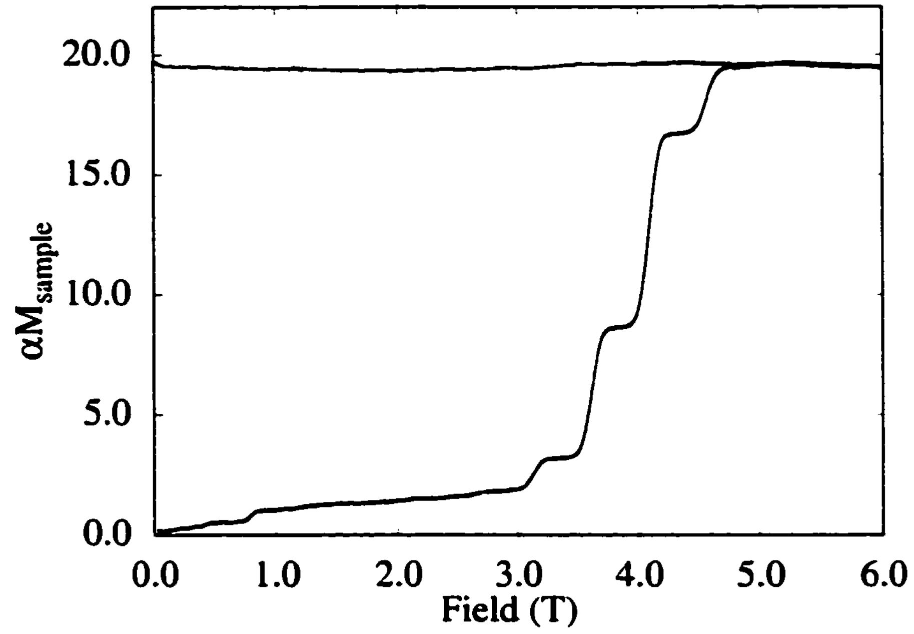

Figure 14: Once the misalignment of the Hall detector is determined, the linear component due to the external field can be "subtracted off" by using the formula $\alpha M = R_{Hall} - \alpha\sin(\theta)\mu_0 H$, where $\alpha\sin(\theta)$ is the slope of R_{Hall} after the sample has been fully magnetized and is no longer dependent on field.

Most of the data analysis performed later concentrates on determining the probability of tunneling from the magnetization measurements. To facilitate these calculations, the magnetization measurements need to be normalized. Thus, the last step to perform is to divide each αM by its value at saturation, αM_{sat}. The normalized magnetization is shown in Fig. 15.

Please note that all the measurements that will be presented later in this thesis were taken with a near zero misalignment of the Hall detector. The misalignment is estimated to be less than 0.5°. The misaligned measurement presented here was chosen for illustration purposes only.

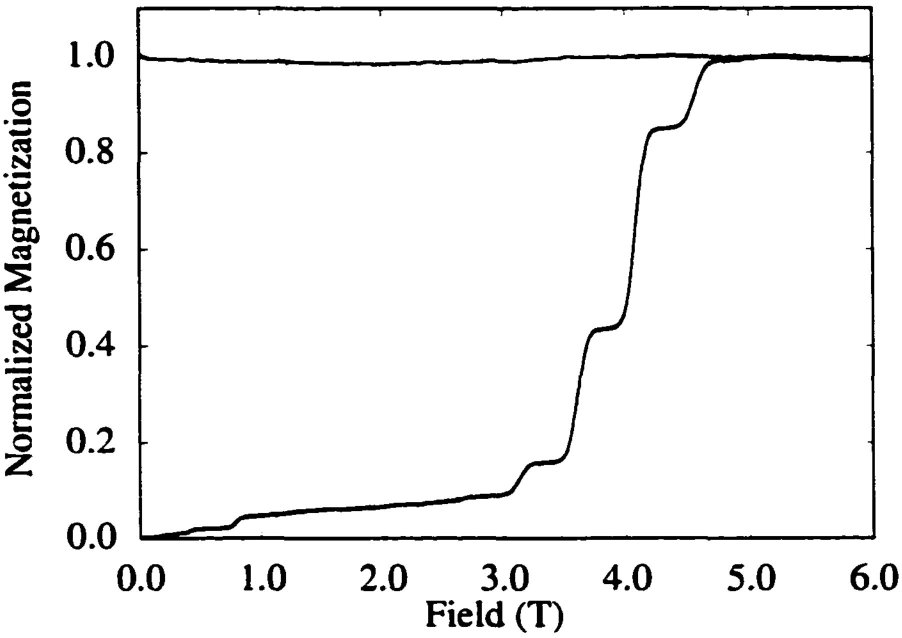

Figure 15: Since the coupling of the sample to the detector is not precisely known, it is not possible to accurately determine the field produced by the sample. Instead the data is normalized by dividing each point by its average value after the sample reaches saturation.

2.8 Summary of Experimental Techniques

To summarize, the experimental techniques outlined in this section provide accurate and reliable temperature control of the sample under investigation. The detector that will be used to measure the magnetization of the sample is closely linear and has no temperature dependence for the temperature range under consideration. Even though the magnetic moment of the sample cannot be determined directly, the Hall sensor does provide a means of obtaining the normalized magnetization curves of the sample.

3 Experimental Studies

Three experiments were performed on Mn_{12}-acetate. The first experiment studied the temperature dependence of quantum tunneling of magnetization. The second experiment studied the dependence of tunneling on the rate at which the field is swept. The third experiment investigated the tunneling process as the field is swept back and forth through a resonance. The results of each of these studies will be presented in the following subsections.

3.1 Temperature Dependence

3.1.1 Experimental Method

The magnetization of Mn_{12}-acetate was measured at various temperatures. Before each measurement the state of the sample was prepared in the following way. First the sample was heated in zero magnetic field to 10 K, well above the blocking temperature.

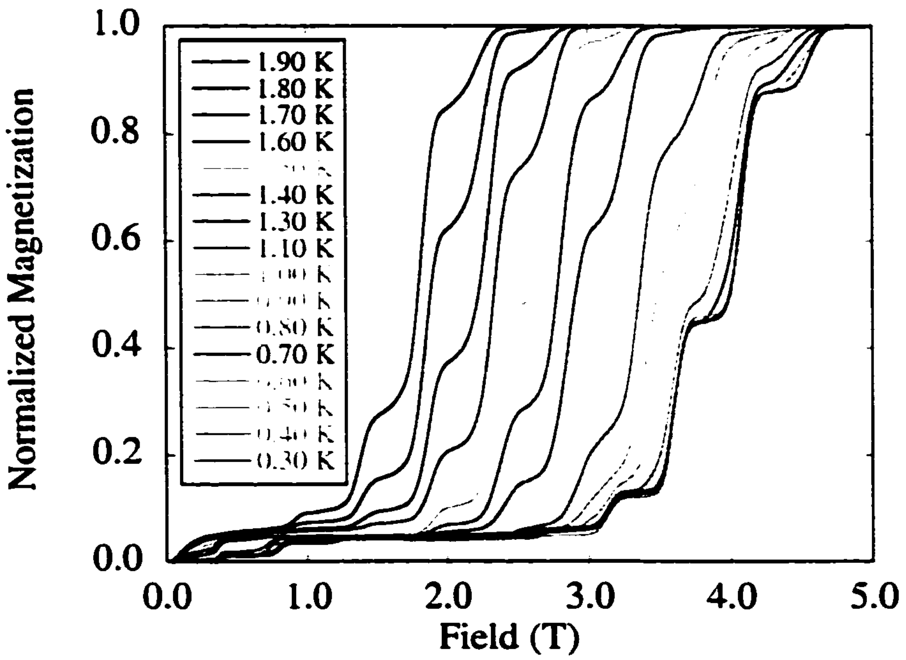

Figure 16: Normalized magnetization curves of a Mn_{12}-acetate sample taken at various temperatures. The steps in the magnetization curves are indications of quantum tunneling of magnetization. The magnetization curves are independent of temperature below ≈ 0.50 K.

$T_B \approx 3\,\mathrm{K}$. The magnetization of the sample was monitored to make certain that the sample was completely demagnetized, so that the spin populations were distributed equally between the two potential wells. The sample was then cooled to 0.24 K (the lowest temperature obtainable in the He^3 cryostat). Then the sample was heated to the desired temperature until stable temperature control was achieved. While maintaining temperature control, the externally applied magnetic field was swept from 0 T to 5.5 T at a constant sweep rate of 1.85 mT/s.

Fig. 16 shows the magnetization measurements between 1.90 K and 0.30 K in 0.10 K increments. For clarity only a partial data set is presented here. The steps in the magnetization curves are indications that the magnetization is relaxing faster at certain fields than at others. Friedman *et al.* were the first to observe and interpret these steps[1, 2] as evidence of quantum tunneling of magnetization. This was later confirmed by others[54, 55, 56, 3, 57, 58]. From Fig. 16, it is clear that at higher temperatures the magnetization relaxes at lower fields.

3.1.2 Ground State Tunneling

An important observation to make is that the magnetization curves become independent of temperature below $T_G = 0.50\,\mathrm{K}$[59, 60, 61]. This can be seen in Fig. 17 which is plot of the magnetization curves for temperatures between 0.54 K and 0.24 K. All the curves overlap, indicating that the tunneling process has become independent of temperature.

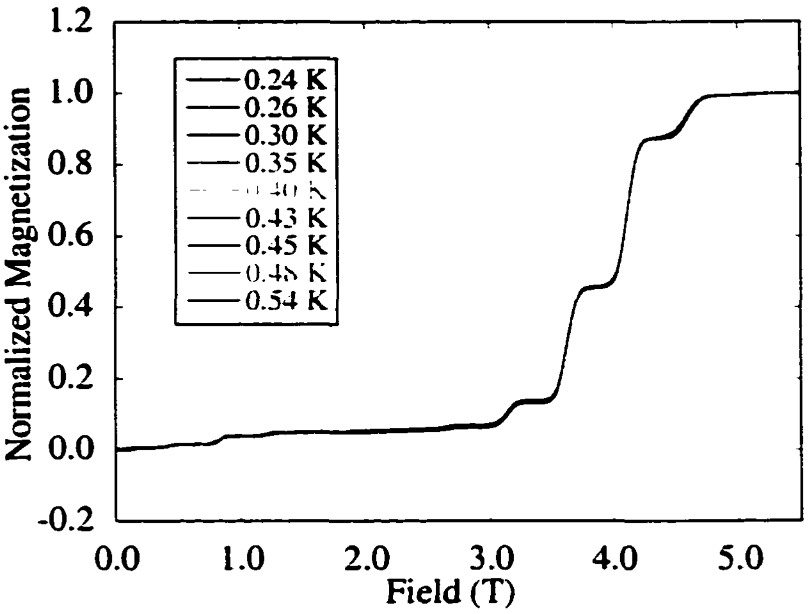

Figure 17: Magnetization curves of Mn_{12}-acetate for temperatures between 0.50 K and 0.24 K. The curves overlap indicating that the tunneling process has become independent of temperature.

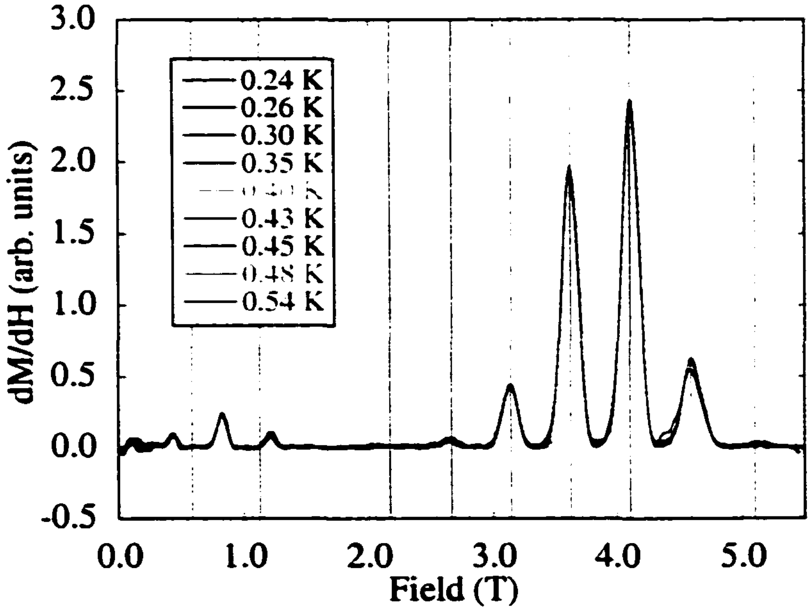

Figure 18: The derivative of the normalized magnetization curves with respect to applied field. The position of the peaks indicate the transition fields. The fact that these peaks are temperature independent and that the transition fields correspond to tunneling from lowest lying state $m' = -10$ of the metastable well are strong indications that this is ground state tunneling. The vertical lines are the transition fields corresponding to ground state tunneling (solid line) and to tunneling from the first excited state (dashed line).

Fig. 18 is a plot of dM/dH as a function of field. Plotting dM/dH is a convenient means of determining the fields at which tunneling occurs. Also plotted in Fig. 18 are the fields at which energy resonances occur for ground state tunneling ($m' = -10$) shown by the vertical solid lines as well as the energy resonances corresponding to tunneling from the first excited state ($m' = -9$) shown by the vertical dashed lines. The fact that the magnetization curves are independent of temperature as well as the fact that the peaks occur at fields corresponding to energy resonances of the ground state are strong evidence that this is ground state tunneling.

Also visible in Fig. 18 are several peaks that appear at fields below $\approx 1.2\,\mathrm{T}$. These peaks are due to a second species or complex of Mn_{12}-acetate. Although several isomeric forms[62, 8, 6, 28, 63, 55] of Mn_{12}-acetate have been chemically identified, only one minority species is present in the samples studied here with sufficient concentration to produce measurable effects. Since the magnetization from this species saturates below 1.5 T, its presence does not affect the results presented in this section. This second species was not studied extensively in this thesis.

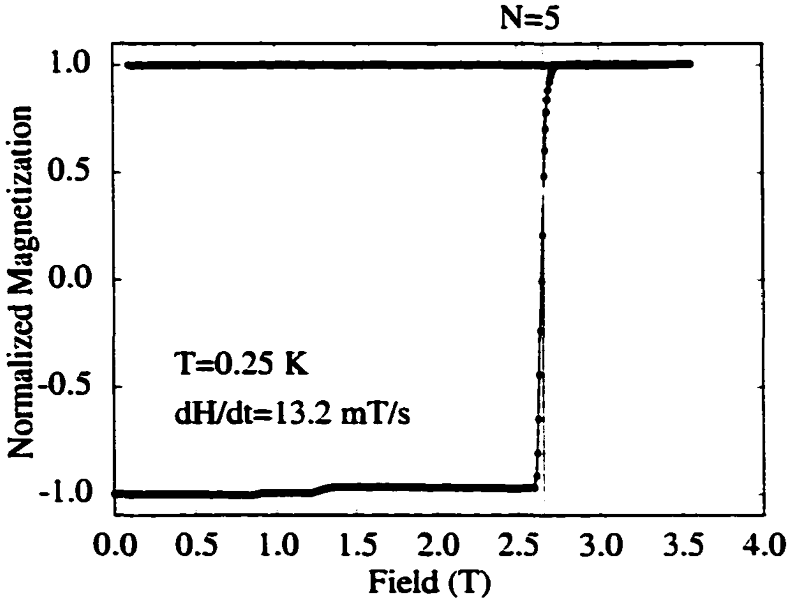

Figure 19: Avalanches in the magnetization may occur if the field is swept quickly and the magnetization starts from the fully saturated state. Notice that the avalanche occurred at an energy resonance.

In addition, a dramatic effect known as the avalanche effect may occur, as shown in Fig. 19. Paulsen *et al.* were the first to observe this phenomenon[46, 64]. Paulsen, showed that there is a tremendous amount of heat released during an avalanche. For the samples studied here, this effect was only seen under specific reproducible conditions. Namely, if the field is swept very quickly and magnetization starts from the fully saturated state. To avoid the avalanche effect, the magnetization measurements always began with the sample in the demagnetized state.

3.1.3 Transition to Thermally Assisted Tunneling

For Mn_{12}-acetate the distinction between thermally assisted tunneling and ground state tunneling can be seen in magnetization measurements as the temperature is increased above the ground state tunneling temperature, $T_G \approx 0.5\,\mathrm{K}$. Because of the fourth order anisotropy term, $A\hat{S}_z^4$, only one pair of energy levels comes into resonance at a time as the field is swept. As can be seen by the double well potential diagrams for the $N = 7$ step in Fig. 20, the first excited state come into resonance at a lower magnetic field, $H_z = 3.48\,\mathrm{T}$, than the field at which the ground state comes into resonance, $H_z = 3.63\,\mathrm{T}$.

This means that if the molecules are thermally activated to excited states in the metastable well, then tunneling will occur at lower fields compared with ground state tunneling. This can be more clearly seen by plotting all the energies at which resonances occur as a function of magnetic field, as is shown in Fig. 21. Each dot represents an energy resonance, $E_m = E_{m'}$. The energies were determined from Eq. 5. The corresponding fields were determined from Eq. 6. The lower mark encircles the first 10 ground state resonances. The other mark encircles the $N = 7$ family of resonances.

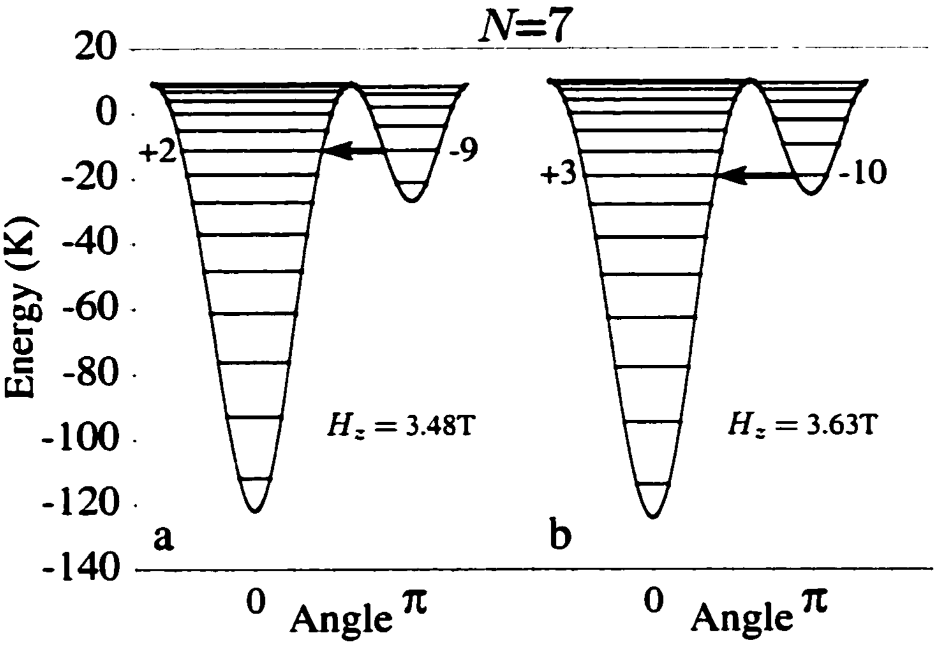

Figure 20: Double well potential for Mn_{12}-acetate. Only one pair of eigenvalues come into resonance at a time.

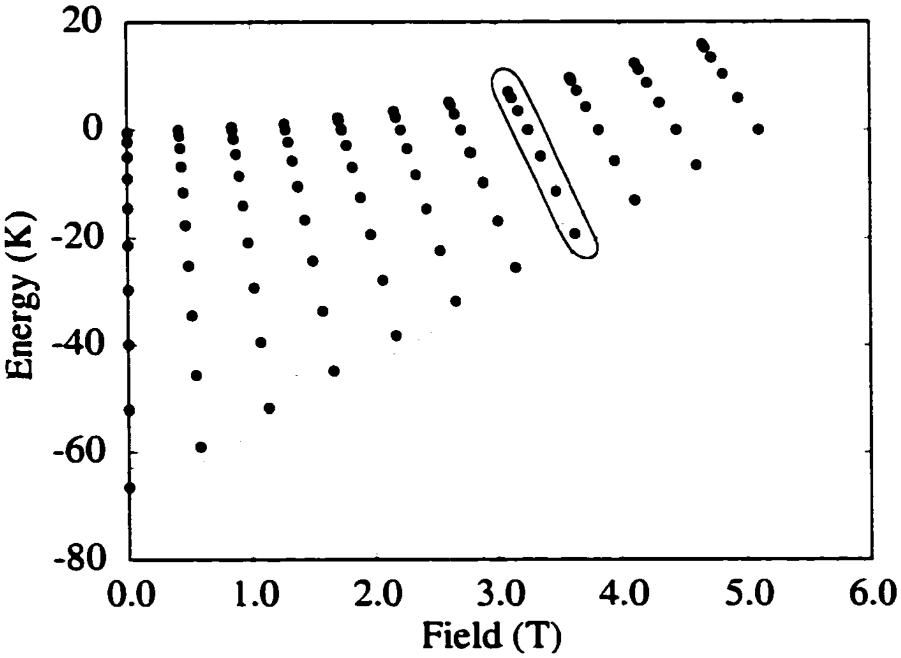

Figure 21: Energies at which resonances occur as a function of magnetic field. Each dot represents an energy resonance. The lower mark encircles the first 10 ground state resonances. The other mark encircles the resonances for the $N = 7$ family of resonances.

Thus, as the temperature is increased above T_G, shoulders in each peak should and do occur as is shown in Fig. 22. The solid curve corresponds to ground state tunneling. The dashed curve corresponds to a combination of ground state tunneling and thermally assisted tunneling at $T = 0.88\,\mathrm{K}$. The thin gray curves correspond to measurement made between these two temperatures. The two vertical thin lines depict the resonance field for ground state tunneling (solid lines) and tunneling from the first excited state (dotted lines). Only the peaks associated with $N = 5...9$ are shown since the other peaks at lower fields correspond to a second complex of Mn_{12}-acetate[62, 8, 65, 28, 63, 55].

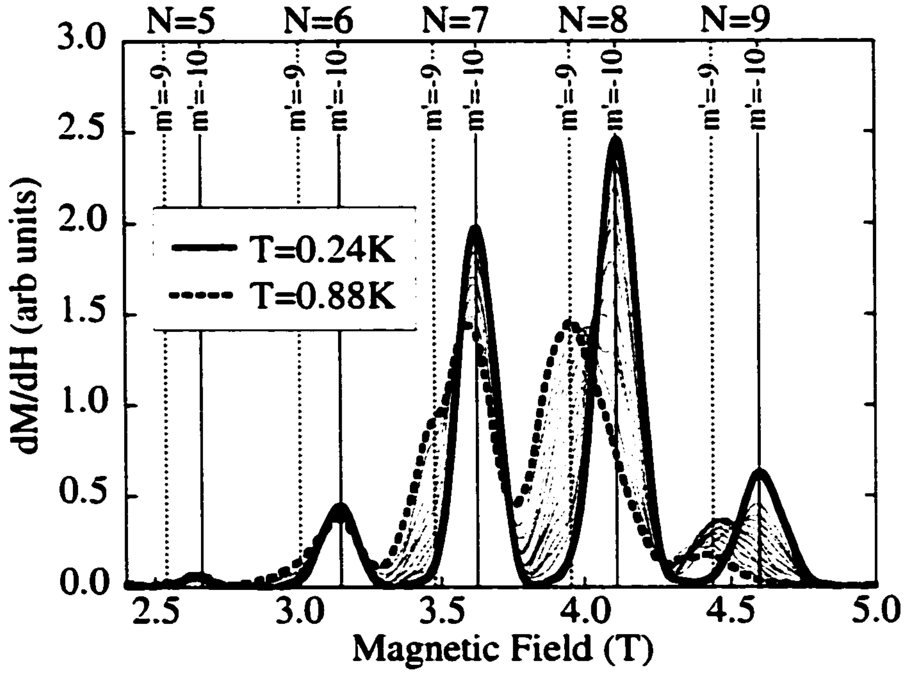

Figure 22: Transition from ground state tunneling to thermally assisted tunneling. The thick solid curve corresponds to ground state tunneling. The dashed curve corresponds to a combination of ground state tunneling and thermally assisted tunneling at $T = 0.88\,\mathrm{K}$. The two vertical thin lines depict the resonance field for ground state tunneling (solid lines) and tunneling from the first excited state (dotted lines).

It should be noted that the shoulders appear at lower temperatures for $N = 9$ than they do for $N = 6$. This phenomenon can be understood qualitatively by considering both the probability of tunneling together with the probability of occupying the excited states. The probability of tunneling can be related to the penetration of the wavefunctions of each state into the potential barrier. As N increases, the height of the potential barrier decreases so that the decay of the wave function into the potential barrier is smaller for larger N. Also, the amplitude of the wavefunction as it penetrates the stable well increases as N increases, since the width of the potential barrier decreases with increasing N. Thus, the probability of tunneling increases with increasing N. On the other hand, the spacing between the energy levels is roughly the same for $N = 5$ through $N = 9$, so that the probability of occupying the excited states for each N is roughly the same at any given temperature. Since the probability of occupying the excited states is about the same for each N at any given temperature, but the probability of tunneling is greatly enhanced for higher N, the transition to thermally assisted tunneling will occur at lower temperature for higher N.

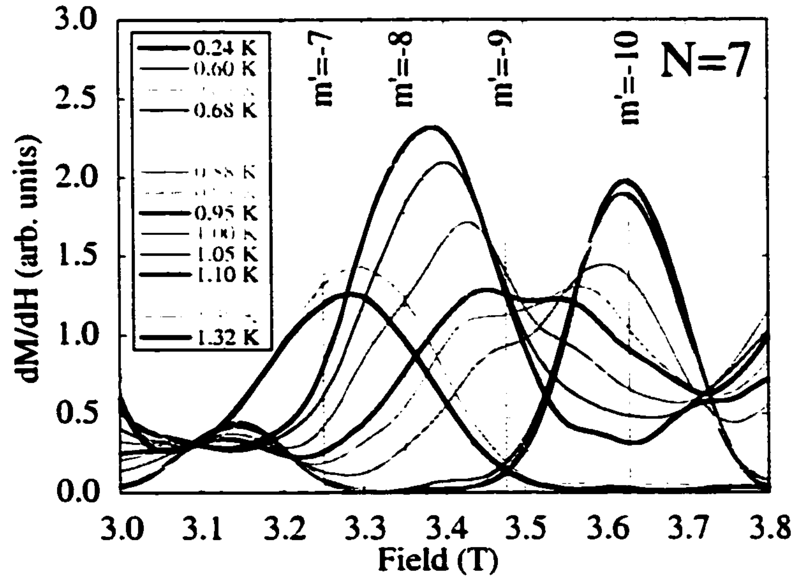

Figure 23: The transition from Thermally Assisted Tunneling to Ground State tunneling for the $N = 7$ family of transitions.

As the temperature is increased even further, the higher excited states become more populated. Thus the expectation is that the peaks associated with thermally assisted tunneling for the second ($m' = -8$) and third ($m' = -7$) excited states should also appear as is shown in Fig. 23, which is a detailed view of dM/dH for the $N = 7$ family for temperatures between 0.24 K and 1.32 K.

It is clear from Fig. 23 that the position of the peaks moves to lower fields as the temperature increases. On the other hand, the amplitudes of the peaks have a complicated behavior. For example, the amplitude of dM/dH is maximum for the peaks associated with tunneling for the $N = 7$ family at 1.10 K and the amplitude of the peaks decreases for higher temperatures. This artifact occurs because this is a plot of dM/dH which is a measure of the absolute change in the normalized magnetization, it is not a direct measure of the tunneling probability. The reason why the amplitude begins to decrease for temperatures above 1.10 K for $N = 7$ is that most of the magnetization has already tunneled from the excited states associated with $N = 5$ and $N = 6$. In other words, since there is less magnetization remaining in the metastable well the total change in M is smaller. In particular, at 1.32 K only 33% of the magnetization is remaining just before the $N = 7$ transition. Whereas, at 0.95 K, 77% of the magnetization remains. So, even though the probability of tunneling is higher for transitions that are occupied at 1.32 K than it is for transitions that are occupied at 0.95 K, the peak will be smaller at 1.32 K because the amount of magnetization remaining is *significantly* smaller.

3.1.4 Abrupt Transitions

An interesting feature is that there is an apparent minimum in dM/dH around the $m' = -9$ transition at $0.95K$. To better see how the transition depends on temperature, the same data is plotted in the $H - T$ plane in Fig. 24, with dM/dH shown in the third dimension by different shading, with lighter shade corresponding to larger amplitude. The data is also shown in a topological view in Fig. 26. From these figures it is clear that the tunneling appears to be skipped for the first excited state ($m' = -9$) in favor of either the higher excited states or the ground state. Kent *et al.* interpreted this skipping effect[59, 60] in terms of a theory by Chudnovsky and Garanin[66, 18]. Chudnovsky and Garanin showed that the crossover from thermally assisted tunneling to pure ground state tunneling can occur either continuously ("second order" transition) or abruptly ("first order" transition) as the temperature is reduced.

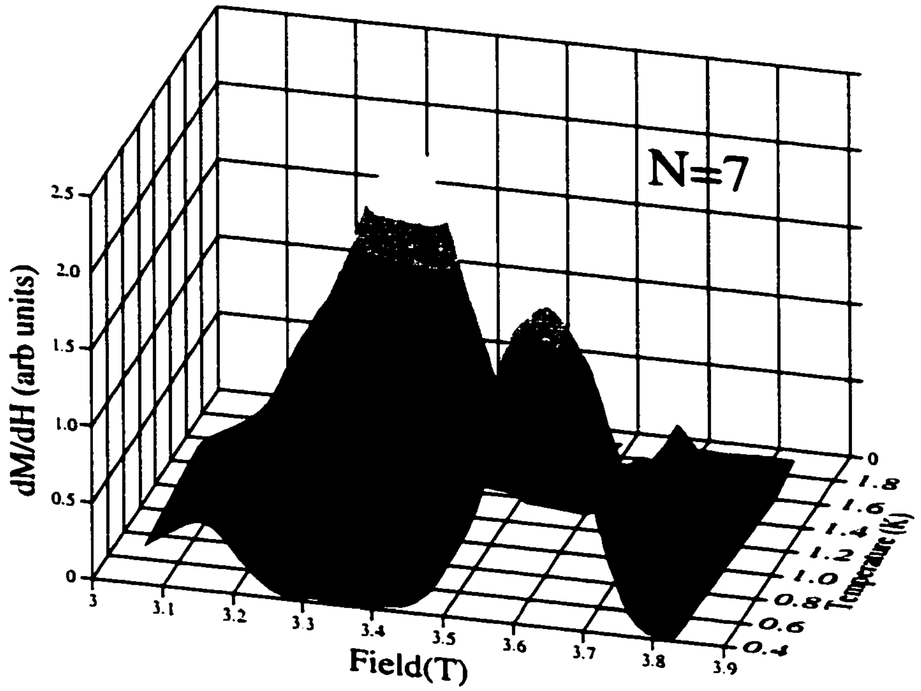

Figure 24: dM/dH for the $N = 7$ family of transitions. The amplitude has a complicated temperature dependence.

Each family of transitions $N = 6...9$ show similar behavior, as can be seen in Fig. 25 through Fig. 28, where the topological views of the other family of transitions is shown in separate graphs. For $N = 6$, the peak jumps over two excited state transitions to tunneling from the ground state. The ground state tunnelling is difficult to see in this graph because the amplitude is much smaller than the peak associated with thermally assisted tunneling. Ground state tunneling for $N = 6$ is more evident in Fig. 22. For $N = 7$, as was stated earlier, the tunneling skips over the first excited state. For $N = 8$ and $N = 9$, the transition is more gradual.

To understand Chudnovsky and Garanin's idea of an abrupt transition, recall that thermal activation becomes exponentially more difficult as one proceeds up the ladder to higher energy levels. On the other hand, the barrier is lower and more penetrable, so that the tunneling process becomes exponentially easier. Which level dominates the tunneling is determined by competition between the two effects. As the temperature is reduced and thermal activation becomes more difficult, tunneling proceeds from progressively lower energy levels deeper in the potential well. The levels which dominate the tunneling at any particular temperature depend upon the shape of the potential barrier and the spacing of energy levels.

For example, if the barrier is steep with little change in thickness for the ground state and the first few excited states, then the probability of tunneling will be approximately the same for each of these levels. On the other hand, the population decreases exponentially for higher levels, so it is expected that most of the tunneling will occur for ground state tunneling at low and moderately low temperatures. However, near the top of the barrier the width of the barrier may become thin quickly with increasing energy. For these high excited states, the probability of tunneling may be significantly greater than it is for the ground state and first few excited states. Thus if the temperature is increased above a certain threshold the tunneling will be suddenly dominated by tunneling from these high excited states. This is an abrupt transition. A smooth transition will occur if the probability of tunneling increases more gradually with increasing energy.

It should be noted that the history dependence of the peaks cannot explain the effect of the skipped $m' = -9$ transition. For example, just before the $N = 7$ transition at 0.95 K, 85% of the magnetization is remaining, whereas at 0.24 K, 87% is remaining. So in both cases the amount of magnetization available for tunneling is roughly the same. However, the amplitude of the peak in dM/dH at 0.95 K is significantly smaller than it is at 0.24 K. Thus, the history dependence cannot account for the fact that the *effective* probability of tunneling from the first excited state is smaller than the ground state.

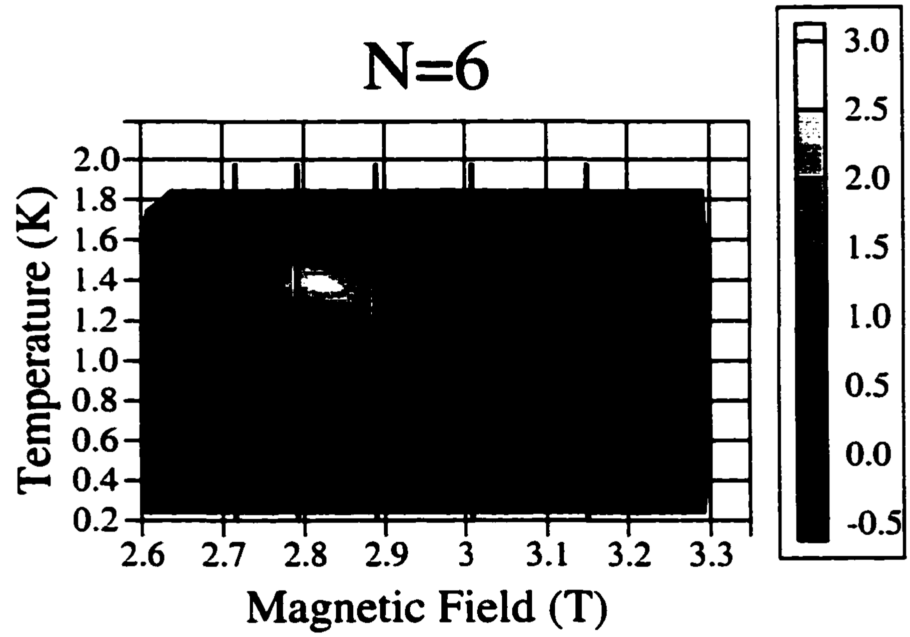

Figure 25: *dM/dH* for the $N = 6$ family of transitions. The amplitude seems to skip over two excited states. The yellow shading that appears near 3.3 T and 1.2 K is the beginning of the thermally assisted tunneling peaks for $N = 7$.

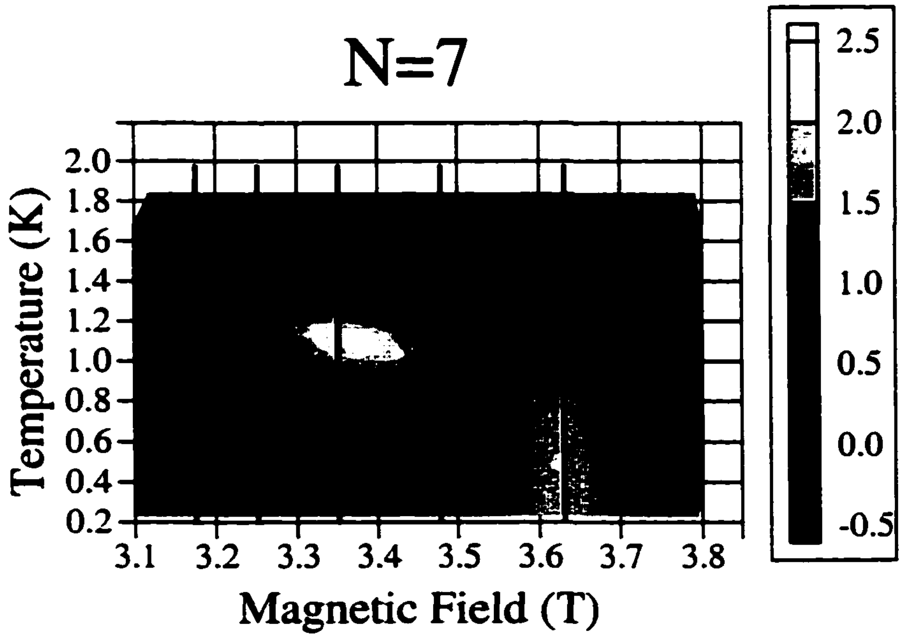

Figure 26: *dM/dH* for the $N = 7$ family of transitions. The vertical black lines indicate the transition fields. The right most corresponds to ground state tunneling (m'=-10). The amplitude seems to "skip" over the first excited state ($m' = -9$).

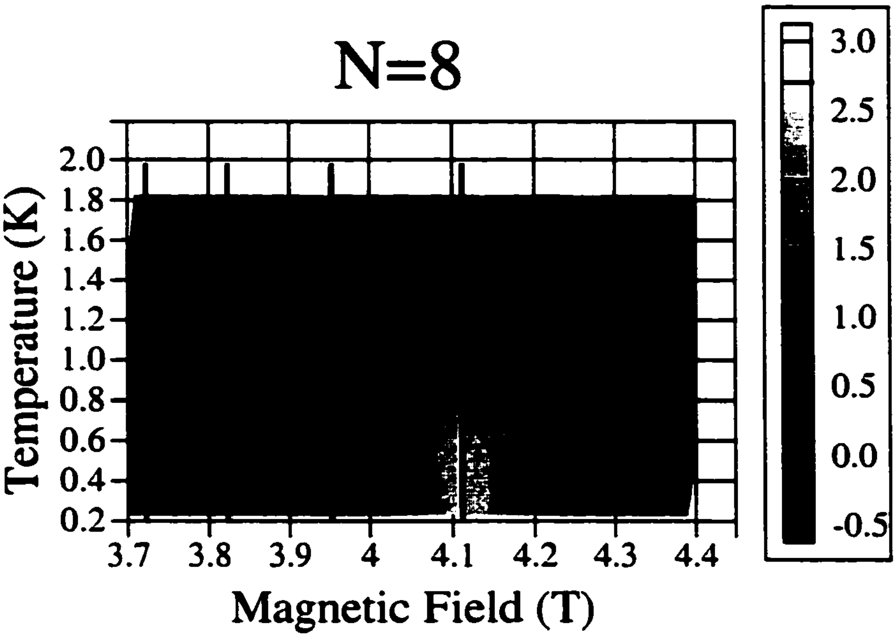

Figure 27: *dM/dH* for the $N = 8$ family of transitions. The transition to ground state tunneling is more gradual.

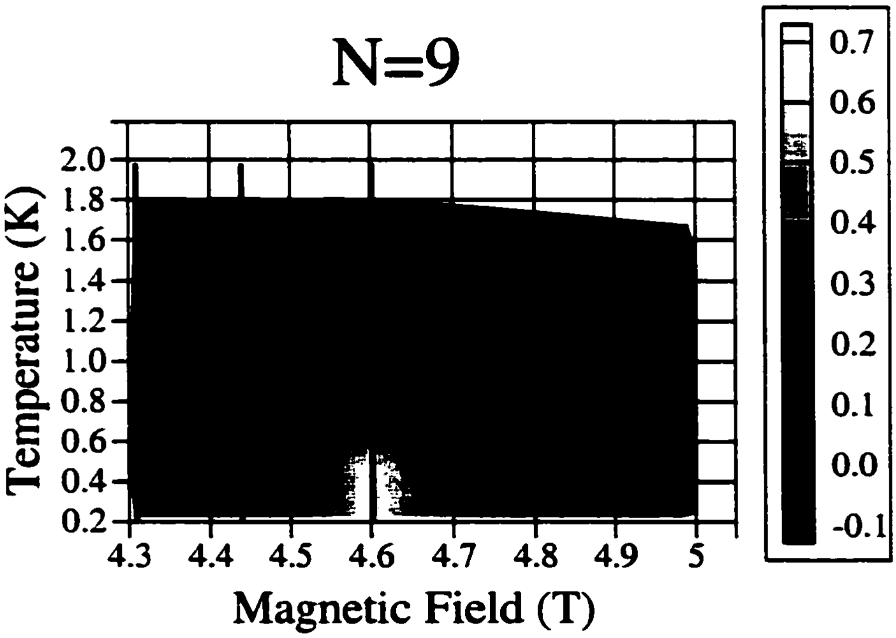

Figure 28: *dM/dH* for the $N = 9$ family of transitions. The transition to ground state tunneling is more gradual.

3.1.5 Suppression of Ground State Tunneling Probability

There is an additional subtle feature seen in these plots that cannot be explained by the history dependence. From these graphs it is clear that transitions associated with ground state tunneling for $N = 7$ are nearly absent for 1.10 K (see Fig. 23). At the onset of ground state tunneling at 0.24 K the magnetization remaining is 87%, whereas for 1.10 K, the magnetization remaining is 60%. One would thus expect a small change in the height of the peak for ground state tunneling as the temperature is increased. The amplitude at 1.10 K should be reduced to 60/87 of the height at 0.24 K. However, there is a dramatic decrease in the height of the peak. So the history dependence effect cannot explain why ground state tunneling is nearly absent at 1.10 K. Also, the theory of Chudnovsky and Garanin claims that the level that *dominates* tunneling can shift abruptly with temperature. It does not state that the probability of tunneling should decrease with increasing temperature.

The above discussions suggest the observed temperature dependence cannot be fully explained within the Chudnovsky-Garanin theory and that other factors play a role. The peaks in dM/dH provide accurate means of determining the field of each transition. However, the amplitudes are complicated by the history dependence of the magnetization. This history dependence can be folded out of the problem by dividing by the amount of magnetization remaining in the metastable well. Defined this way,

$$\Gamma = \frac{dM/dH}{M_{sat} - M} \tag{11}$$

represents the instantaneous tunneling rate because it is the total amount of magnetization that *did* tunnel divided by the total amount of magnetization that *could* have tunneled as the field changed from H to $H + dH$. Γ is not well defined for tunneling from the excited states since dM/dH is divided by the total magnetization in the metastable well. In other words, it does not take into account the population distribution of the excited states:

$$n_{m'} = n_0^- e^{-\Delta E_{m'}/k_B T}/\mathcal{N}, \tag{12}$$

where n_0^- is the number of molecules in the metastable well, $\Delta E_{m'} = E_{m'} - E_{-10}$ is the energy difference between the excited state m' and the ground state $m' = -10$ and $\mathcal{N} = \sum\limits_m e^{-\Delta E_m/k_B T}$ is the normalization factor. However, it *is* well defined for ground state tunneling for temperatures between T_B and T_G because the population of the ground state is given by, $n_G = n_0/\mathcal{N}$. As can be seen by the energy level diagram shown in Fig. 20, $\Delta E_{m'} >> k_B T$, so that $\mathcal{N} \approx 1$ for the temperatures under consideration ($T < 2\,\mathrm{K}$). Therefore, the population of the ground state is simply given by,

$$n_G \approx n_0^-. \tag{13}$$

Γ for $T = 0.24\,\mathrm{K}$ is plotted as a function of H in part (c) of Fig. 29. As expected the instantaneous tunneling probability, Γ, increases as N increases, since it becomes easier to tunnel as the potential wells become more unbalanced. The skewing of the peaks is due to the fact that the amount of magnetization remaining, $M_{sat} - M$ changes during the transition. This means that dM/dH is divided by a smaller amount above the transition than it is for fields below the transition. The reason the peaks shift off resonance will be discussed later in Section 3.1.6. For comparison M and dM/dH are plotted as a function H in parts (a) and (b) respectively. The solid vertical lines indicate the ground state transition fields for each step, N.

For temperatures above T_G, Γ begins to show anomalous behavior. As stated earlier, the measured tunneling rate depends on both the probability of occupying the ground state as well as the quantum mechanical probability of tunneling from the ground state:

$$P_{Measured} \sim P_{Occupying}\, P_{Tunneling}, \tag{14}$$

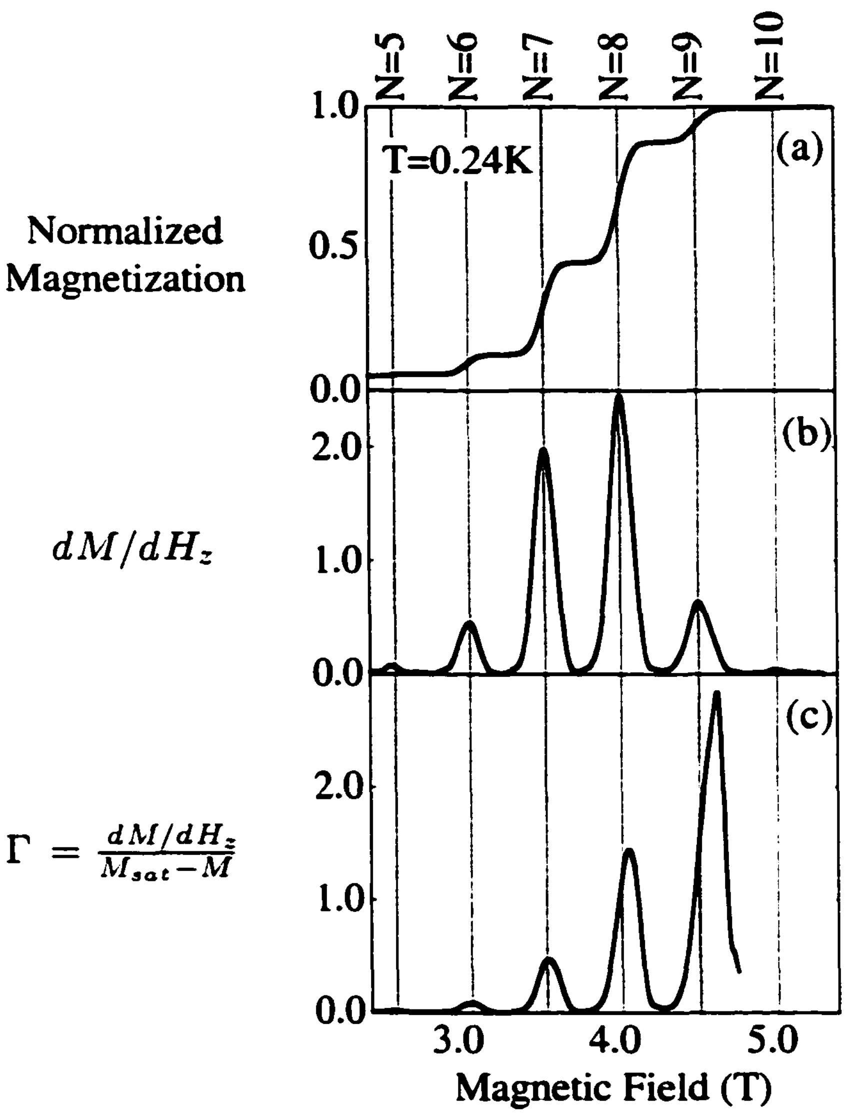

Figure 29: Ground state tunneling data for Mn_{12}-acetate taken at $T = 0.24\,K$. Part (a), (b) and (c) are the normalized magnetization data, dM/dH and Γ, respectively.

where the ground state population, $P_{Occupying} \approx 1$ is essentially independent of temperature and $P_{Tunneling}$ is the tunneling probability which is also independent of temperature. Therefore, the expectation is that Γ at the ground state transition field should be independent of temperature. Fig. 30 is a plot of Γ near the $N = 7$ family of transitions. The solid vertical line indicates the ground state ($m' = -10$) transition field. As can be clearly seen, the measured probability of tunneling from the ground state has decreased significantly as the temperature is increased. In fact, the decrease may be even more significant since the tail for the $N = 8$ peak for 1.10 K seems to increase the value of Γ.

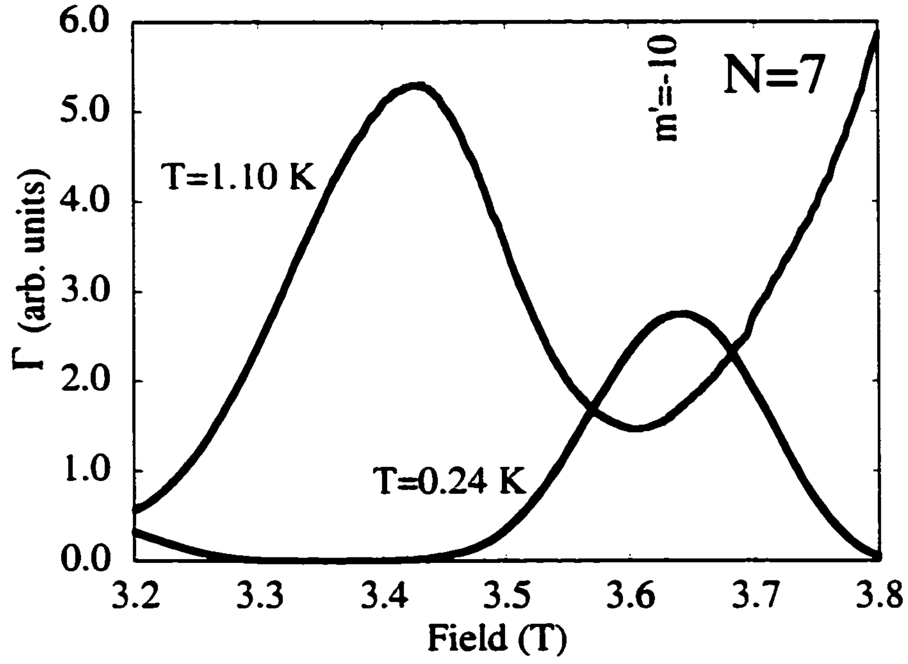

Figure 30: Comparison of ground state tunneling rate, Γ, for $N = 7$ at high temperature ($T = 1.05\,\mathrm{K}$) and low temperature ($T = 0.24\,\mathrm{K}$). The measured probability of tunneling has decreased as the temperature increased.

Since by its definition Γ removes the history dependence from dM/dH peaks, the probability should not change as the population is changed due to the differing amounts of magnetization remaining in the metastable well. However, Fig. 30 clearly shows that the probability as determined from magnetization has indeed changed.

3.1.6 Distributions of Tunnel Splittings

This anomalous behavior[61], is completely unexpected for an ensemble of identical molecules. The fact that the instantaneous tunneling rate, Γ, still depends on past history implies that not only is the total population important, but also the demographics of this population. It was suggested by Garanin that the suppressed ground state enigma can be understood if there is a distribution of tunneling probabilities[67].

In real crystals of Mn_{12}-acetate there are many environmental effects that have been ignored. Some of these effects include interactions such as nuclear hyperfine interactions, dipole-dipole interactions, or transverse fields due to misalignment of the crystal as well as transverse fields and anisotropies due to imperfections in the crystal. Imperfections can occur at the molecular level by isomeric molecules or molecules with "missing parts"[62]. Imperfections may also occur at the crystal level due to chemical impurities and crystal dislocations[68].

All of these effects may have measurable consequences. The most important consequence is that the molecules may not be identical. Each molecule will experience these effects to varying degrees. The Hamiltonian will have the same form for each molecule. However, the prefactors (D, A, H_x, E, C,...) which determine the strength of each effect, will vary from molecule to molecule. Since the tunnel splitting is determined by the size of the prefactors, there may be a *distribution* of tunnel splittings in the sample.

To understand the consequences of a distribution of tunnel splittings on magnetization measurements, consider the case of a very broad distribution. In reality the distribution may not be so broad, but the physics is much easier to understand and the behavior remains essentially the same. With a very broad distribution some molecules will have very large tunnel splittings and some will have very small tunnel splittings. As can be seen from Eq. 9, the probability of tunneling depends sensitively on the tunnel splitting. Consequently, for each energy resonance, N, those molecules with very small tunnel splittings will have near zero probability of tunneling. Whereas, those molecules with very large tunnel splittings will tunnel very easily. In other words, each transition acts like a filter that separates very fast molecules from very slow molecules.

To understand how a broad distribution explains why the tunneling ground state disappears at higher temperatures, consider Fig. 31, which is a plot of a hypothetical lognormal distribution of the "tunneling parameter". The tunneling parameter is simply the prefactor of the symmetry-breaking term responsible for the tunneling. The tunnel splitting depends on the tunneling parameter and the probability of tunneling depends on the tunnel splitting. The distribution shown in Fig. 31 gives the fraction of molecules that have a tunneling parameter between δ and $\delta + d\delta$.

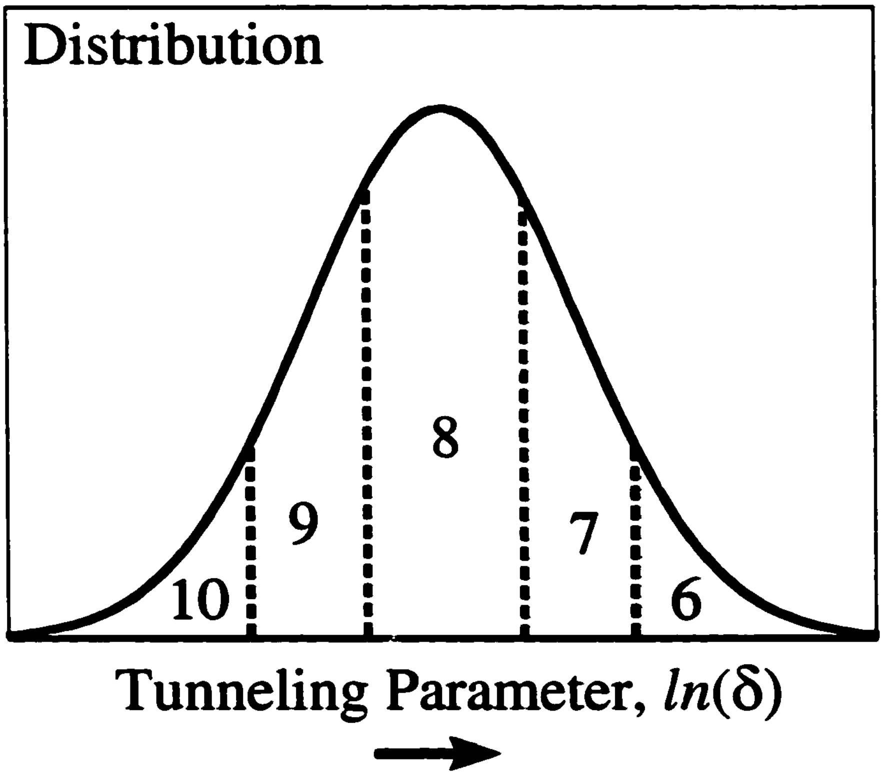

Figure 31: Hypothetical lognormal distribution of the tunneling parameter (the prefactor of the symmetry-breaking term). With a broad distribution, only certain molecules will tunnel at each transition as shown by the different regions.

Fig. 31 breaks the distribution into different regions. Each vertical line depicts the threshold that separates fast tunneling molecules from slowly tunneling molecules for each ground state resonance, N. As the field is swept up to an energy resonance, different parts of the distribution will tunnel. For example, for $N = 6$ all the molecules with a tunnelling parameter in region marked 6 in Fig. 31 will tunnel. None of the other molecules will tunnel because they tunnel too slowly since the potential barrier is too high. At the next transition, $N = 7$, the potential barrier is lower, so another group of molecules will be able to tunnel. A similar effect occurs at the other transitions, $N = 8...10$.

Now consider the same situation at higher temperature. As the temperature is increased the distribution of tunneling parameters does not change. However, there are now additional tunneling channels available to the molecules since each molecule now will spend a fraction of its time in the excited states. Since these additional tunneling channels occur at lower fields, the molecules that would have tunneled at the ground state transition will *definitely* tunnel from the excited states since it is so much easier to tunnel from these states. By the time the field reaches the ground state transition field, there are no molecules remaining in the distribution to tunnel. Thus, the magnetization will not change much at the field corresponding to ground state tunneling and the ground state will seem to have "disappeared". Thus, the idea of a distribution provides a natural explanation of the suppression of ground state tunneling.

3.1.7 Summary of Temperature Dependence Study

The detailed temperature dependence of Mn_{12}-acetate was measured and analyzed. Fig. 32 shows a topological view in the $H-T$ plane of dM/dH. The shading indicates the value of dM/dH for various isothermic field sweeps. Since dM/dH varies over a wide range of values, the intensity of dM/dH is shown on a logarithmic scale.

Fig. 32 summarizes the findings of the temperature dependence study. There is a transition from thermally assisted tunneling to ground state tunneling. The curved line denotes the fields and temperatures where this transition occurs. Below this curve are the ground state peaks that are clearly temperature independent. Above this transition curve are the peaks associated with thermally assisted tunneling. It is clear that the amplitude of the thermally assisted peaks for any given family of transitions, N, increase and decrease. This behavior has been attributed to the history

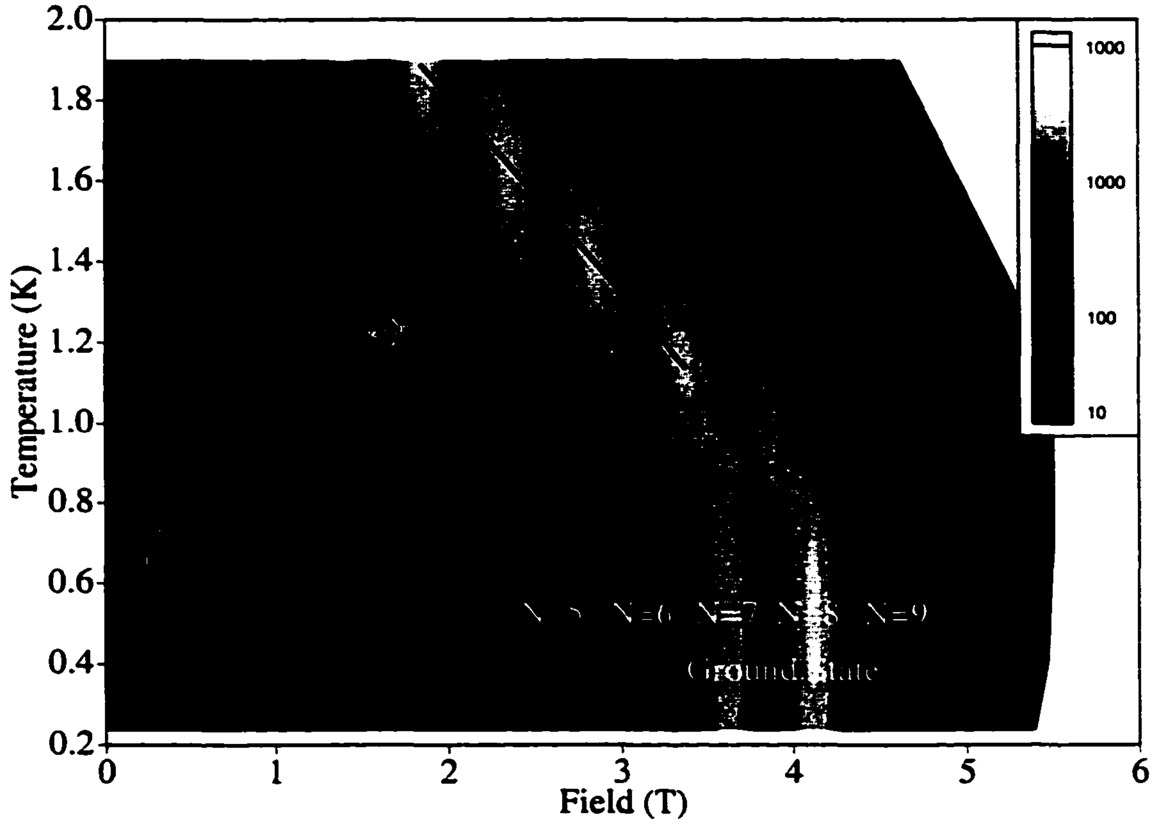

Figure 32: A "phase diagram" for the tunneling of magnetization of Mn_{12}-acetate summarizes all the phenomenon discovered by measuring the temperature dependence in detail.

dependence of dM/dH. The straight line joining the thermally assisted peaks illustrate how the peaks march toward lower field (i.e. to lower N) as the temperature increases. If this line is extrapolated to $H = 0$ ($N = 0$) it intercepts at $\approx 3\,\mathrm{K}$. This corresponds to the blocking temperature as expected, since near the blocking temperature most of the tunneling will occur for $N = 0$ and $N = 1$. At this temperature it is difficult to distinguish between over the barrier hopping and thermally assisted tunneling. Also evident in the diagram are the peaks associated with tunneling of the second complex of Mn_{12}-acetate. Fortunately, these occur in a separate region of the $H - T$ plane and it is thus easy to separately identify their presence in the data.

It was found that as the temperature increases, tunneling from the ground state decreases, even though there is plenty of magnetization remaining. The dots in Fig. 32

locate the regions where the ground state tunneling is suppressed. This phenomenon could not be explained in terms of the history dependence of dM/dH of identical molecules. However, it was argued that a distribution provides a very simple and elegant explanation. The next study confirms more directly that there is indeed a distribution of tunnel splittings in Mn_{12}-acetate crystals.

3.2 Sweep Rate Dependence

3.2.1 Experimental Method

The magnetization of Mn_{12}-acetate was measured at different rates of the swept external magnetic field. Before each measurement the state of the sample was prepared in a fashion similar to the temperature dependence study. First the sample was heated in zero magnetic field to 10 K, well above the blocking temperature, $T_B \approx 3\,K$. The magnetization of the sample was monitored to make certain that the magnetization of the sample was completely removed. The sample was then cooled to 0.24 K. While keeping the sample at base temperature, the externally applied magnetic field was swept up to 5.5 T at some fixed sweep rate. The procedure was then repeated for a different field sweep rate.

3.2.2 Sweep Rate Data

Fig. 33 through Fig. 35 show the magnetization measurements for various sweep rates. Each graph depicts the measurements performed on a different Mn_{12}-acetate sample. Each curve represents one sweep of the external field and each sweep was conducted at a different sweep rate. Fig. 33 shows the measurements for the same sample measured in the temperature dependence experiment. This sample was not taken out of the He^3 cryostat between the temperature dependence measurements and the sweep rate dependence measurements. The other two samples were taken from a freshly prepared batch. The major difference between the samples is their size and surface quality. Sample #1 and #3 both had smooth surfaces with sharp edges and corners. Sample #2 had a rough surface and broken corners. Table 1 lists the approximate dimensions of each sample.

	a-axis	b-axis	c-axis	Quality
Sample #1	40 μm	40 μm	100 μm	Good
Sample #2	20 μm	20 μm	50 μm	Poor
Sample #3	40 μm	40 μm	150 μm	Good

Table 1: Approximate dimensions of the three parallelepiped shaped samples measured in the sweep rate dependence study. The c-axis is the easy axis of magnetization. The field was aligned along this axis. All three axes are mutually perpendicular. The "Poor" quality sample #2 had broken corners and rough surfaces.

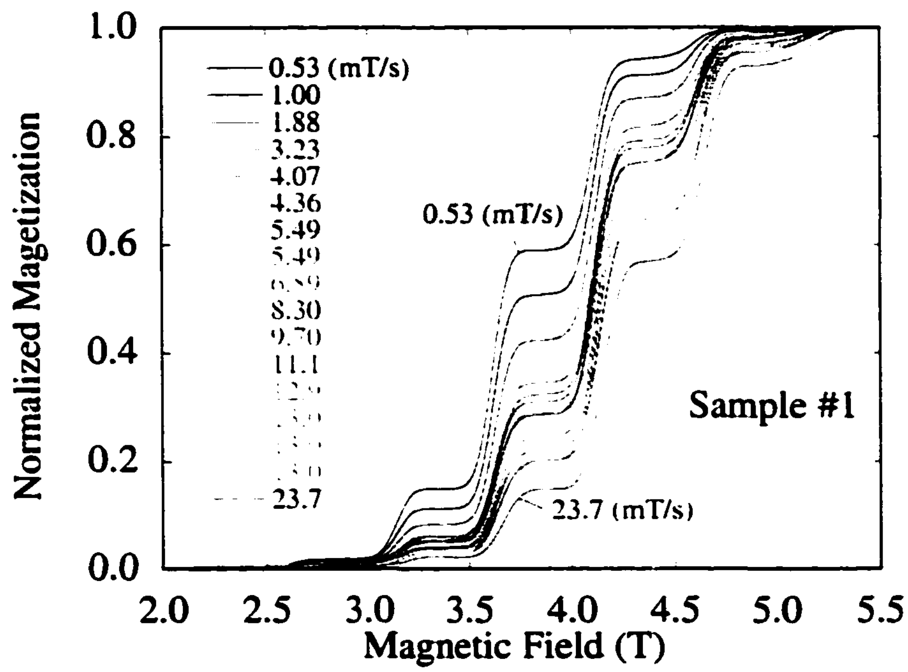

Figure 33: Tunneling Sweep Rate Dependence for sample #1. Each curve depicts the normalized magnetization for a different sweep rate.

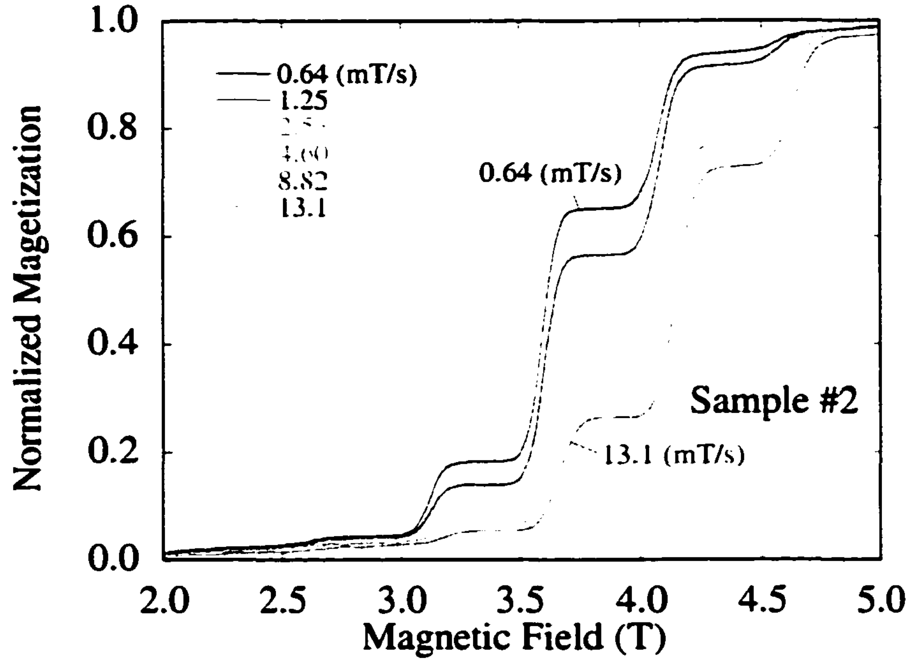

Figure 34: Tunneling Sweep Rate Dependence for sample #2. Each curve depicts the normalized magnetization for a different sweep rate.

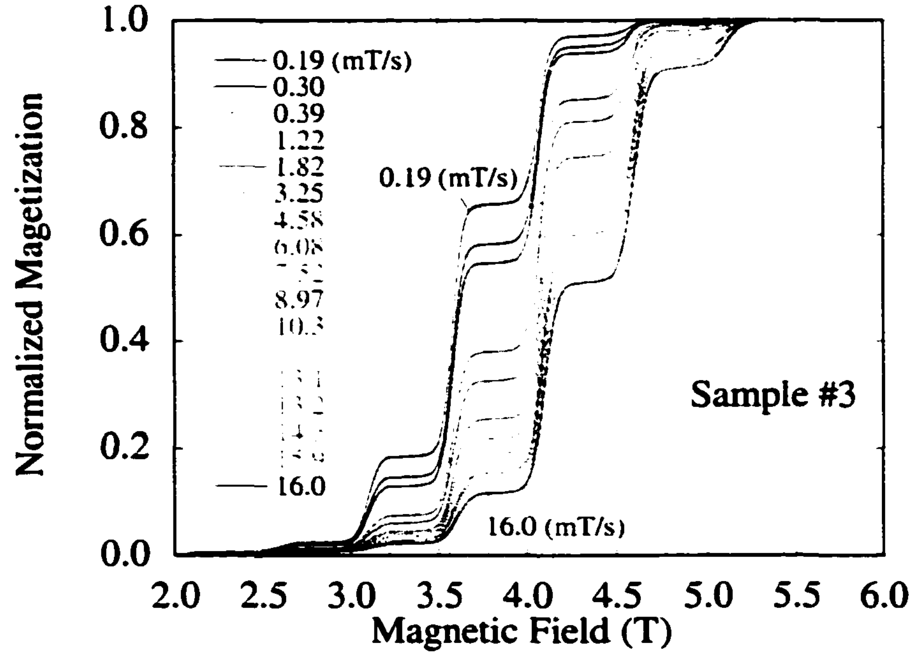

Figure 35: Tunneling Sweep Rate Dependence for sample #3. Each curve depicts the normalized magnetization for a different sweep rate.

All these field sweeps were taken at 0.24 K so that only ground state tunneling occurs. This makes analyzing the data significantly easier since only one tunneling channel is available. For thermally assisted tunneling, the energy resonances are sufficiently close to one another and the widths of the peaks sufficiently broad that it is difficult to resolve the energy resonances.

The magnetization due to the second species has been removed from the data by first determining the saturation level for the second species, then subtracting this amount from the magnetization curves and then normalizing. This is important since, as will be seen shortly, the normalized magnetization curves will be used to determine the tunneling probabilities.

From these curves it is clear that the sweep rate plays an important role in determining how many molecules tunnel at each energy resonance. For all three samples the magnetization relaxes at lower fields when the field is swept more slowly. This is in agreement with the predictions of the incoherent (and coherent) Landau-Zener-Stueckelberg formalism, since the tunneling probability increases with decrease energy sweep rate. The next two sections will analyze this data in terms of the probability of remaining in the metastable well.

3.2.3 Tunnel Splittings for Identical Molecules

The incoherent Landau-Zener-Stueckelberg formula can be used to determine the tunnel splittings from the normalized magnetization curves. When determined under the assumption that all the molecules are identical, the tunnel splittings have an unexpected dependence on sweep rate[69, 70, 71, 72, 73]. For an ensemble of identical molecules, at a particular energy resonance, every molecule has the same probability of *remaining* in the metastable well given by Eq. 15.

$$P_N = \exp(-\pi\Delta_N^2/2v_N\hbar), \tag{15}$$

where Δ_N is the tunnel splitting formed at the N^{th} anti-crossing (see Fig. 4) and $v_N = (g_z\mu_B)(2S - N)dH_z/dt$ is the rate at which the energy levels approach each other (in the absence of any symmetry breaking terms). Notice that it is proportional to the magnetic field sweep rate, dH_z/dt.

Since each molecule has the same probability of remaining in the metastable well. the number of molecules remaining after sweeping the field through a resonance is given by:

$$n_N^- = n_{N-1}^- P_N, \tag{16}$$

where n_N^- is the number of molecules in the metastable well *after* the N^{th} energy resonance, n_{N-1}^- is the number of molecules remaining in the metastable well *after* the $(N-1)^{th}$ energy resonance (which is the same as the number of molecules in the metastable well *before* the N^{th} resonance) and P_N is the probability that a molecule remains in the metastable well for the N^{th} resonance. In other words. the number of molecules remaining after a transition is just the number of molecules remaining before the transition times the probability of remaining.

For temperatures below, T_G, the magnetization of the sample is related to the number of molecules in the metastable well and the stable well by:

$$M = g_z\mu_B S(n^+ - n^-), \tag{17}$$

where g_z is the g-factor, μ_B is the Bohr magneton and n^+ and n^- are the number of molecules in the stable well and metastable well respectively. Since the total number of molecules is constant, the saturation value of the magnetization is given by:

$$M_{sat} = g_z\mu_B S(n^+ + n^-). \tag{18}$$

Eq. 17 can be combined with Eq. 18 to express the number of molecules in the metastable well as:

$$n^- = (M_{sat} - M)/2g_z\mu_B S. \tag{19}$$

Finally, using Eq. 19 and rearranging Eq. 15, the probability of remaining in the metastable well can be related to the measured magnetization:

$$P_N = \frac{n_N^-}{n_{N-1}^-} = \frac{M_{sat} - M_N}{M_{sat} - M_{N-1}}, \tag{20}$$

where M_N is the magnetization of the sample just after a resonance and M_{N-1} is the magnetization just before the resonance. Fig. 36 shows how the magnetization can be used to measure the probability of remaining in the metastable well for each resonance. In this diagram, R_N, R_{N-1} and T_N are chosen at the plateaux. $R_N = M_{sat} - M_N$ is the fraction of molecules remaining in the metastable well after the Nth resonance. $R_{N-1} = M_{sat} - M_{N-1}$ and is the fraction of molecules remaining in the metastable well after the $(N-1)th$ resonance. $T_N = R_{N-1} - R_N$ is the fraction of molecules that tunneled during the Nth resonance. Under the assumption that all the molecules tunnel with the same probability, the probability of remaining is given by,

$$P_N = R_N / R_{N-1}. \tag{21}$$

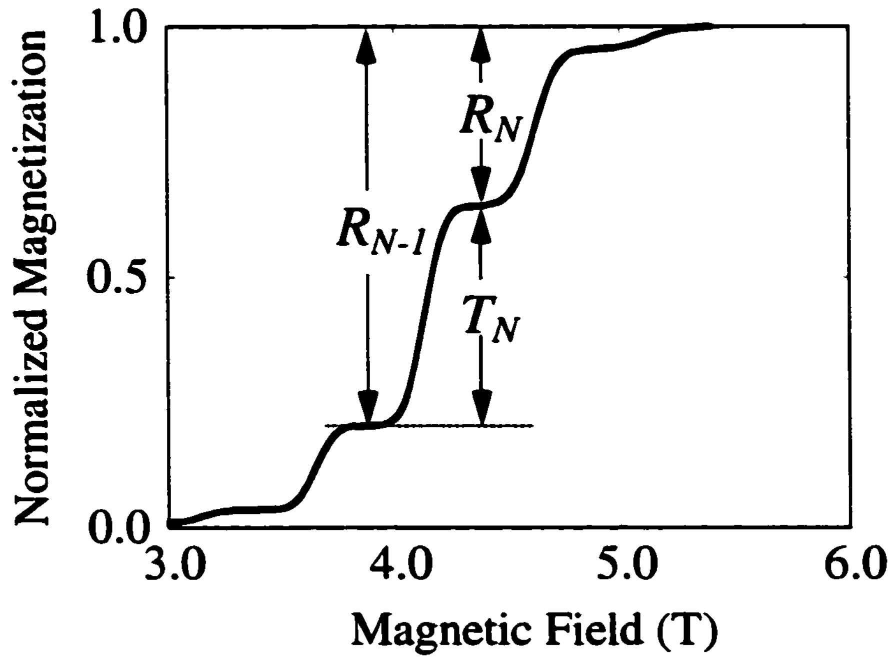

Figure 36: Determining the probability of remaining in the metastable wellfor an ensemble of identical molecules. The magnetization remaining after each plateaux is labeled by R_N. $T_N = R_{N-1} - R_N$ is the fraction that tunneled after the Nth resonance.

Using the probabilities determined from Eq. 21, the tunnel splitting can be determined from the incoherent Landau-Zener-Stueckelberg formula, Eq. 15,

$$\Delta_N = \sqrt{-2v_N \ln(P_N)/\pi} = \sqrt{-2(g_z\mu_B\hbar)(2S-N)dH_z/dt\,\ln(R_N/R_{N-1})/\pi}. \qquad (22)$$

Fig. 37 shows the values of Δ_N as a function of the field sweep rate for sample #1. From this diagram it is clear that the tunnel splittings determined from Eq. 15 have a strong dependence of on the sweep rate. However, in the incoherent Landau-Zener-Stueckelberg formalism, the tunnel splitting is independent of the sweep rate. The other samples show similar behavior.

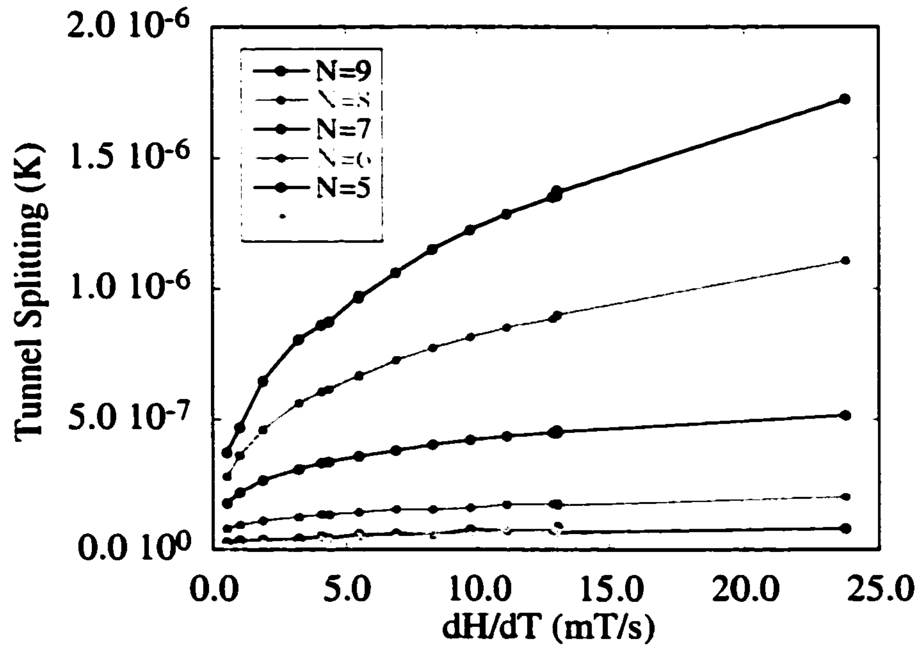

Figure 37: Tunnel splittings determined from incoherent Landau-Zener-Stueckelberg formula. Under the assumption of identical molecules, the tunnel splittings have an unexpected dependence on sweep rate.

3.2.4 Failure of Assumption that Molecules are Identical

Many authors[70, 71, 20, 74, 26] attribute the unexpected dependence of tunnel splittings on sweep rate as an effect due to the fact that the internal dipole field is changing so that the values used to determine the energy sweep rate are incorrect. So, for very slow external sweep rates, application of this formula may be invalid. This explanation does not seem plausible, for the following reasons. Consider the following worst case scenario. The slowest external sweep rate is $dH_z/dt = 0.53\,\mathrm{mT/s}$. For the largest step in the magnetization at this sweep rate, the magnetization changes in about 600 s. If it is assumed that the internal field is about 0.06 T (which is a large estimate), then during this time the internal field changes by 0.02 T. This means that the fastest change in internal field is $0.03\,\mathrm{mT/s}$. So even in this worst case scenario, the change in the mean dipole field is trivially small compared with the external sweep rate.

If, instead, one considers the change in the field due to a neighboring molecule having tunneled, then one must consider the time of tunneling. Mullen[75] has estimated this time (in the adiabatic limit) to be $\tau_N = \Delta_N/v_N$. This is an extremely short time interval, for $N = 6$, $\tau_6 \approx 5\,\mathrm{ns}$. In this time, a molecule neighboring a molecule that tunnels will experience a field that changes by $\Delta B_{dip} \approx 20\mu_B/r^3 \approx 0.01\,\mathrm{T}$. So the rate of change of the field due to a neighboring dipole flipping is, $\Delta B_{dip}/\tau_6 \approx 2 \times 10^6\,\mathrm{T/s}$. Since the probability of tunneling decreases exponentially with increasing sweep rate, the neighboring molecule will not tunnel with such a rapidly changing field. Compared with the time scale associated with sweeping the field through a resonance, the change in energy due to a neighboring molecule that tunnels is instantaneous. In other words, the change in field due to a dipole flip is just the sudden approximation considered earlier.

The above analysis suggests that the unexpected sweep rate dependence of the tunnel splittings determined from the incoherent Landau-Zener-Stueckelberg formula cannot be due to the internal dipole field. The next section analyzes the data quantitatively in terms of a distribution of tunnel splittings.

3.2.5 Reinterpreting Steps in the Magnetization Curves

As suggested by Chudnovsky and Garanin, the magnetization curves can also be analyzed in terms of a distribution of tunnel splittings. Care must be taken, however, because the physical interpretation of the curves changes. For an ensemble of identical molecules, the plateaux in the ground state magnetization curves are related to the *probability* of remaining in the metastable well, $P_N = R_N / R_{N-1}$. With a distribution this notion is no longer valid, as will now be shown.

For a single molecule, the probability of remaining in the metastable well is given by the incoherent Landau-Zener-Stueckelberg formula $P_N = \exp(-\pi\Delta_N^2/2v_N\hbar)$ [43, 44, 18, 50]. For a distribution of tunnel splittings, $\Delta_{N,i}$, (where i denotes the ith molecule) the probability that a spin remain in the metastable well must be averaged over all the molecules: $\langle P_{N,i}\rangle = \frac{1}{N_T}\sum_i \exp(-\pi\Delta_{N,i}^2/2v_N)$, where N_T is the total number of molecules. If the distribution is sufficiently broad, then $\langle P_{N,i}\rangle$ is best examined on a logarithmic scale where an exponential can be approximated by a step function, so that $\exp(-\pi\Delta_{N,i}^2/2v_N) \approx \Theta(1 - \pi\Delta_{N,i}^2/2v_N)$. This means that for a fixed field sweep rate, dH_z/dt, those molecules that have tunnel splittings obeying:

$$\pi\Delta_{N,i}^2 < 2v_N \tag{23}$$

will remain in the metastable well for each N. In essence,

$$R_N = \langle P_{N,i}\rangle = \frac{1}{N_T}\sum_i \Theta(1 - \pi\Delta_{N,i}^2/2v_N). \tag{24}$$

and each curve in Fig. 38 denotes the *fraction* of molecules that remain in the metastable well after each energy resonance because they tunnel too slowly[67, 76, 72, 73]. Thus, each tunneling transition acts like a filter separating fast tunneling molecules from slow tunneling molecules with the threshold condition, $\pi\Delta_{N,i}^2 = 2v_N\hbar$. This is summarized by the following equation for the tunneling probability:

$$P_{N,i} = \begin{cases} 1, & \pi\Delta_{N,i}^2 \gg 2v_N\hbar \\ 1,0, & \pi\Delta_{N,i}^2 \ll 2v_N\hbar \\ 0, & \end{cases} . \tag{25}$$

With a sufficiently broad distribution only a few molecules have $\pi\Delta_{N,i}^2 \approx 2v_N\hbar$ and most of the molecules fall into one of the two categories listed in Eq. 25.

In this new interpretation, the height of each plateaux, labeled by T_N in the ground state magnetization curve shown in Fig. 38, represents the fraction of molecules that tunnel fast enough for that transition. Likewise, R_N represents the fraction of molecules that tunnel too slowly for N^{th} transition. Also notice that since $\Delta_{N,i}$ is greater than $\Delta_{N-1,i}$, each step probes a set of molecules in the crystal belonging to a different range of the (initial) distribution of tunnel splittings as was shown earlier in Fig. 31.

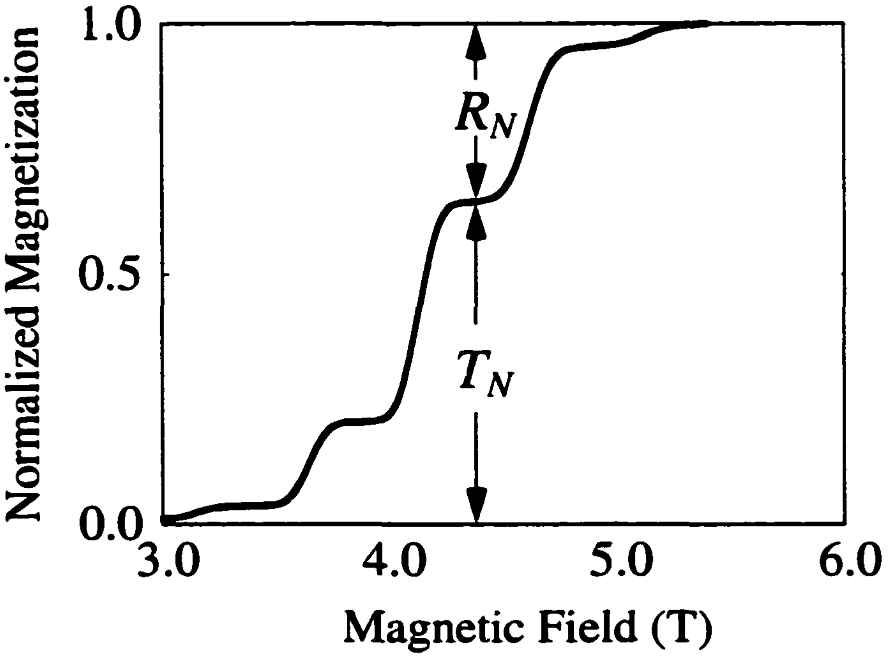

Figure 38: With a distribution of tunnel splittings, the height of each plateaux in the normalized magnetization data, labeled by T_N, represents the fraction of molecules that tunnel fast enough for that transition.

The physical meaning of the plateaux in the magnetization data for the two interpretations is summarized by the following equations:

$$R_N^{Identical} = R_{N-1}^{Identical} e^{-\Delta_N^2/2v_N} \qquad (26)$$

$$R_N^{Distribution} = \frac{1}{N_T}\sum_i \Theta(1 - \pi\Delta_{N,i}^2/2v_N), \qquad (27)$$

where $R_N^{Identical}$ is the fraction of remaining in the metastable well for an ensemble of identical molecules and $R_N^{Distribution}$ is the fraction of molecules that tunnel too slowly when there is a broad distribution of tunnel splittings. Fig. 39 summarizes the dependence of the measured values of R_N as a function of $-ln(dH_z/dt)$ for sample #1. The other samples exhibit similar behavior.

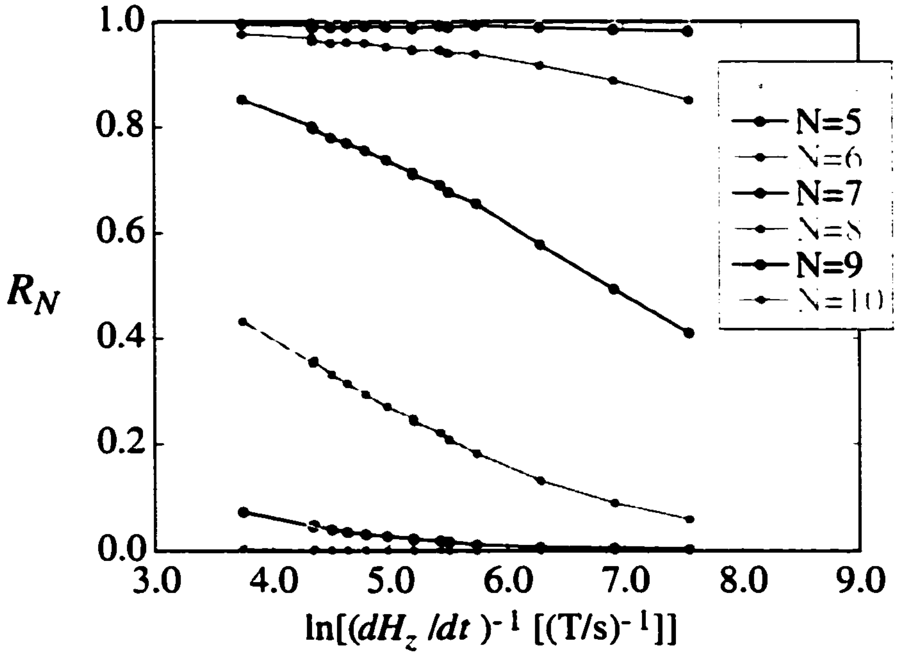

Figure 39: Fraction of molecules remaining in the metastable well for each resonance N plotted as a function of $-ln(dH_z/dt)$ for sample #1

3.2.6 Determining Distributions

Eq. 24 shows that varying the sweep rate changes the fraction of molecules that remain in the metastable well after the field sweeps through a particular energy resonance. In fact, R_N is the fraction of molecules which satisfy Eq. 23 up to the threshold condition $\pi\Delta_{N,i}^2 = 2v_N$,

$$R_N = \int_0^{\Delta^{threshold}} f_N(\Delta)\, d\Delta, \tag{28}$$

where $\Delta^{threshold} = \sqrt{2v_N/\pi}$ and $f_N(\Delta)$ is the normalized distribution of tunnel splittings for the N^{th} transition (i.e. $f_N(\Delta)d\Delta$ is the fraction of molecules with a tunnel splitting between Δ and $\Delta + d\Delta$). Application of Leibnitz's rule for differentiation of integrals,

$$\frac{\partial}{\partial z}\int_{\phi_1(z)}^{\phi_2(z)} g(x,z)\,dx = \int_{\phi_1(z)}^{\phi_2(z)} \frac{\partial g}{\partial z}\,dx + g(\phi_2(z))\frac{\partial \phi_2}{\partial z} - g(\phi_1(z))\frac{\partial \phi_1}{\partial z} \tag{29}$$

gives the distribution of tunnel splittings,

$$f_N(\Delta) = \sqrt{2\pi v_N}\,\frac{dR_N}{dv_N}. \tag{30}$$

In order to obtain $f_N(\Delta)$ for all molecules, dH_z/dt must range over several orders of magnitude, which is experimentally unobtainable. Also, this method will only produce the tunnel splittings. Garanin and Chudnovsky have shown[67, 68] that if the tunneling process is dominated by a single distributed term in the Hamiltonian, then all the curves for each R_N will scale onto a universal curve and each R_N will determine a different portion of $f_N(\Delta)$.

The scaling depends on the dominant tunneling process. Thus, in order to apply their methodology, the dominate term in the Hamiltonian must be chosen first. The idea is to try various terms to see which term will scale the R_N data and once a term is found, the distribution of that term can be determined from R_N. The next section will attempt to scale the R_N data in terms of different models. All the models satisfy the requirement of attributing the tunneling process to a single (or nearly single) term in the Hamiltonian that is distributed.

3.2.7 Distributions of Transverse Anisotropy

In Ref. [67, 68], Chudnovsky and Garanin considered a distribution of tunnel splittings due to transverse anisotropies caused by crystal dislocations. In their model, dislocations have the strong effect of producing deformations that require inclusion of a magnetoelastic term in the Hamiltonian. The dislocation will create transverse anisotropy, $E(\hat{S}_x^2 - \hat{S}_y^2)$ that varies with the distance from the dislocation. Thus, the second order transverse anisotropy prefactor, E, will be distributed.

Cornia *et al.* have also pointed out that there are six different isomers of Mn_{12}-acetate[62], four of which are only two-fold symmetric. This lowers the symmetry group for the Hamiltonian and permits inclusion of transverse anisotropy terms. They too found a second order transverse anisotropy that is distributed.

The following analysis is valid regardless of which micro-theory is correct. The only assumption made is that the second order transverse anisotropy prefactor, E, is distributed.

The tunnel splittings can be computed from high order degenerate perturbation theory[41]. To make the calculations simpler, the following Hamiltonian was used when calculating the tunnel splittings:

$$\hat{\mathcal{H}} = -D\hat{S}_z^2 - g\mu_B H_z \hat{S}_z + E_i(\hat{S}_x^2 - \hat{S}_y^2), \tag{31}$$

where the value of $D = 0.65\,\mathrm{K}$ has been adjusted to compensate for the neglected quartic longitudinal anisotropy term, AS_z^4. Fig. 40 compares the energy levels for the new Hamiltonian given in Eq. 31 with the energy levels of the full Hamiltonian, Eq. 4. It is clear that the energy levels are in good agreement, thus the expectation is that the simplified Hamiltonian of Eq. 31 will yield reasonably accurate tunnel splittings.

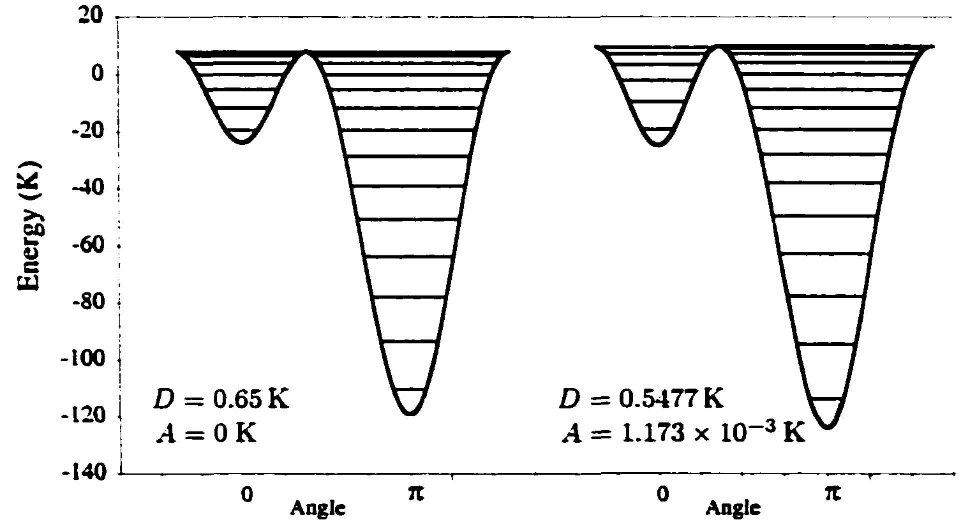

Figure 40: Comparison of energy levels between the simplified Hamiltonian of Eq. 1 with $D = 0.65\,\mathrm{K}$ and $A = 0$ and the full Hamiltonian of Eq. 4 with $D = 0.5477\,\mathrm{K}$ and $A = 1.127^{-3}\,\mathrm{K}$

The tunnel splitting of molecule i due primarily to second-order transverse anisotropy, $E(\hat{S}_x^2 - \hat{S}_y^2)$, is then given by:

$$\Delta_{N,i} = \eta_N g_N \left(\frac{\mid E_i \mid}{2D}\right)^{\xi_N}, \tag{32}$$

where $g_N = \frac{2D}{[(2S-N-2)!!]^2}\sqrt{\frac{(2S-N)!(2S)!}{(N)!}}$. The value of η_N and ξ_N have different forms depending whether N is even or odd. This is because transverse anisotropy generates selection rules that only allow even-numbered resonances. The leading contribution to even-numbered resonances involves $\xi_N = S - N/2$ virtual transitions with $\Delta m = \pm 2$ and for even N, $\eta_N = 1$. However, odd numbered resonances could also occur due to the presence of internal transverse magnetic fields of hyperfine or dipolar origin, or transverse fields due to the defects suggested by Chudnovsky and Garanin which locally tilt the easy axis so that the applied longitudinal field has a transverse component[67, 68]. The largest contribution to odd-numbered resonances entails $S - (N+1)/2$ virtual transitions with $\Delta m = \pm 2$ due to the transverse anisotropy and a single virtual transition with $\Delta m = \pm 1$ due to the transverse field. Since transverse anisotropy and transverse field created by dislocations are of the same order of magnitude [67, 68], the transverse field is proportional to the transverse anisotropy. This leads to the exponent $\xi_N = S - (N-1)/2$. Under these assumptions, the tunnel splitting for even and odd N should be roughly comparable, as is observed. For odd N, the tunnel splitting has the same form as Eq. 32. However, in this case, $\eta_N = CN/2$ and $\xi_N = S - (N-1)/2$, where C is an adjustable parameter of order 1.

By rearranging Eq. 32 it is found that

$$-\ln\left(\mid E_i \mid /2D\right) = -\ln\left(\Delta_{N,i}/\eta_N g_N\right)/\xi_N \equiv X \tag{33}$$

is independent of N. Substituting the threshold condition, $\pi\Delta_{N,i}^2 = 2v_N$, into Eq. 33 means that,

$$-\ln\left[\frac{1}{\eta_N g_N}\sqrt{\frac{2}{\pi}v_N}\right]/\xi_N \equiv X_E \tag{34}$$

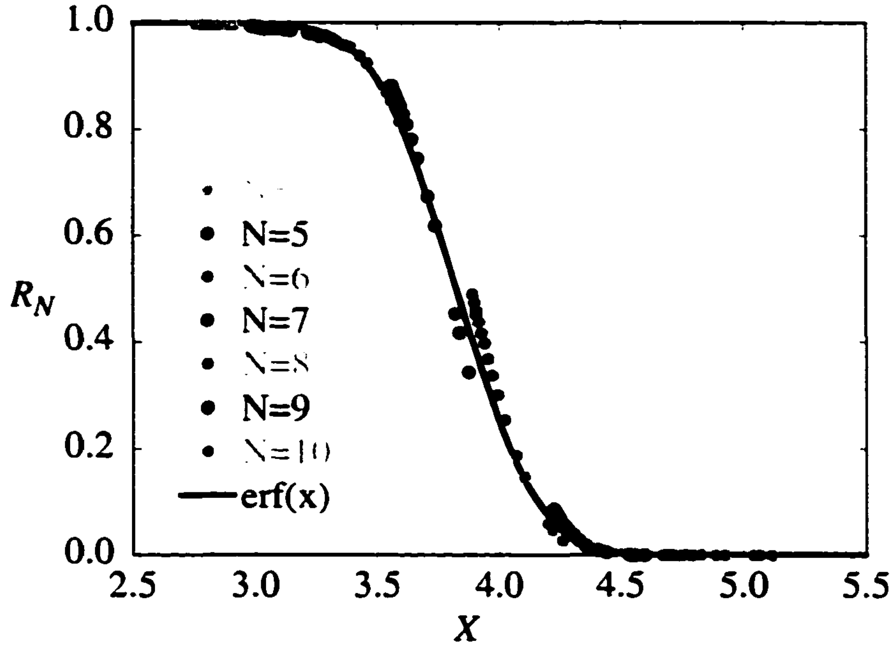

Figure 41: Scaling for distribution in second order transverse anisotropy. The fraction of molecules, R_N, that remain in the metastable well following the N^{th} level crossing is plotted as a function of the scaling parameter X. The solid continuous curve is a best fit to the data using the error function.

is also independent of N. This implies that all the curves for R_N shown in Fig. 39 should collapse onto a single curve when plotted as a function of X_E (if second-order anisotropy is responsible for the tunneling). This is shown in Fig. 41. For the odd resonance scaling, a good fit was obtained for $C = 1$.

Although the scaling obtained is of good quality, deviations should and do occur. This is due to the fact that the scaling parameter, X_E, was calculated exactly for even-numbered steps involving transverse anisotropy, while the expression for X_E is only approximate in the case of odd-numbered steps requiring an admixture of effects due to transverse magnetic fields. It should also be noted that whenever more than one process contributes to tunneling, perfect scaling cannot occur. Moreover, although second order anisotropy is the dominant mechanism causing tunneling, other processes not included in the Hamiltonian used may cause deviations.

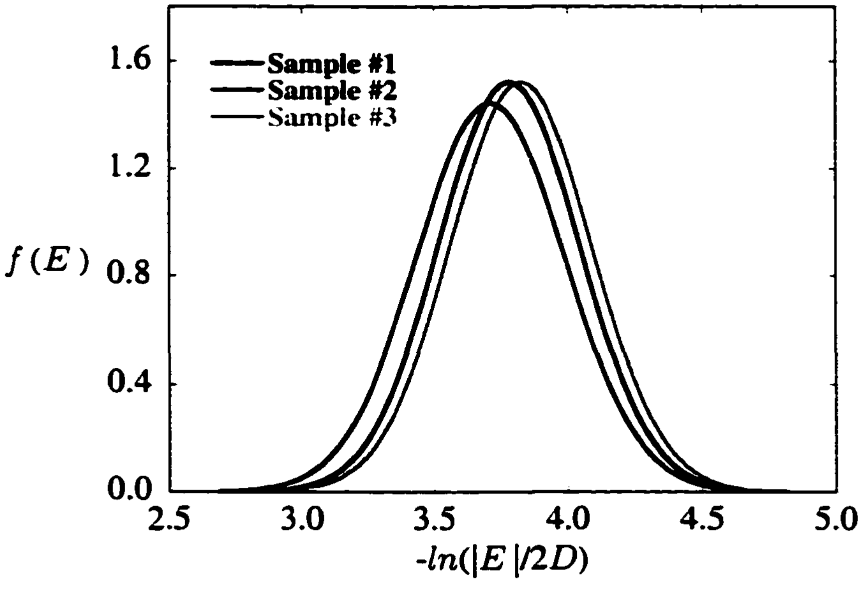

Figure 42: Distribution determined by differentiating the fraction of molecules,R_N, that remain in the metastable well following the N^{th} level crossing with respect to the scaling parameter X_E. The solid continuous curves are Gaussian.

One of the benefits of analyzing the data in this manner is that the distribution can be obtained. Eq. 28 can be rewritten in terms of a distribution in X_E,

$$R = -\int_{X_E}^{+\infty} f(X)\,dX, \tag{35}$$

where the subscript on R has been dropped since X_E is independent of N. Differentiating R with respect to X_E gives,

$$\frac{dR}{dX_E} = f(X) = f(-\ln(\mid E_i \mid /2D)). \tag{36}$$

In other words, the derivative of R in Fig. 41 gives the distribution of $X_E = -\ln(\mid E \mid /2D)$. On a log scale, the integral of any Gaussian-like function will provide a good fit to the scaled curves. The fitting function chosen in Fig. 41 is the error function. The derivative of this curve is shown in Fig. 42. Also shown are the distributions obtained by following the same procedures for the other two samples.

Other fitting functions such as the integral of a Lorentzian were also tried but they did not fit the scaled R curves. The error function was chosen for its symmetry.

The values of R very close to 1 and very close to 0 have larger error compared with the other values of R. Deviations from the error function are hard to see on the logarithmic scale and other Gaussian-like functions could have been chosen such as integrals of weighted exponentials of Gaussians. If the integral of a weighted exponential of a Gaussian were chosen, then the distribution in E would become Gaussian. Using the error function as a fitting function gives a Gaussian distribution in $X_E = -\ln(\mid E \mid /2D)$.

The collapse of R_N onto one curve supports the assumption that the tunnel splittings vary locally within the Mn_{12} crystal with a very broad distribution. The fact that they collapse with scaling parameter, X_E, indicates that transverse anisotropy is the dominant term in the Hamiltonian that drives the tunneling process.

The distribution in E can be obtained by use of the fundamental transformation law of distributions,

$$\mid f(x)\,dx \mid = \mid f(y)\,dy \mid \tag{37}$$

and then normalizing the new distribution. The result is,

$$f(E) = -\frac{e^{-\ln^2(E/E_0)/4\sigma^2}/E}{2\sigma\left[1-\mathrm{erf}\left(\ln\left(E_0/2D\right)\right)\right]} \tag{38}$$

From the distribution in E, the distribution in tunnel splittings can be determined with the aid of Eq. 32. This is shown for sample #3 in Fig. 43. Notice that the peaks come in pairs. This is because tunneling for even steps was determined by considering $S - N/2$ virtual transitions with $\Delta m = \pm 2$. Whereas, the next higher odd step was determined by simply incorporating one additional virtual transition with $\Delta m = \pm 1$.

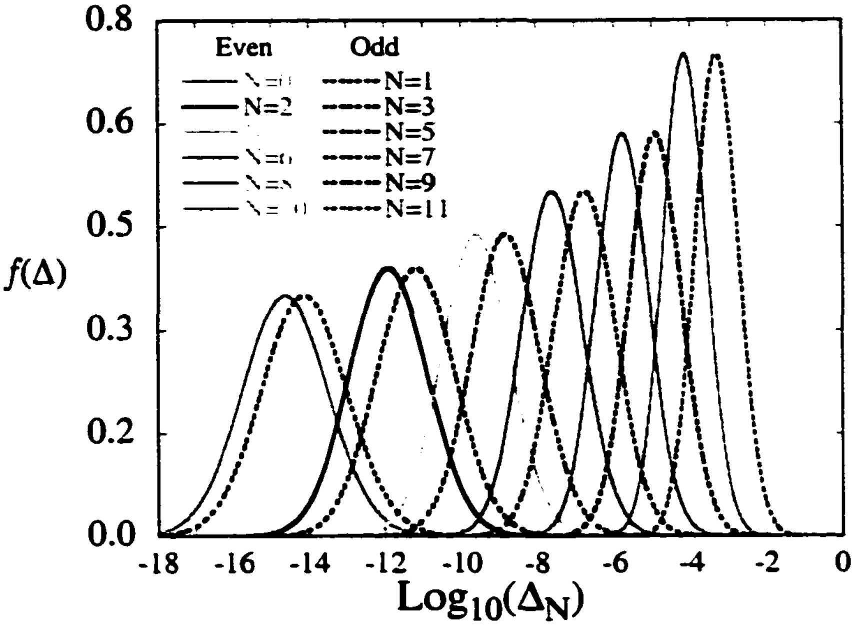

Figure 43: Distribution in tunnel splittings for each observed ground state resonance N for Sample #3.

3.2.8 Distributions of Transverse Field

The same formalism can be applied to the case of a distribution of tunnel splittings due to a distribution of transverse magnetic fields. A distribution of transverse fields could be due to the internal dipole field or the due to the nuclear hyperfine interaction. In this case, the system would be modeled by,

$$\hat{\mathcal{H}} = -D\hat{S}_z^2 - g_z\mu_B H_z\hat{S}_z + g_x\mu_B H_{x,i}\hat{S}_x, \tag{39}$$

where $H_{x,i}$ is the transverse field felt by the i^{th} molecule.

With $\hat{V}_T = g_x\mu_B H_{x,i}\hat{S}_x$ as the symmetry-breaking term, the tunnel splitting has the form[41, 67, 73]:

$$\Delta'_{N,i} = g'_N\left(\frac{g_x\mu_B H_{x,i}}{2D}\right)^{(2S-N)}, \tag{40}$$

where $g'_N = \frac{2D}{[(2S-N-1)!]^2}\sqrt{\frac{(2S-N)!(2S)!}{(N)!}}$. Repeating the same steps as before, the following expression,

$$-\ln\left(g_x\mu_B H_{x,i}/2D\right) = -\ln\left(\Delta'_{N,i}/g'_N\right)/(2S-N) \equiv X' \tag{41}$$

is independent of N. Substituting the threshold condition, $\pi\Delta_{N,i}^2 = 2v_N$, into Eq. 33 means that,

$$-\ln\left(g_x\mu_B H_{x,i}/2D\right) = -\ln\left(\frac{1}{g_N'}\sqrt{\frac{2}{\pi}v_N}\right)/(2S-N) \equiv X_H' \tag{42}$$

is also independent of N.

If the tunnel splitting were due to transverse field alone the data should scale when plotted as a function of the scaling parameter, X_H'. As can be seen in Fig. 44, the data does not scale by this procedure. Thus the tunneling is not dominated a distribution of transverse fields.

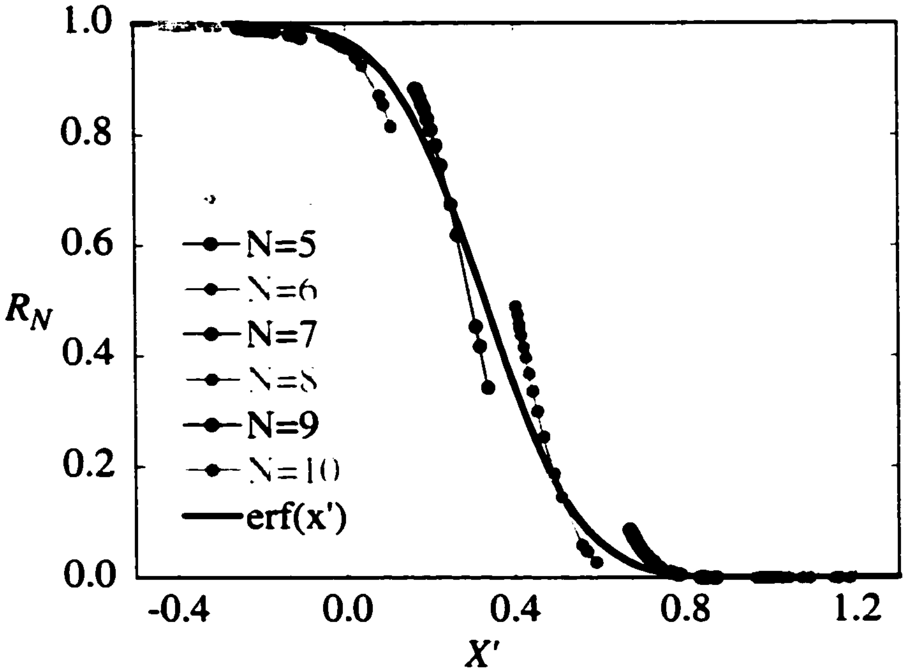

Figure 44: Scaling for distribution in transverse field. The fraction of molecules, R_N, that remain in the metastable well following the N^{th} level crossing is plotted as a function of the scaling parameter X'. The solid continuous curve is a best fit to the data using the error function. The curves do not scale, indicating that transverse field is not the dominant process driving the tunneling.

A slight variation of the above analysis is to consider the case of an angular distribution. If each molecule is tilted by varying amounts, θ_i, then the Hamiltonian will have the same form as Eq. 39. However, $H_{x,i} = H_z\tan(\theta_i) = ND\tan(\theta_i)/g_z\mu_B$

is dependent on N. Thus rearranging Eq. 40 leads to,

$$-\ln\left(g_x\tan(\theta_i)/g_z\right) = -\ln\left(\Delta'_{N,i}/g'_N\right)/(2S-N)+\ln\left(N/2\right)\equiv X'' \qquad (43)$$

and substituting the threshold condition, $\pi\Delta^2_{N,i} = 2v_N$, into Eq. 43 leads to,

$$-\ln\left(g_x\tan(\theta_i)/g_z\right) = -\ln\left(\frac{1}{g'_N}\sqrt{\frac{2}{\pi}v_N}\right)/(2S-N)+\ln\left(N/2\right)\equiv X''_\theta \qquad (44)$$

as the N independent scaling parameter. Scaling R_N in terms of X''_θ is shown in Fig. 45. Clearly, Fig. 45 shows the data does not scale in this case.

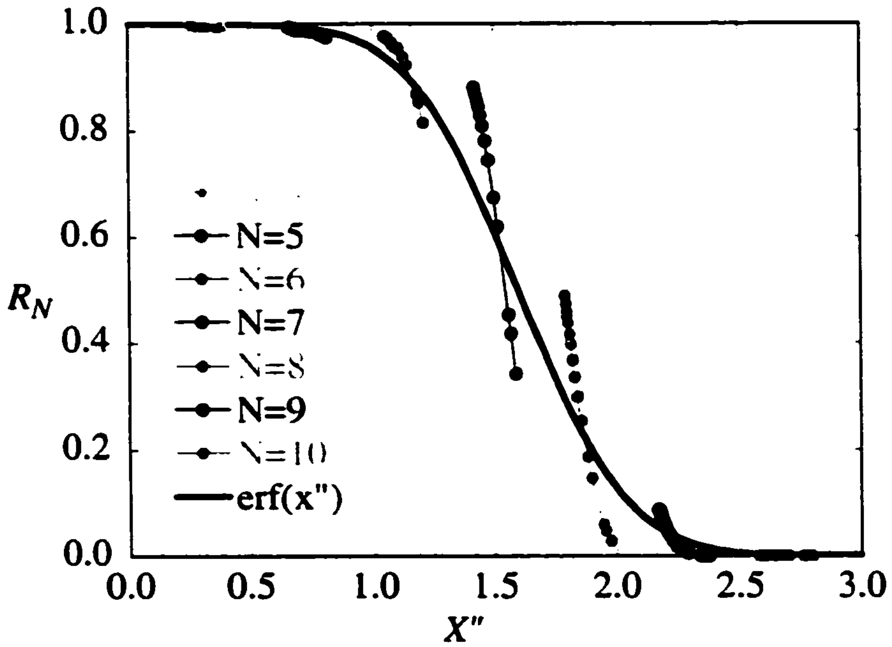

Figure 45: Scaling for distribution in tilt angle. The fraction of molecules, R_N, that remain in the metastable well following the N^{th} level crossing is plotted as a function of the scaling parameter X''. The solid continuous curve is a best fit to the data using the error function. The curves do not scale, indicating that the transverse field caused by a distribution in tilt angles is not the dominant process driving the tunneling.

Thus, it has been shown that if there is a broad distribution of tunnel splittings that is due primarily to one dominant term in the Hamiltonian, then this term cannot be related to transverse field as has been assumed in the past by others[20, 4]. However, the data is consistent with the notion of a distribution of transverse anisotropy.

The micro-theories considered by Chudnovsky and Garanin as well as the one by Cornia and Sessoli both predict that in addition to a distribution of transverse anisotropy, there is also a distribution of *longitudinal* anisotropy. The consequences of this fact will be discussed in the next section.

3.2.9 Width and Shape of Ground State Peaks

It should be noted that the magnitude of the transverse anisotropy, E, has little effect on the position of energy resonance since $E << D$. So the distribution of tunnel splittings does not directly affect the width of the peaks in dM/dH. Experimentally, the shape of the peaks for ground state tunneling have been found to be Gaussian. The fitting for $N = 7$ is shown in Fig. 46. The dotted curve is the data and the thin solid curve is the curve fit determined by minimizing the standard deviation between the data and the function, $A \exp(-(H - H_0)^2/\sigma^2)$. For this fitting function, the full width at half maximum, FWHM is related to σ by,

$$\mathrm{FWHM} = 2\sqrt{\ln(2)}\sigma \approx \frac{5}{3}\sigma. \qquad (45)$$

Interestingly, the width of the peaks in dM/dH have a FWHM $\approx 0.2\,\mathrm{T}$, which is significantly larger than what is expected for a combination of a distribution of nuclear magnetic fields and dipole fields. The nuclear magnetic field is estimated to be about $0.03\,\mathrm{T}$[77, 22, 17]. Thus if the nuclear moment is distributed uniformly over all directions, the distribution would be too small to account for such broad peaks. Also, studies on the effect of sample shape preclude the possibility that the width of the peaks is due to a distribution of dipole fields - nano-sized samples studied by Wernsdorfer *et al.* , micro-sized samples studied here and milli-sized oriented powders studied by Friedman *et al.* all show similar widths in the peaks of dM/dH. The distribution in dipole fields have also been estimated to be around $0.03\,\mathrm{T}$[7, 77, 78]. Thus it is clear that the width is not solely due to a distribution of dipole fields.

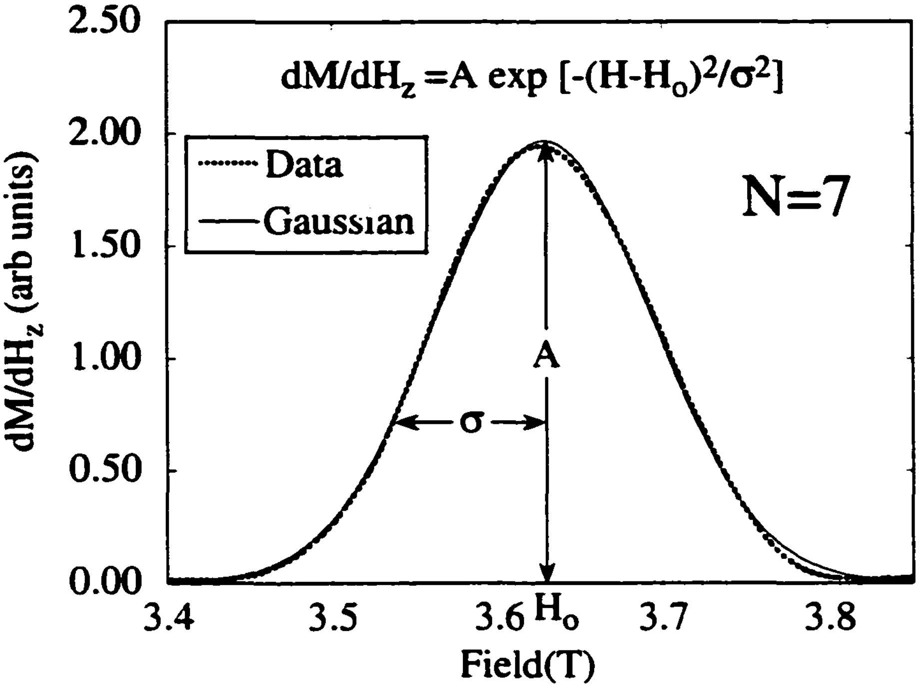

Figure 46: The peaks in dM/dH for ground state tunneling have a Gaussian shape. Shown here is the peak for $N = 7$.

The cause for such broad peaks is not known for certain, but Chudnovsky[67, 68] and Garanin, Cornia *et al.*, Parks *et al.*, Hill *et al.* and Park *et al.* have suggested that there is a distribution in D. Cornia has attributed this distribution to the presence of isomeric forms of Mn_{12}-acetate due to different coordination geometry of the ligands and has estimated the distribution to be about 2%[62]. Chudnovsky has also shown that dislocations will produce a distribution of D of about 3%[68]. Parks *et al.* has also found a distribution in D of about 1%[78]. Hill *et al.* and Park *et al.* found a 2% distribution in D from detailed EPR line shape measurements[79, 35].

These value are consistent with the widths of the peaks found in dM/dH. If the widths are due to a distribution in D then the distribution can be determined by.

$$H_z = N\frac{D}{g_z\mu_B}\left[1 + \frac{A}{D}\left(m^2 + m'^2\right)\right] \Rightarrow \delta H_z = \delta D\frac{N}{g_z\mu_B}, \tag{46}$$

which indicates that the widths of the peaks, δH_z, in dM/dH must vary with N. Plots of the dependence in the widths of the peaks on N for two different samples are shown in Fig. 47 and Fig. 48. The different data sets in each plot are for different sweep rates. Notice that there *is* a dependence on N. Also notice that they do not extrapolate to zero as $N \rightarrow 0$. The finite intercept is a measure of other N-independent sources of broadening.

If there are two sources of broadening and if these two sources are uncorrelated, then the peaks should be considered a convolution of the two distributions. This implies that to separate these two effects, σ^2 should be plotted as a function of N^2. The square-root of the intercept will give the N-independent part, $\sigma_{intercept}$, and the square-root of the slope will give the N-dependent part. Fig. 49 and Fig. 50 show σ^2 as a function of N^2 for Samples #1 and #2, respectively.

Table 2 summarizes the data obtained by examining the dependence of the widths of the peaks on N. The values of the distribution in D are in agreement with other experiments and with theory. The values determined for the distribution of $\sigma_{intercept}$ is in good agreement with the values determined for a distribution of internal dipole and nuclear fields.

	$\sigma_{intercept}$	σ_D	FWHM$_D$	$\delta D/D$
Sample #1	0.071 T	5.6 mT	9.3 mT	2.2%
Sample #2	0.065 T	8.6 mT	14. mT	3.3%

Table 2: Distribution in D determined from slope in Fig. 49 and Fig. 50 for Sample #1 and Sample #2, respectively. $\text{FWHM}_D = 2\sqrt{\ln(2)}\sigma_D$, $\delta D/D = \text{FWHM}_D g_z \mu_B / D$

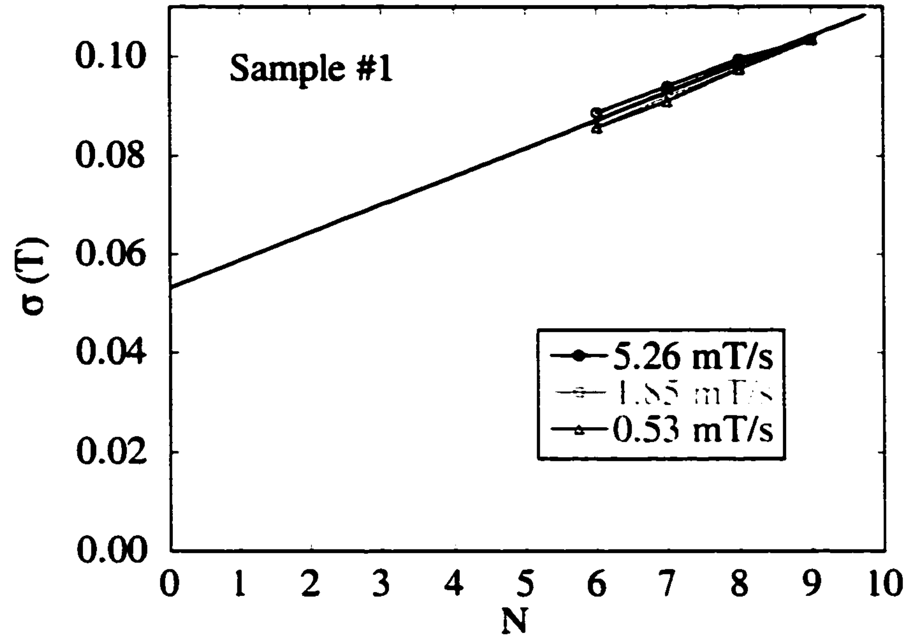

Figure 47: Peak Width Dependence for Sample #1. The finite interecept suggests that there is an internal distribution. The non-zero slope is consistent with a distribution in *D*.

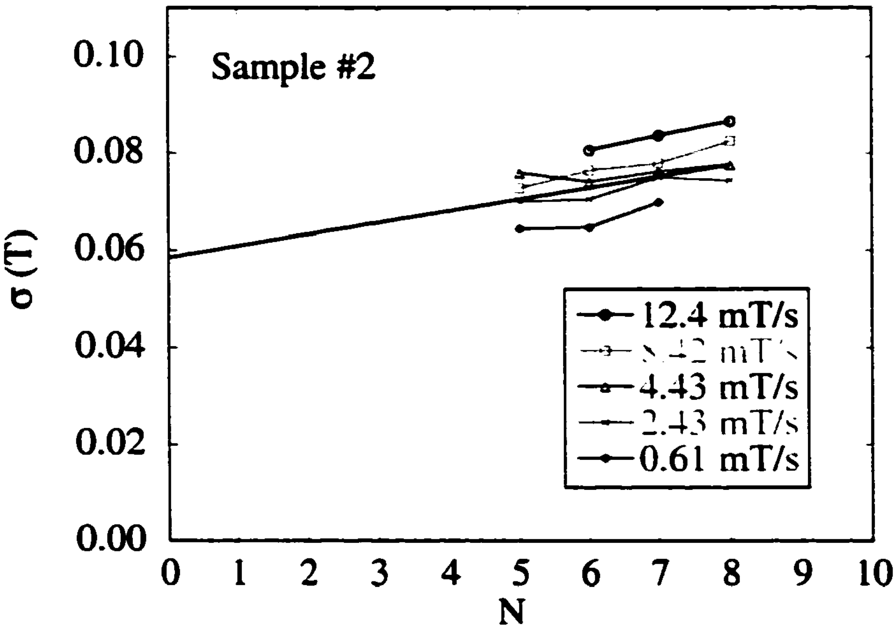

Figure 48: Peak Width Dependence for Sample #2. The finite interecept suggests that there is an internal distribution. The *N* dependent slope is consistent with a distribution in *D*.

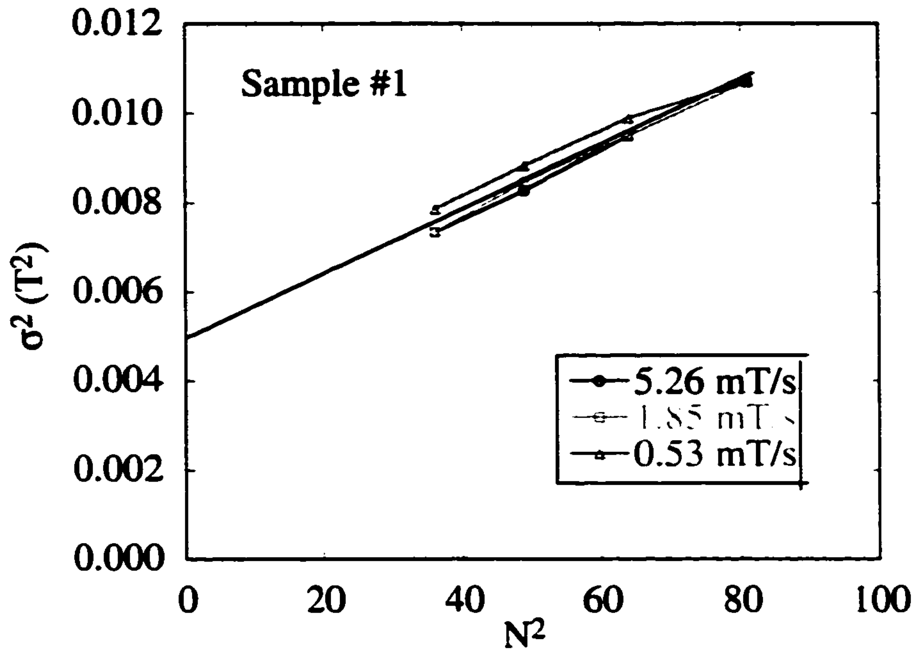

Figure 49: Convolution of Distributions for Sample #1. The square-root of the intercept will give the N-independent part, $\sigma_{intercept}$, and the square-root of the slope will give the N-dependent part.

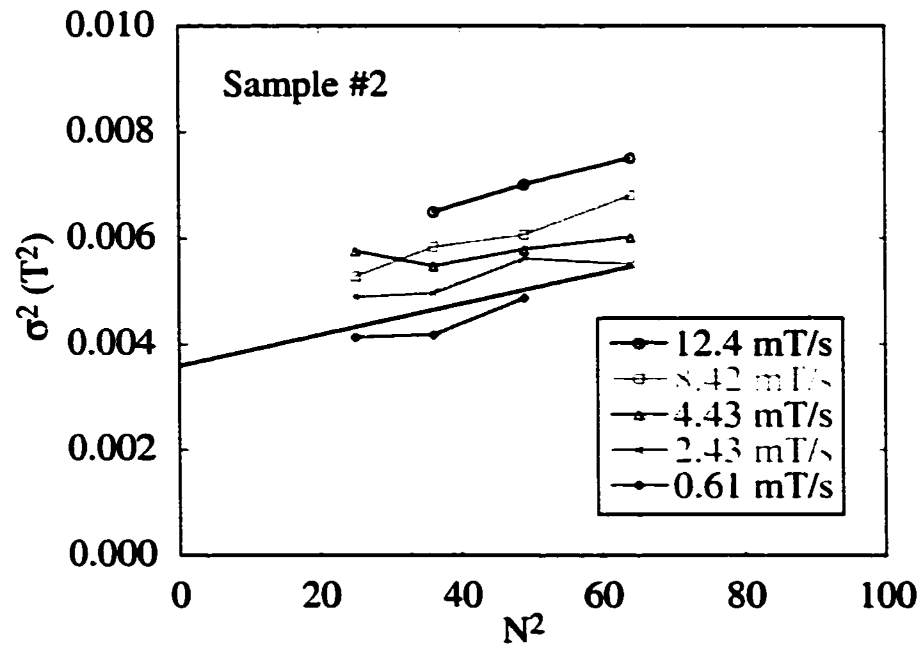

Figure 50: Convolution of Distributions for Sample #2. The square-root of the intercept will give the N-independent part, $\sigma_{intercept}$, and the square-root of the slope will give the N-dependent part.

3.2.10 Summary of Sweep Rate Dependence

In summary, the dependence of the steps in the magnetization curves on the rate at which the external field is swept was studied. It was shown that the unexpected dependence of the experimentally determined tunnel splittings on the sweep rate could be easily explained by the notion of a distribution of tunnel splittings. Under the assumption of a distribution of tunnel splittings, the plateaux in the magnetization curves now yield the *fraction* of molecules remaining in the metastable well, rather than yielding the *probability* of tunneling. It was shown that if the tunneling process is driven by one dominant term in the Hamiltonian, then the fraction of molecules, R_N, remaining in the metastable well after each resonance, N will scale onto a universal curve. The derivative of this curve directly gives the distribution in terms of the scaling parameter. It was found that the data does not scale if one assumes a distribution of transverse fields. The data scales best on the assumption there is a distribution of second order transverse anisotropy, $E(\hat{S}_x^2 - \hat{S}_y^2)$.

Two micro-physical models have been proposed to explain why there is a distribution of transverse anisotropy: isomeric forms of Mn_{12}-acetate molecules and dislocations. The data presented here cannot distinguish between these models.

These micro-theories also predict distributions of longitudinal anisotropy. This may explain the dependence of the widths of the peaks in dM/dH on N. The fact that the widths extrapolate to a finite value as $N \rightarrow 0$, indicates there is an internal distribution of fields.

3.3 Oscillating Field Experiments

3.3.1 Experimental Method

The relaxation of the magnetization was studied for each observable ground state transition by sweeping the field back and forth repeatedly across each transition, N. The sample was prepared in the same way as in the sweep rate dependence experiment described in Section 3.2. Starting from zero magnetization, the external field was swept up to and beyond the first observed transition, $N = 5$. When the field reached the middle of the plateau, it was reversed and swept back across the transition. When the field reached the middle of the previous plateau, the field was swept back up and the process was repeated many times. The same process was repeated for the next transition, $N = 6$ and so forth. The turning points of the field were chosen so that the amplitude of the oscillations of the field were the same for each N and the turning points of the field occurred near the center of a plateau.

3.3.2 Motivation of Oscillation Experiment

The purpose of this experiment is to obtain additional evidence for a distribution of transverse anisotropy. In this experiment, as the field is swept back and forth across the transition, the magnetization relaxes in steps. As will be shown, the manner in which it relaxes is expected to be different for a set of identical molecules than for the case of a distribution of tunnel splittings. The data presented here will be examined under both assumptions. It will be shown that an ensemble of identical molecules cannot describe the oscillation data presented here. A method of fitting different distributions to the magnetization data will be developed that gives an approximate fit to the data.

3.3.3 Oscillation Data

Fig. 51 shows the normalized magnetization data as the field was swept back and forth across each transition as a function of field. Notice that for each transition, as the field sweeps back and forth, the magnetization relaxes in decreasing amounts. Also notice that only for steps $N = 8$ and $N = 9$ does the magnetization effectively reach saturation. This is because the experiment was terminated before the system relaxed completely.

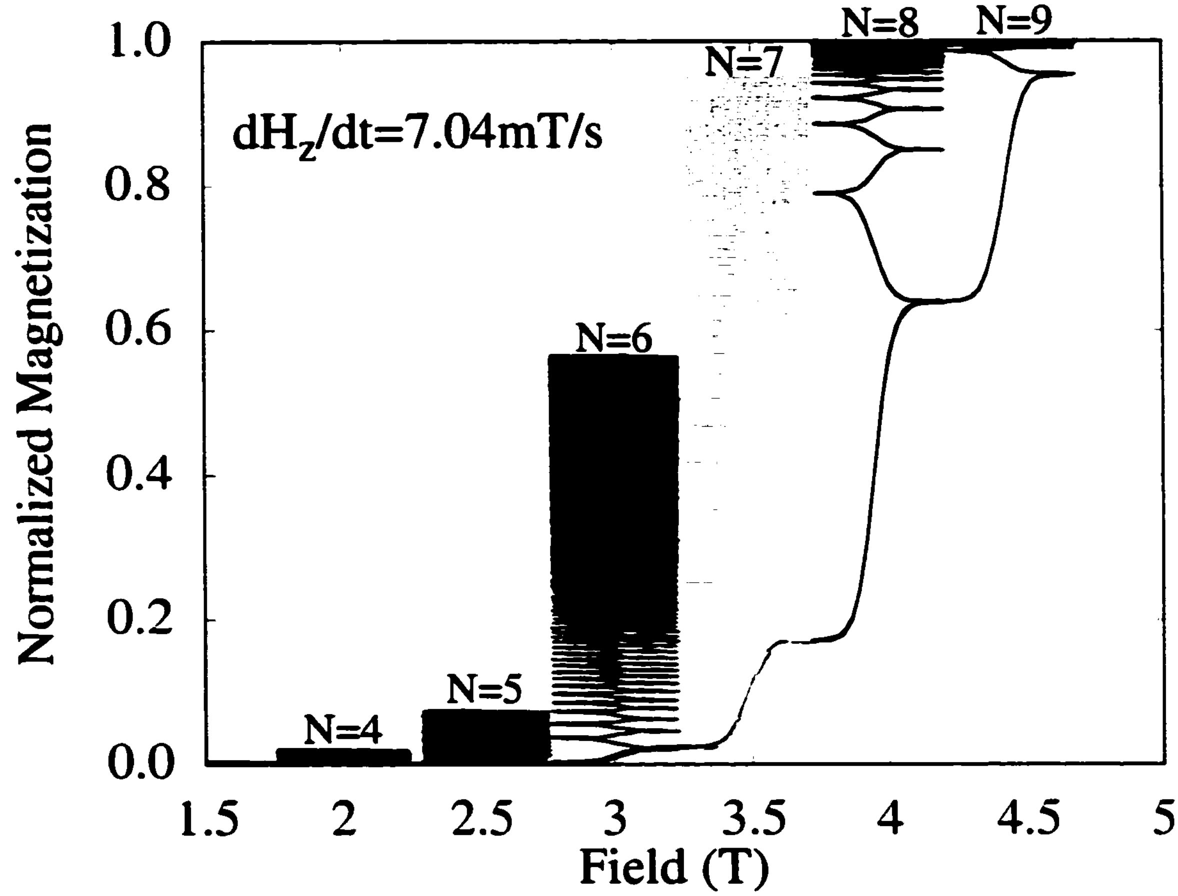

Figure 51: Normalized magnetization data for Sample #3 as the field was swept back and forth across each resonance.

As can be seen in Fig. 52, which shows the same data of Fig. 51 as a function of time. Since the amplitude of the oscillation in field was the same for each measurement and the sweep rate was also the same, the time dependence for different N can be safely compared. From the time dependence data of Fig. 52, it is clear that the magnetization relaxation rate is significantly faster for higher N than it is for lower N, which is consistent with the expectation that the tunnel splitting increases with increasing N. The issue is whether or not the relaxation rate is consistent with the model of an ensemble of identical molecules or with a distribution of tunnel splittings.

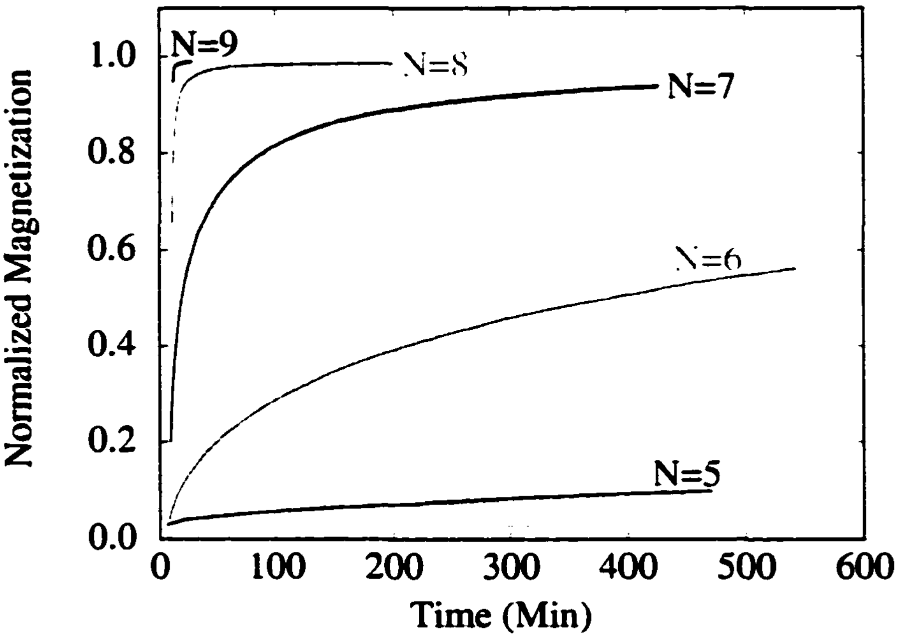

Figure 52: Normalized magnetization data for Sample #3 as the field was swept back and forth across each resonance plotted as a function of time. The magnetization relaxes faster for higher N.

Proceeding in a manner similar to Section 3.2.5, the fraction of molecules remaining after each step can be measured from the oscillation data. Fig. 53 shows the first few oscillations in detail for the $N = 7$ ground state transition. At the turning points of the field, labeled by f_1, f_2,..., the fraction of molecules remaining in the metastable well can be determined with the help of Eq. 18 and Eq. 19:

$$f_i = \frac{n_i^-}{n_i^- + n_i^+} = \frac{M_{sat} - M_i}{2M_{sat}}, \tag{47}$$

where M_i is the normalized magnetization at the turning points of the field.

For each N, Fig. 54 shows the fraction of molecules remaining in the metastable well after each pass of the field plotted as a function of how many times the field was swept past the transition. This later quantity shall be called the "oscillation number", j.

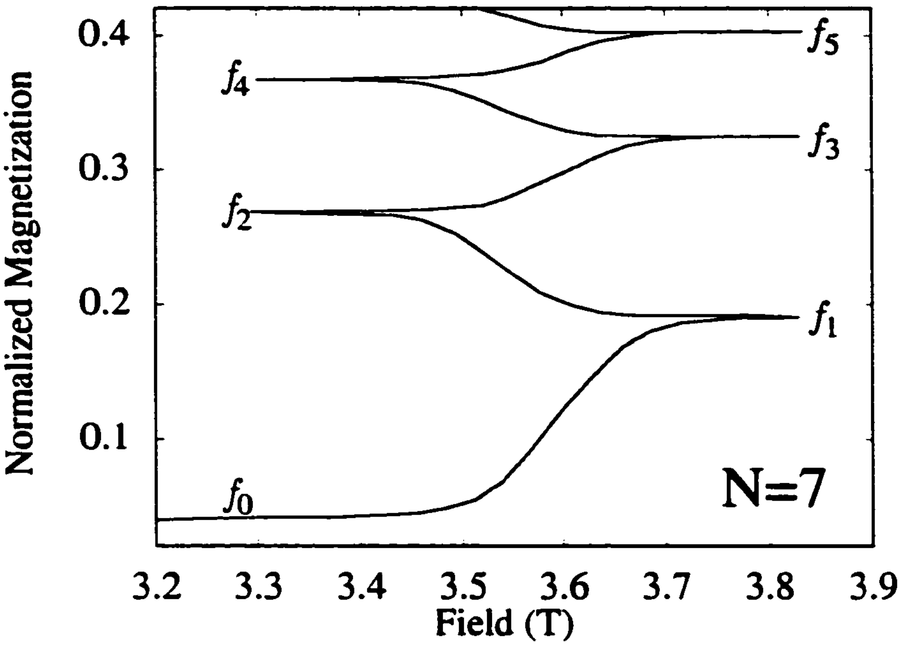

Figure 53: First few oscillations in field of the normalized magnetization data for $N = 7$. The turning points in the field are labeled by $f_1, f_2, \ldots$ in terms of the oscillation number. j.

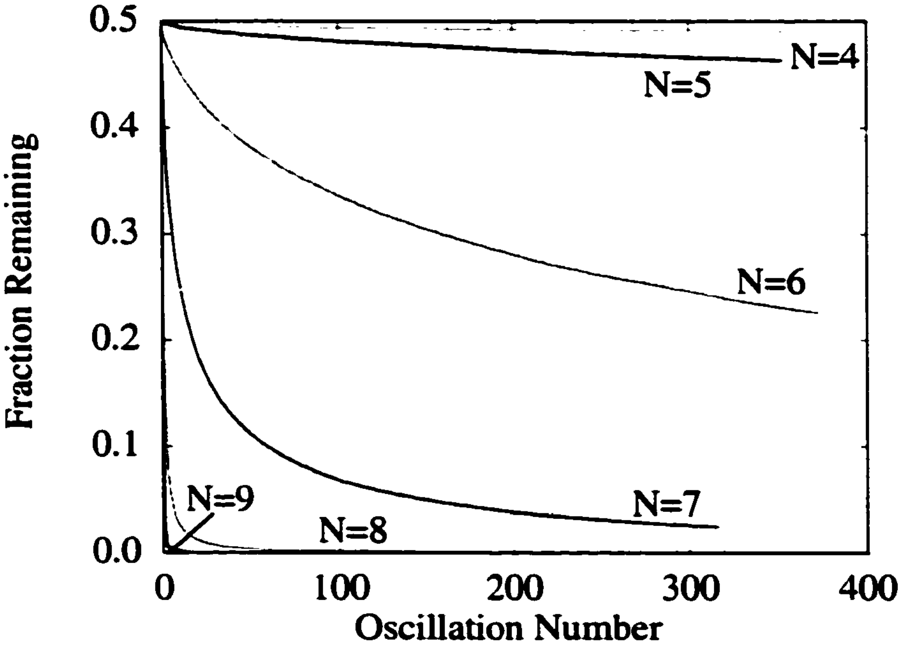

Figure 54: Fraction of molecules remaining in the metastable well plotted as a function of the oscillation number, j.

The question is, "How much magnetization tunnels from the metastable well after each pass of the magnetic field?" The data can be analyzed under the two models described earlier: 1) as an ensemble of identical molecules, 2) as a set of molecules with a distribution of tunnel splittings. The data will be analyzed in terms of both of these models in the next two sections.

3.3.4 Ensemble of Identical Molecules

The easiest way to analyze the data is under the assumption that all the molecules are identical and will tunnel with the same probability, P_N, for each resonance, N. If the fraction of molecules in the metastable well before sweeping past the transition is f_0, then since each molecule has the probability, P_N, of remaining in the metastable well, the number of molecules remaining will be

$$f_1 = f_0 P_N. \tag{48}$$

As the field is swept back down across the transition a second time, another set of molecules will tunnel. The fraction remaining after the second pass can be determined from the fraction remaining after the first pass:

$$f_2 = f_1 P_N = f_0 (P_N)^2. \tag{49}$$

In general, after j passes of the field, the fraction of molecules remaining in the metastable well will be:

$$f_j = f_0 (P_N)^j \tag{50}$$

Taking the $\log_{10}$ of both sides yields,

$$\log_{10}(f_j) = \log_{10}(f_0) + j \log_{10}(P_N). \tag{51}$$

Thus a semi-log plot of the fraction remaining as a function of oscillation number, j, should yield straight lines for each N. As can be seen in Fig. 55 this is clearly not the case. So the simple assumption that all the molecules are identical cannot explain the non-exponential relaxation of the oscillation data.

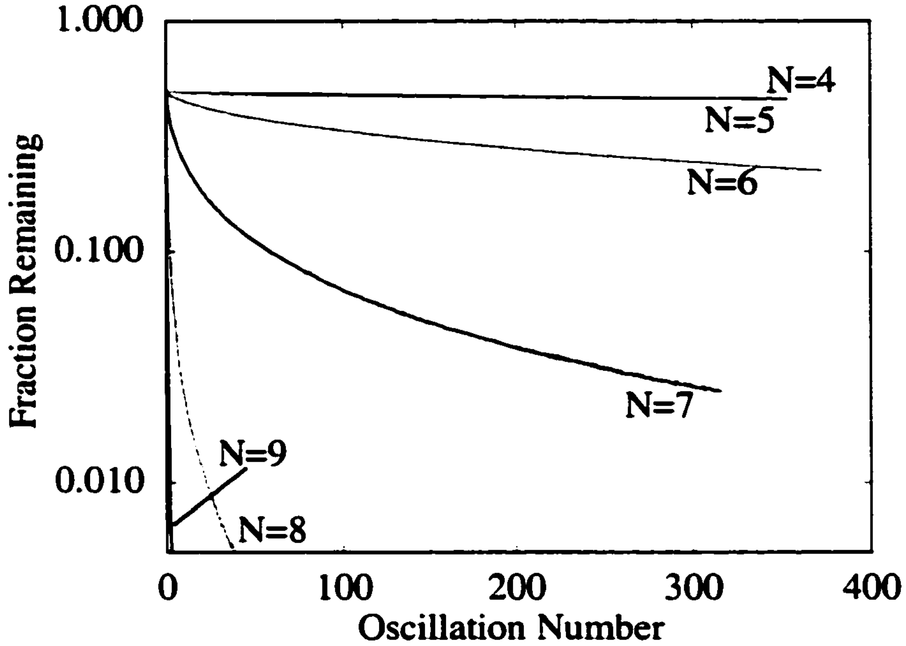

Figure 55: Fraction of molecules remaining in the metastable well under the assumption of an ensemble of identical molecules should have an exponential dependence on the oscillation number, j. Since, the data is not linear on a semilog plot, the data is inconsistent with the notion that all the molecules are identical.

3.3.5 Probing the Distribution of Tunnel Splittings

The notion of a distribution can be used to fit the data in the following way. Under the assumption of a distribution of second order transverse anisotropy, when the system starts out at zero magnetic field there is an initial distribution of the tunneling parameter, E. Consider the case of the distribution found from the scaling technique discussed in Section 3.2.7,

$$f_0(X_E) = \frac{1}{2\sqrt{\pi}} e^{-(X_E - X_0)^2/4\sigma^2}, \tag{52}$$

where $X_E = -\ln(\mid E \mid /2D)$, X_0 determines the maximum of the distribution and σ is the width. This distribution has been normalized to 1/2 since only half the molecules start out in the metastable well. After sweeping through the first resonance, the fraction of molecules remaining in the metastable well between X_E and $X_E + dX_E$, will be,

$$f_1(X_E)\,dX_E = P_1(X_E)f_0(X_E)\,dX_E, \tag{53}$$

where $P_1(X_E)$ is the probability of remaining in the metastable well for molecules with a tunneling parameter, X_E. Integrating Eq. 53 over all possible tunneling parameters, will give the fraction of molecules remaining in the metastable well after having swept the field entirely through the transition,

$$\bar{f}_1 = \int_{-\infty}^{+\infty} P_1(X_E)f_0(X_E)\,dX_E. \tag{54}$$

If the field is swept back down, then the fraction of molecules between X_E and $X_E + dX_E$ changes again, this time it is,

$$f_2(X_E)\,dX_E = P_1(X_E)f_1(X_E)\,dX_E = (P_1(X_E))^2 f_0(X_E)\,dX_E, \tag{55}$$

and the fraction remaining after having swept through the transition a second time is,

$$\bar{f}_2 = \int_{-\infty}^{+\infty} (P_1(X_E))^2 f_0(X_E)\,dX_E. \tag{56}$$

In general, the total fraction of molecules remaining in the metastable well, after having swept the field back and forth across the first transition j times is,

$$\bar{f}_j = \int_{-\infty}^{+\infty} (P_1(X_E))^j f_0(X_E)\,dX_E. \tag{57}$$

Care must be exercised when determining the fraction of molecules remaining for the other transitions. For higher N, the field is swept once through each of the $N-1$ transitions. So the fraction of molecules remaining in the metastable well, after sweeping the field back and forth across transition N, j times is given by,

$$\bar{f}_{Nj} = \int_{-\infty}^{+\infty} \prod_{k=0}^{N-1} P_k(X_E)\,(P_1(X_E))^j f_0(X_E)\,dX_E, \tag{58}$$

where $\prod_{k=0}^{N-1} P_k(X_E)$ determines how much of the distribution is remaining after having swept through the previous $N-1$ transitions. Eq. 58 can be used to model the oscillation data. Different distributions, $f_0(X_E)$, can be chosen and all the curves in Fig. 54 should be fit *simultaneously* by adjusting the parameters defining the shape of $f_0(X_E)$.

Fig. 56 shows the results of applying a distribution of the form, $f(X_E) = e^{-(X_E-X_0)^2/4\sigma^2}$. The fitting function Eq. 58 captures the shape of the curves remarkably well for all observed resonances. However, a single value for the X_0 could not be found. This could be due to the fact that the distribution may not be of the form chosen due perhaps to the existence of other symmetry-breaking terms in the Hamiltonian. The values of X_0 chosen for each N in the fit are shown in Fig. 57. The value of σ was not adjusted. If σ were also adjusted then the fits would be even better. The values for X_0 and σ agree with those obtained in the sweep rate dependence experiment.

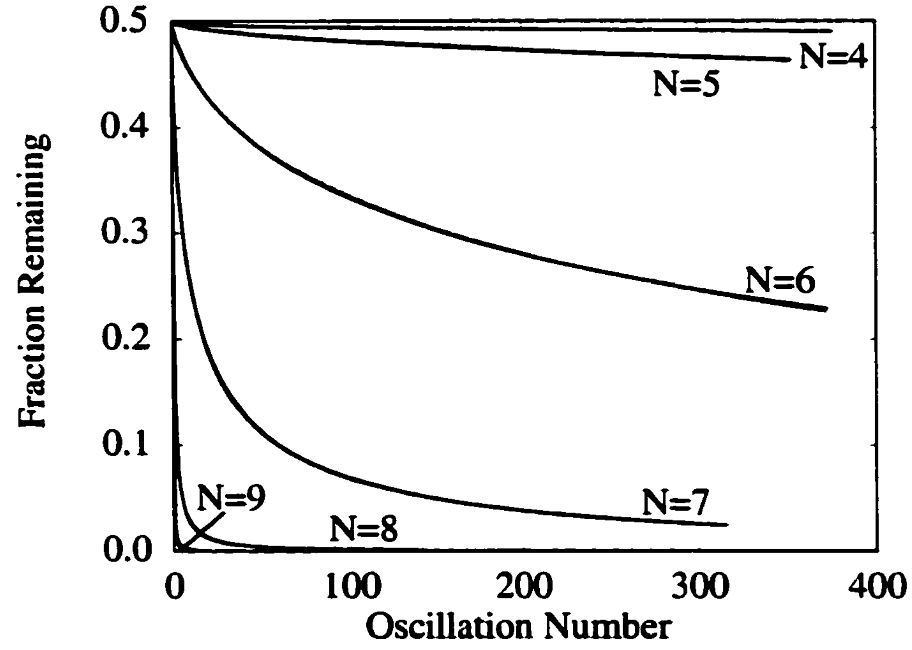

Figure 56: Fraction of molecules remaining compared with the notion of a distribution of second order transverse anisotropy. The fit function of Eq. 58 is indistinguishable from the measured data for all observed resonances.

Other fitting functions were chosen, for example a distribution that was Gaussian in $|E|/2D$. In this case it was possible to approximate all the curves with just one set of parameters. However, the fit for each curve was not as good as it is for Gaussian in $X = -\ln(|E|/2D)$. This indicates that there probably is a distribution but it is neither Gaussian in X_E, nor is it Gaussian in $|E|/2D$. This issue requires additional research.

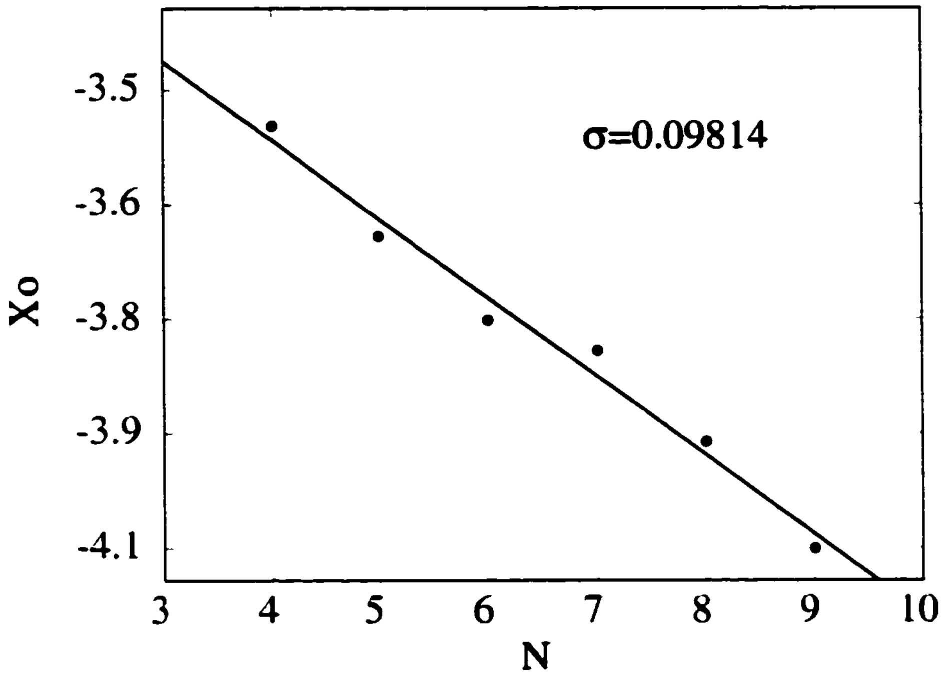

Figure 57: Fitting parameters used to fit oscillation data. The values for X_0 and σ agree with those obtained in the sweep rate dependence experiment.

3.3.6 Summary of Oscillating Field Experiment

In summary, the dependence of the measured tunneling probability on the amount of magnetization remaining in the metastable well was studied by sweeping the field back and forth across each transition. The fraction of molecules remaining in the metastable well after each sweep through the resonance was shown to be inconsistent with the model of an ensemble of identical molecules. It was also shown that the data could be analyzed in terms an arbitrary distribution. A Gaussian distribution in $X = -\ln(|E|/2D)$ as predicted in Section 3.2 gave an approximate fit to all the data simultaneously. When used to fit the data of a single curve, the fit is remarkably good. Thus the oscillating field experiment provides additional verification of the finding that tunneling of magnetization in Mn_{12}-acetate is dominated by second order transverse anisotropy and that there is a distribution of tunnel splittings.

4 Conclusion

4.1 Summary of Research

The research presented describes three experiments performed on crystals of Mn_{12}-acetate. The first was a detailed measurement of the temperature dependence of the magnetization. The transition from thermally assisted tunneling to ground state tunneling was studied. An abrupt transition to ground state tunneling was observed. Also, the puzzling phenomenon of the suppressed ground state was discussed. The latter suggests there is a distribution of tunnel splittings.

The second experiment measured the dependence of ground state tunneling on sweep rate. It was found that the notion of an ensemble of identical molecules was inconsistent with experiment. The theory of Chudnovsky and Garanin showed that a distribution of tunnel splittings leads to a scaling law for systems dominated by a single tunneling process. It was found that the data could in fact be described by a distribution of second order transverse anisotropy which gives rise to a distribution of tunnel splittings. It was also shown that with a broad distribution of tunnel splittings, the heights of the plateaux in the magnetization curves should be interpreted as a measure of the *fraction* of molecules in the distribution that tunnel fast enough for each transition, rather than as a measure of the *probability* of tunneling. The second order transverse anisotropy could derive from the presence of dislocations or the fact that there are several isomeric forms of molecules of Mn_{12}-acetate. Implicit in both the theory of dislocations and the chemistry of isomeric forms, is the expectation that there is also a distribution in longitudinal anisotropy. The widths of the peaks in dM/dH were shown to depend in a way consistent with a distribution in longitudinal anisotropy. This analysis led to an estimation of the combined effects of a distribution of dipolar and hyperfine fields.

The third experiment measured magnetic relaxation as the field was swept back and forth across each resonance. It was found that the data was inconsistent with the notion of an ensemble of identical molecules. It was also shown that the data could be analyzed in terms of an arbitrary distribution. A Gaussian distribution in $X = -\ln(|E|/2D)$ as predicted in Section 3.2 gave an approximate fit to all the data simultaneously and gave a distribution similar in size as the one found in the sweep rate experiment. Thus the oscillating field experiment provides additional verification of the finding that tunneling of magnetization in Mn_{12}-acetate is dominated by second order transverse anisotropy and that there is a distribution of tunnel splittings.

4.2 Future Research

The discovery of a distribution of transverse anisotropy has had a measurable impact in the field of single molecule magnets. Since its publication, several authors[80, 81, 82, 62] have published results supporting this claim. The idea of a distribution provides a simple explanation of many puzzling aspects of the behavior of Mn_{12}-acetate. For example, in relaxation measurements the magnetic field is swept to a fixed value and then the magnetization is monitored as it relaxes toward equilibrium. The magnetic relaxation is non-exponential[36, 20]. Wernsdorfer *et al.* reported that the magnetization for Fe_8 has a $\sqrt{t}$-dependence[83] as it relaxes toward equilibrium for short times and then displays an exponential relaxation at longer times. However for Mn_{12}-acetate, a $\sqrt{t}$-dependence was not found[55, 84] and the long time tail is not strictly exponential[36, 85]. These data should be reanalyzed in terms of a distribution of tunnel splittings. Perhaps a distribution of second order transverse anisotropy can explain these unexpected deviations.

A second area that needs to be investigated further is the puzzling behavior found by YiCheng Zhong, a former student of Myriam Sarachik at City College of New York. In relaxation measurements he found that the lineshape determined from the relaxation rate measured at different small longitudinal fields centered around the $N = 0$ step develops a peculiar shape as a function of transverse field. His observations are consistent with the presence of two different processes and may be due to a transition from tunneling arising from a broad distribution of second order transverse anisotropy to tunneling induced by the transverse field.

A third area that needs further investigation are the oscillating field experiments. The fractions of molecules remaining after each oscillation of the field are essentially integral transforms of the distribution of the tunnel splittings. Even though inverting the integral transform is an ill-posed problem, perhaps the added constraint that each resonance probes the same distribution will facilitate inversion of the integral transform. If this is possible, then the oscillating field experiments will directly measure the distribution of tunnel splittings.

The above ideas are applications of the notion of a distribution of tunnel splittings to recent measurements in Mn_{12}-acetate. The techniques developed during the experimental stages of this research can be easily applied to rapidly characterize new single molecule magnets. Interesting candidates are variants of Mn_4. With the tools in place, many different single molecule magnets can be analyzed quickly.

All these ideas can be applied now to existing materials. However, in the long term it will be necessary to move away from bulk crystals and study individual molecules. To this end it will be profitable to arrange the single molecule magnets in an array so that each molecule can be individually addressed. This will permit development of the application of single molecule magnets as the building blocks for molecular based memory storage devices or even quantum computers. Standard photolithographic techniques may not provide the best means to this end. An alternative approach is to develop the chemistry of self-assembled nano-structures. This is long term goal, but hopefully will be achieved one day.

Bibliography

[1] J. R. Friedman, M. P. Sarachik, J. Tejada, and R. Ziolo, *Phys. Rev. Lett.*, **76**(20), 3830 (1996).

[2] J. R. Friedman, *Ph.D. Thesis, The City University of New York* (1996).

[3] J. M. Hernandez, X. X. Zhang, F. Luis, J. Tejada, J. R. Friedman, M. P. Sarachik. and R. Ziolo, *Phys. Rev. Lett.*, **55**(9), 5858–5865 (1997).

[4] W. Wernsdorfer, I. Chiorescu, R. Sessoli, D. Gatteschi. and D. Mailly, *Physica B*, **284-288**, 1231–1232 (2000).

[5] W. Wernsdorfer and R. Sessoli, *Science*, **284**, 133 (1999).

[6] A. Caneschi, D. Gatteschi, R. Sessoli, A. L. Barra, L. C. Brunel, and M. Guillot. *J. Am. Chem. Soc.*, **113**, 5873–5874 (1991).

[7] M. A. Novak and R. Sessoli, in *Quantum Tunneling of Magnetization*, edited by L. Gunther and B. Barbara, pages 171–188, Kluwer, Amsterdam, 1995.

[8] R. Sessoli, D. Gatteschi. A. Caneschi, and M. A. Novak, *Nature*, **365**, 141 (1993).

[9] C. Paulsen, J. G. Park, B. Barbara, R. Sessoli, and A. Caneschi. *J. Magn. Magn. Mater.*, **140-144**, 379–380 (1995).

[10] A. O. Caldeira and A. J. Leggett, *Phys. Rev. Lett.*, **46**(4), 211–214 (1981).

[11] A. J. Leggett, S. Chakravarty, A. T. Dorsey, M. P. A. Fisher. A. Garg, and W. Zwerger, *Rev. Mod. Phys.*, **59**(1), 1–85 (1995).

[12] A. Garg and G.-H. Kim, *Phys. Rev. Lett.*, **63**(22), 2512–2515 (1989).

[13] E. M. Chudnovsky and L. Gunther, *Phys. Rev. Lett.*, **60**(8), 661–664 (1988).

[14] A. Garg, *Phys. Rev. Lett.*, **70**(10), 1541–1544 (1993).

[15] J. Villain, F. Hartman-Boutron, R. Sessoli, and A. Rettori, *Europhys. Lett.*, **27**(2), 159–164 (1994).

[16] A. Garg, *Phys. Rev. B*, **51**(21), 15592–15595 (1995).

[17] P. Politi, A. Rettori, F. Hartmann-Boutron, and J. Villain, *Phys. Rev. Lett.*, **75**(3), 537–540 (1995).

[18] D. A. Garanin and E. M. Chudnovsky, *Phys. Rev. B*, **56**(17), 11102–11118 (1997).

[19] J. R. Friedman, M. P. Sarachik, and R. Ziolo, *Phys. Rev. B*, **58**(22), R14729–R14732 (1998).

[20] B. Barbara, L. Thomas, F. Lionti, I. Chiorescu, and A. Sulpice, *J. Magn. Magn. Mater.*, **200**, 167–181 (1999).

[21] D. A. Garanin, E. M. Chudnovsky, and R. Schilling, *Phys. Rev. B*, **61**(18), 12204–12208 (2000).

[22] T. Kubo, T. Goto, T. Koshiba, K. Takeda, and K. Awaga, *preprint cond-mat/0201297* (2002).

[23] D. Deutsch, *Proc. Roy. Soc. A*, **400**, 97–117 (1985).

[24] D. Deutsch, A. Ekert, and R. Lupacchini, *preprint cond-mat/9911150* (1999).

[25] M. N. Leuenberger and D. Loss, *Nature*, **410**, 789 (2001).

[26] I. Tupitsyn and B. Barbara, *Quantum Tunneling of Magnetization in Molecular Complexes with Large Spins, Effects of the Environment.*

[27] W. Wernsdorfer, *Classical and quantum magnetization reversal studied in nanometer-sized particles and clusters*, John Wiley & Sons, 2002.

[28] S. M. J. Aubin, Z. Sun, I. A. Guzei, A. L. Rheingold, G. Christou, and D. N. Hndrickson, *Chem. Commun.*, page 2239 (1997).

[29] A. Caneschi, T. Ohm, C. Paulsen, C. Sangregorio, and R. Sessoli, *J. Am. Chem. Soc.*, **113**, 5873–5874 (1991).

[30] R. Sessoli, H.-L. Tsai, A. R. Schake, S. Wang, J. B. Vincent, K. Folting, D. Gatteschi, G. Christou, and D. N. Hendrickson, *J. Am. Chem. Soc.*, **115**(5), 1804–1816 (1993).

[31] M. R. Pederon and S. N. Khanna, *Phys. Rev. B*, **59**(2), R693–R696 (1999).

[32] M. R. Pederon and S. N. Khanna, *Phys. Rev. B*, **60**(13), 9566–9572 (1999).

[33] T. Lis, *Acta Cryst. B*, **36**, 2042 (1980).

[34] R. Sessoli, *Mol. Cryst. Liq. Cryst.*, **274**, 145–157 (1995).

[35] S. Hill, J. A. A. J. Perenboom, N. S. Dalal, T. Hathaway, T. Stalcup, and J. S. Brooks, *Phys. Rev. Lett.*, **80**(11), 2453–2456 (1998).

[36] Y. Zhong, M. P. Sarachik, J. R. Friedman, R. A. Robinson, T. M. Kelley, H. Nakotte, A. C. Christianson, F. Trouw, S. M. J. Aubin, and D. N. Hendrickson, *J. Appl. Phys.*, **85**(8), 5636 (1999).

[37] M. Hennion, L. Pardi, I. Mirebeau, E. Suard, R. Sessoli, and A. Caneschi, *Phys. Rev. B*, **56**, 8819 (1997).

[38] I. Mirebeau, M. Hennion, H. Casalta, H. Andres, H. U. Gudel, A. V. Irodova, and A. Caneschi, *Phys. Rev. Lett.*, **83**(3), 628–631 (1999).

[39] A. L. Barra, A. Caneschi, D. Gatteschi, and R. Sessoli, *J. Am. Chem. Soc.*, **117**, 8855 (1995).

[40] A. L. Barra, D. Gatteschi, and R. Sessoli, *Phys. Rev. B*, **56**(13), 8192–8198 (1997).

[41] D. A. Garanin, *J. Phys. A.*, **24**, L61–L62 (1991).

[42] D. Bohm, *Quantum Mechanics*, Dover Publicaitons, New York, 1989.

[43] L. D. Landau, *Phys. Z. Sowjetunion*, **2**, 46 (1932).

[44] C. Zener, *Proc. R. Soc. London A*, **137**, 696 (1932).

[45] E. C. G. Stueckelberg, *Helv. Phys. Acta*, **5**, 370–422 (1932).

[46] C. Paulsen and J. G. Park, "Evidence for Quantum Tunneling of the Magnetization in $\mathrm{Mn}_{12}Ac$", in *Quantum Tunneling of Magnetization*, edited by L. Gunther and B. Barbara, pages 189–207, Kluwer, Amsterdam, 1995.

[47] M. A. Novak, R. Sessoli, A. Caneschi, and D. Gatteschi, *J. Magn. Magn. Mater.*, **146**, 211–213 (1995).

[48] S. Miyashita, *J. Phys. Soc. Jpn.*, **64**(9), 3207–3214 (1995).

[49] M. Nishino, K. Saito, and S. Miyashita, *preprint cond-mat/0103553* (2001).

[50] M. N. Leuenberger and D. Loss, *Phys. Rev. B*, **61**(18), 12200–12203 (2000).

[51] E. Zeldov, D. Majer, M. Konczykowski, V. B. Geshkenbein, V. M. Vinokur, and H. Shtrikman, *Nature*, **375**, 373–376 (1995).

[52] Y. Abulafia, M. McElfresh, A. Shaulov, Y. Yeshurun, Y. Paltiel, D. Majer, H. Shtrikman, and E. Zeldov, *Appl. Phys. Lett.*, **72**(22), 2891–2893 (1998).

[53] D. Majer, E. Zeldov, H. Shtrikman, and M. Konczykowski, in *World Scientific*, edited by G. Deutscher and A. Revcolevschi, pages 271–296, World Scientific, Singapore, 1996.

[54] L. Thomas, F. Lionti, R. Ballou, D. Gatteschi, R. Sessoli, and B. Barbara, *Nature*, **383**, 145–147 (1996).

[55] W. Wernsdorfer, R. Sessoli, and D. Gatteschi, *Europhys. Lett.*, **47**(2), 254–259 (1999).

[56] F. Luis, J. Bartolomé, J. F. Fernández, J. Tejada, J. M. Hernández, X. X. Zhang, and R. Ziolo, *Phys. Rev. B*, **55**(17), 11448–11456 (1997).

[57] I. Chiorescu, R. Giraud, A. G. M. Jansen, A. Caneschi, and B. Barbara, *Phys. Rev. Lett.*, **85**(22), 4807–4810 (2000).

[58] J. A. A. J. Perenboom, J. S. Brooks, S. Hill, T. Hathaway, and N. S. Dalal, *Phys. Rev. B*, **58**(1), 330–338 (1998).

[59] A. D. Kent, Y. Zhong, L. Bokacheva, D. Ruiz, D. N. Hendrickson, and M. P. Sarachik, *Europhys. Lett.*, **49**, 521 (2000).

[60] L. Bokacheva, A. D.Kent, and M. A. Walters, *Phys. Rev. Lett.*, **85**, 4803 (2000).

[61] K. M. Mertes, Y. Zhong, M. P. Sarachik, Y. Paltiel, H. Shtrikman, E. Zeldov, E. M. Rumberger, and D. N. Hendrickson, *Europhys. Lett.*, **55**(6), 874–879 (2001).

[62] A. Cornia, R. Sessoli, L. Sorace, D. Gatteschi, A. L. Barra, and C. Daiguebonne, *preprint cond-mat/0112112* (2001).

[63] Z. Sun, D. Ruiz, E. Rumberger, C. D. Incarvito, K. Folting, A. L. Rheingold, and G. Christou, *Inorg. Chem.*, **37**(19), 4758–4759 (1998).

[64] C. Paulsen, J. G. Park, B. Barbara, R. Sessoli, and A. Caneschi, *J. Magn. Magn. Mater.*, **140-144**, 379–380 (1995).

[65] A. Caneschi and *et al.* , *J. Magn. Magn. Mat.*, **171-181**, 1330 (1998).

[66] E. M. Chudnovsky and D. A. Garanin, *Phys. Rev. Lett.*, **79**(22), 4469–4472 (1997).

[67] D. A. Garanin and E. M. Chudnovsky, *Phys. Rev. B*, **65**(9), 4423–4440 (2002).

[68] E. M. Chudnovsky and D. A. Garanin, *Phys. Rev. Lett.*, **87**(18), 187203 (2001).

[69] W. Wernsdorfer, T. Ohm, C. Sangregorio, R. Sessoli, D. Mailly, and C. Paulsen, *Phys. Rev. Lett.*, **82**(19), 3903–3906 (1999).

[70] W. Wernsdorfer, R. Sessoli, A. Caneschi, D. Gatteschi, A. Cornia, and D. Mailly, *J. Appl. Phys.*, **87**(9), 5481–5846 (2000).

[71] W. Wernsdorfer, R. Sessoli, A. Caneschi, D. Gatteschi, and A. Cornia, *Europhys. Lett.*, **50**, 552 (2000).

[72] K. M. Mertes, Y. Suzuki, M. P. Sarachik, Y. Paltiel, H. Shtrikman, E. Zeldov. E. M. Rumberger, D. N. Hendrickson, and G. Christou, *J. Appl. Phys.*. **91**, 7161 (2002).

[73] K. M. Mertes, Y. Suzuki, M. P. Sarachik, Y. Paltiel, H. Shtrikman, E. Zeldov, E. M. Rumberger, D. N. Hendrickson, and G. Christou, *Phys. Rev. Lett.*, **87**(22), 7205 (2001).

[74] J. Liu, B. Wu, L. Fu, R. B. Diener, and Q. Niu, *Phys. Rev. B*, **65**(22), 4401 (2002).

[75] K. Mullen, E. Ben-Jacob, Y. Gefen, and Z. Schuss, *Phys. Rev. Lett.*, **62**(21), 2543–2546 (1989).

[76] K. M. Mertes, Y. Suzuki, M. P. Sarachik, Y. Paltiel, H. Shtrikman, E. Zeldov, E. M. Rumberger, D. N. Hendrickson, and G. Christou, *Phys. Rev. B*, **65**(21), 212401 (2002).

[77] F. Luis, J. Bartolome, and J. Fernandez, *Phys. Rev. B*, **57**(1), 505–513 (1998).

[78] B. Parks, J. Loomis, E. Rumberger, D. N. Hendrickson, and G. Christou, *Phys. Rev. B*, **64**(18), 184426 (2001).

[79] K. Park, M. A. Novotny, N. S. Dalal, S. Hill, and P. A. Rikvold, *Phys. Rev. B*, **65**(1), 014426 (2002).

[80] R. Amigo, E. del Barco, L. Casas, E. Molins, and J. Tejada, *preprint cond-mat/0111208* (2001).

[81] F. Torres, J. M. Hernandez, E. Molins, A. Garcia-Santiago, and J. Tejada, *preprint cond-mat/0110538* (2001).

[82] J. M. Hernandez, F. Torres, and J. Tejada, *preprint cond-mat/0110515* (2001).

[83] N. V. Prokof'ev and P. C. E. Stamp, *Phys. Rev. Lett.*, **80**(26), 5794–5797 (1998).

[84] W. Wernsdorfer, C. Paulsen, and R. Sessoli, *Phys. Rev. Lett.*, **84**(24), 5678 (2000).

[85] Y. Zhong, *Ph.D. Thesis, The City University of New York* (2000).